ASD-TR-61-523

IN-FLIGHT MEASUREMENT OF HELICOPTER ROTOR SHAFT LOADS UNDER CONTROL CYCLIC TRIM VARIATIONS

TECHNICAL REPORT NO. ASD-TR-61-523
June 1962

Statement A
Approved for Public Release

Flight Dynamics Laboratory
Aeronautical Systems Division
Air Force Systems Command
Wright-Patterson Air Force Base, Ohio

Project No. 1370, Task No. 1370-04

(Also Department of the Army
Project No. 9R-38-11-009-05)

(Prepared under Contract No. AF33(616)-7292
by Vertol Division, The Boeing Company, Morton, Pennsylvania.
Authors: Robert G. Ricks, Peter Shyprykevich, Richard Gabel, and Delbert J. Smyers.)

NOTICES

When Government drawings, specifications, or other data are used for any purpose other than in connection with a definitely related Government procurement operation, the United States Government thereby incurs no responsibility nor any obligation whatsoever; and the fact that the Government may have formulated, furnished, or in any way supplied the said drawings, specifications, or other data, is not to be regarded by implication or otherwise as in any manner licensing the holder or any other person or corporation, or conveying any rights or permission to manufacture, use, or sell any patented invention that may in any way be related thereto.

Qualified requesters may obtain copies of this report from the Armed Services Technical Information Agency, (ASTIA), Arlington Hall Station, Arlington 12, Virginia.

This report has been released to the Office of Technical Services, U.S. Department of Commerce, Washington 25, D.C., in stock quantities for sale to the general public.

Copies of this report should not be returned to the Aeronautical Systems Division unless return is required by security considerations, contractual obligations, or notice on a specific document.

FOREWORD

This report was prepared by the Vertol Division of The Boeing Company, Morton, Pennsylvania, on Air Force Contract AF33(616)-7292 under Task No. 137004, "Methods for Predicting Rotor Induced Helicopter Vibrations", Project No. 1370, "Dynamic Problems in Flight Vehicles". The work was administered under the direction of Flight Dynamics Laboratory, Aeronautical Systems Division. Robert Cook and Channing Pao were the project engineers for the Laboratory. It was funded by the Department of the Army under Project No. 9R38-11009-05 directed by John Yeates.

The studies presented began in March 1959, were terminated in October 1961, and represent the effort of the Dynamics Group of the Vertol Division of The Boeing Company. Although the Studies were a group effort, the chief contributors and their fields of interest were: D. J. Smyers, flight program; R. Gabel, R. G. Ricks and P. Shyprykevich, analytical dynamics, C. Shakespeare, flight instrumentation.

This report concludes the work on Contract AF33(616)-7292.

ABSTRACT

The hub load measurement system developed for the H-21 helicopter has been utilized in this study for the measurement of metal blade loads for both standard controls and combinations of Differential Longitudinal Cyclic Trim. Cockpit floor motions were measured concurrently to permit correlation of load and vibration data. The H-21 helicopter used for this program was flown at 13,500 lb. normal gross weight, through an airspeed sweep and two rotor speed sweeps for metal blade evaluation with standard controls. At the same gross weight, the effect of longitudinal cyclic was investigated during an airspeed sweep at normal rotor speed for each cyclic combination. The data was computer processed to provide rotating and fixed coordinate system loads on the fuselage and correlative vibration data. Torque distribution between rotors and total power for each cyclic configuration was obtained from torque bridges located on the forward and aft synchronizing shafts.

In the standard configuration with metal blades, the third harmonic loads, generally the most significant with a three-bladed rotor helicopter, averaged 400 and 600 lb forward and aft rotor longitudinal, 100 and 200 lb vertical and 200 and 300 lb lateral; rolling and pitching moments averaged 3,500 and 2,000 in.-lb at the forward and aft rotors. Comparison with an earlier wood blade test program showed that metal blade loads were generally much lower; longitudinal metal blade loads were 1/3 the wood blade average. Cockpit floor vertical third harmonic vibration with metal blades was approximately half that with wood blades.

Cyclic control variations were made with three fixed longitudinal link positions at the forward rotor and an electric pilot actuated variable longitudinal link at the aft rotor. Vertical cockpit floor vibration was significantly affected by forward rotor cyclic changes, with forward tilts generally reducing vibration levels. At high speed the lowest vibration level occurred when the forward rotor was set at the most forward cyclic. Aft settings of the forward rotor increased vibration up to five fold. Aft cyclic settings of the aft rotor tended to reduce vibration when the forward rotor settings were forward. In general, forward cyclic at both rotors produced moderate vibration levels while aft cyclic settings at both rotors produced a large increase in vibration. Vibration changes were traceable to phase relation changes between vertical and longitudinal rotor forces, with little actual magnitude change due to the cyclic variations. Total aircraft power decreased linearly for aftward settings of the forward rotor cyclic. At the same time, the proportion of power to the aft rotor increased, and that to the forward rotor decreased. In general, moving the aft rotor cyclic forward linearly increased the power to the aft rotor and linearly decreased the power to the forward rotor.

PUBLICATION REVIEW

This report has been reviewed and is approved.

FOR THE COMMANDER:

William C. Nielsen

WILLIAM C. NIELSEN
Colonel, USAF
Chief, Flight Dynamics Laboratory

TABLE OF CONTENTS

LIST OF ILLUSTRATIONS

LIST OF SYMBOLS

F_x	Shear in the rotor plane in the direction of the master spline
F_y	Shear in the rotor plane in a direction normal to the master spline
$M_x = M_\alpha$	Moment in the rotor plane, about the rotating X axis
$M_y = M_\beta$	Moment in the rotor plane, about the rotating Y axis
F_z	Lift force in the shaft vertical direction
$M_z = M_\gamma$	Torque about the shaft axis
Ψ	Rotation in the plane of the rotor
L_f	Estimated lift, forward rotor
L_a	Estimated lift, aft rotor
L'_f	Steady lift, forward rotor
L'_a	Steady lift, aft rotor
Ω	Rotor speed
ϕ	Phase angle
K	Amplitude correction
P_x	Pitch link location in rotating system
P_y	Pitch link location in rotating system
F_{zRP}	Rotating pitch link load
F_{zRT}	Total vertical load rotating system
M_xR_t, M_yR_t	Total moment rotating system
Ωt	Azimuth angle
ϕR	Angular position between the rotating X axis and accelerometer No. 1

SECTION I

INTRODUCTION

Contract AF33(616)7292, Reference 1, is a research program to evaluate the effect of Differential Longitudinal Cyclic Trim (DLCT) on vibratory hub loads and performance, and the difference between metal and wood blades in regard to vibratory hub loads. Specifically, the purpose of this program was (1) to record and analyze in-flight hub loads, fuselage vibration, and performance data under preset longitudinal cyclic combinations, (2) to correlate the measured data with longitudinal cyclic positions, and (3) to compare the metal blade hub loads with those measured for the standard wood blade under Reference 2. Flight testing was performed using the H-21 helicopter (S/N 55-4141) instrumented under Reference 2 for the recording of in-flight shaft loads. Additional instrumentation was installed to provide data for the calculation of power required and power distribution between rotors.

Longitudinal dihedral was varied by restraining the forward swashplate at each of three longitudinally tilted positions and at the same time permitting longitudinal tilt of the aft swashplate to five positions. In the test program the forward swashplate longitudinal position was set prior to flight and maintained throughout the flight while the aft swash plate longitudinal position was moved in-flight to each of five predetermined positions.

Instrumentation for in-flight shaft loads consisted of strain gage bridges at several shaft levels and two azimuth positions. These permitted the measurement of rotor lift, shaft torsion, transverse shear in two mutually perpendicular directions and shaft bending moments in the same two directions. Prior to installation in the aircraft static load calibrations of all the instrumentation were conducted and means for accounting for load interaction developed. The required accuracy of the oscillograph traces was maintained in the aircraft by a detailed calibration check prior to each flight. Vibratory motions were measured concurrent with load measurement at a sufficient number of locations to define all linear and angular motions of the hubs and transmissions, as well as linear motion at the cockpit floor. Performance data was also measured, but recording equipment limitations prevented simultaneous acquisition of this data. Testing at each longitudinal cyclic configuration consisted of two flights; the first for recording load and vibration data, and the second for performance data.

Flight data for this program was compiled during seven flights which included a metal blade reference flight with standard longitudinal cyclic control and two flights at each preset forward swashplate longitudinal tilt position. The test aircraft was equipped with unweighted, turned root end, metal blades aft and weighted (20 lb cabled at 50% R), metal blades forward. Each flight was ballasted to 13,500 lb at takeoff with a nominal cg 19 in. forward of the centerline between rotors. In-flight measurements for the metal blade reference flight C96X124 included an airspeed sweep at normal rotor speed and five increment rpm sweeps at 40 and 90 knots. During flights C96X125, C96X128, and C96X129, data was obtained for loads and vibration for three forward swashplate longitudinal tilt positions in combination with each of five aft swashplate longitudinal tilt positions; performance data was compiled during flights C96X126, C96X127, and C96X132. The measured data was analyzed to obtain third harmonic fixed system loads and

Manuscript released by the author in October 1961 for publication as an ASD Technical Report.

vibration, and power requirements. Third harmonic fixed system loads were obtained by a direct transformation from the second and fourth harmonics measured in the rotating coordinate system.

Section II presents a brief description of the instrumentation and the method used for analyzing the flight data, together with the program for the conversion of loads from the rotating to the fixed system. A description of the flight configuration together with the flight test program is presented in Section III. Section IV presents load comparisons for wood and metal blades, the effect of longitudinal dihedral on in-flight loads, vibration and power requirements, and a discussion of the results. Conclusions are given in Section V. Appendices A and B give the derivation of the equations used to convert measured rotor loads to fixed system loads and Appendix C gives a more detailed description of the instrumentation.

SECTION II

INSTRUMENTATION AND DATA PROCESSING

In the present test program the instrumentation includes the hub load measuring system and subsidiary deflection measuring instrumentation developed under Reference 4. The test aircraft was further equipped with torque bridges on the interconnecting and engine shafts for defining shaft horsepower. Appendix C presents a detailed description of the instrumentation as well as detailed calibration results and procedures.

Oscillograph records of the load strain data were transferred to punched cards using a Benson Lehner Data Reader, Figure 1. Fixed system loads were obtained from the recorded strain data with a digital computer program which harmonically analyzed the data, corrected for gage interaction and transformed the loads to the fixed system.

A. INSTRUMENTATION

Load and Motion Measuring System

The H-21 helicopter, S/N 55-4141, used in this program was equipped with instrumentation to measure the following loads and motions:

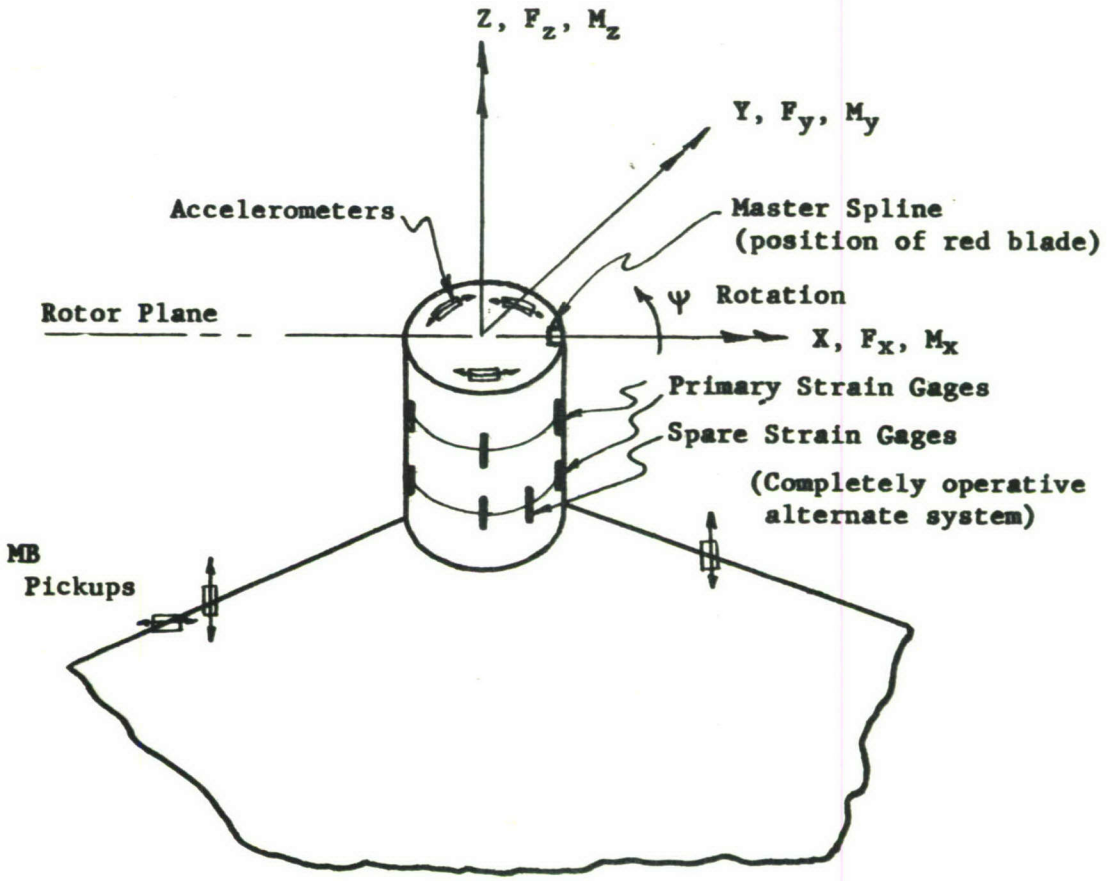

Figure 1 Benson - Lehner Data Reader

Forward and aft transmission and rotor shafts:

1. F_x, Shear in the rotor plane in the direction of the master spline.

2. F_y, Shear in the rotor plane in a direction normal to the master spline.

3. M_x, Moment in the rotor plane, about the rotating X axis.

4. M_y, Moment in the rotor plane, about the rotating Y axis.

5. F_z, Lift force in the shaft vertical direction.

6. M_z, Torque about the shaft axis.

7. Transmission case fixed system motion, referred to longitudinal and lateral motion on the shaft at the rotor hub, MB measurements.

8. Rotor hub motion, oscillation in the rotating x and y axis system, measured by accelerometers on the rotating hub.

9. Blade pitch link loads, 3 links on the forward rotor and 1 link on the aft rotor.

Fuselage:

10. Cockpit floor motion, vertical, lateral and longitudinal, MB measurements.

11. Forward rotor shaft tilt.

Static Load Calibration:

(Performed under Reference 2 contract). Each transmission was installed in a specially constructed fixture and known loads were applied individually at the rotor hub level in all directions. Figures 2, 3 and 4 illustrate the manner of load application. The response of all gages to each load was recorded, regardless of the direction of the load, in order to obtain interaction as well as primary load calibration factors. Both the primary strain gages and the spare gage alternate system were calibrated in this manner.

The results of the primary load calibration are tabulated in Table 1, Page 9, along with an estimate of the load-through-record accuracy based on an assumed oscillograph trace reading error of ± 0.02 inches.

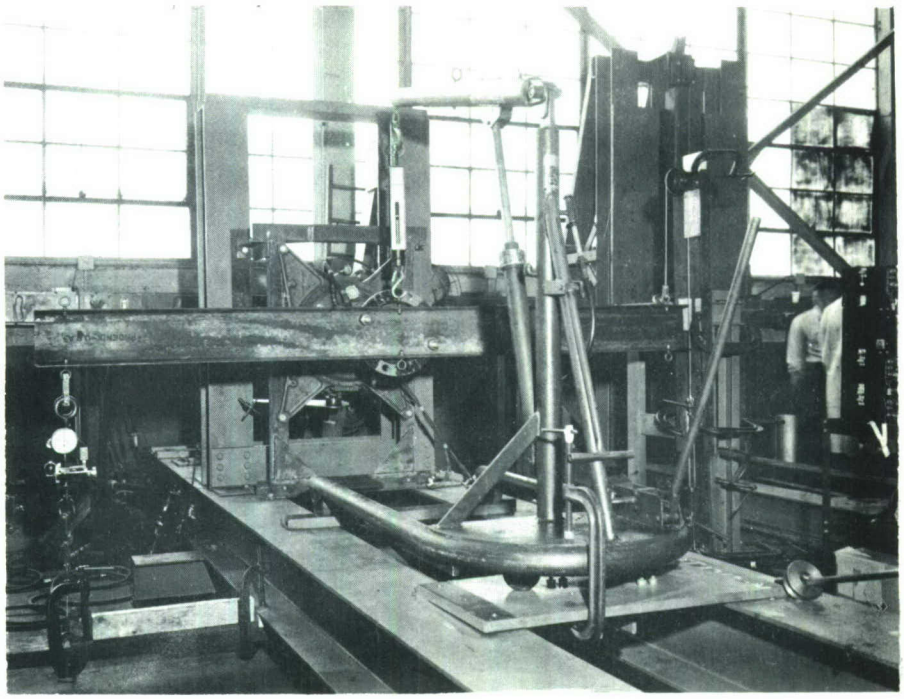

External Weight Couple Load System

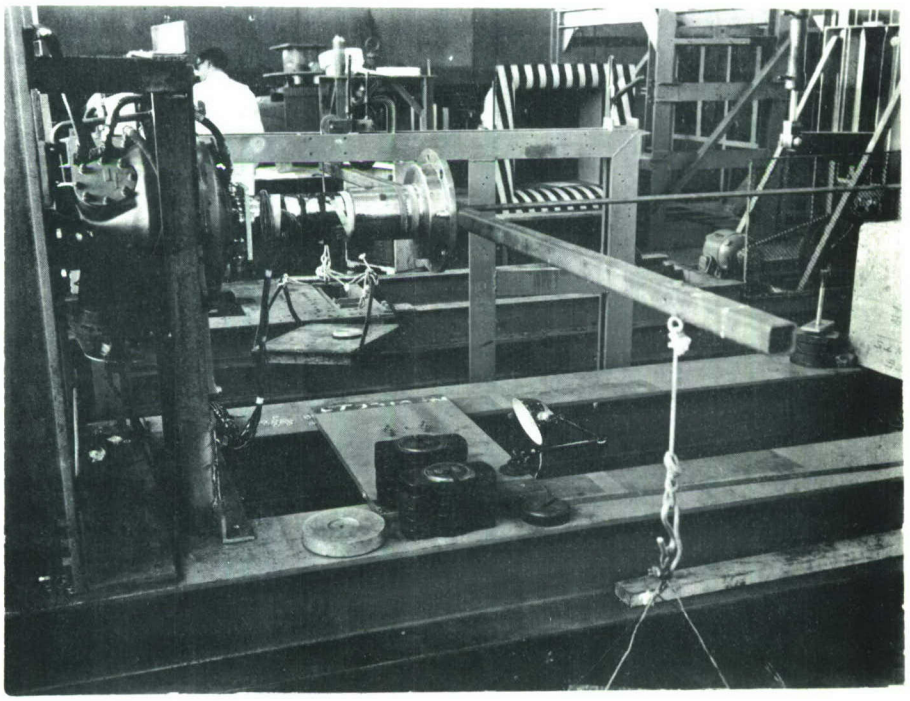

Closed Loop Cable Load System

Figure 2 Rotor Shaft Calibration - Torque Loading

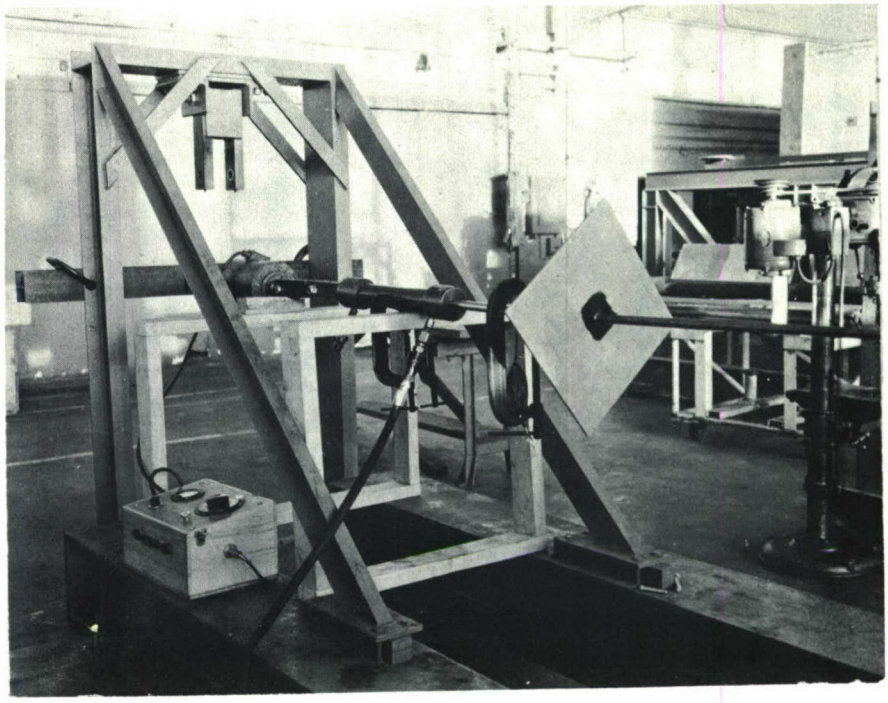

To Rotor Shaft

Hydraulic Jack

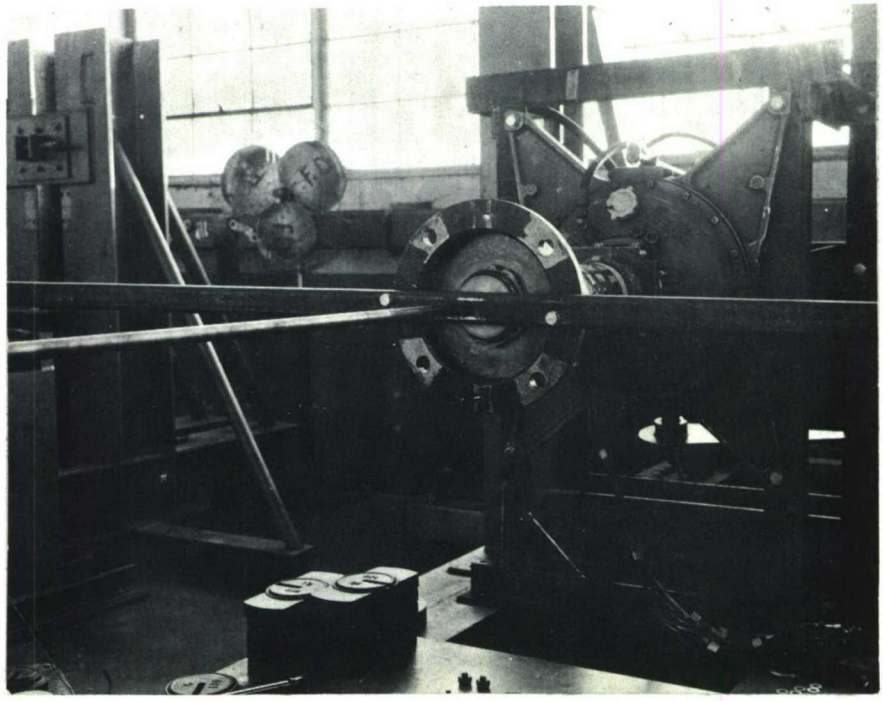

Lift Load at Rotor Shaft
(also used for moment calibration)

Figure 3 Rotor Shaft Calibration - Lift Loading

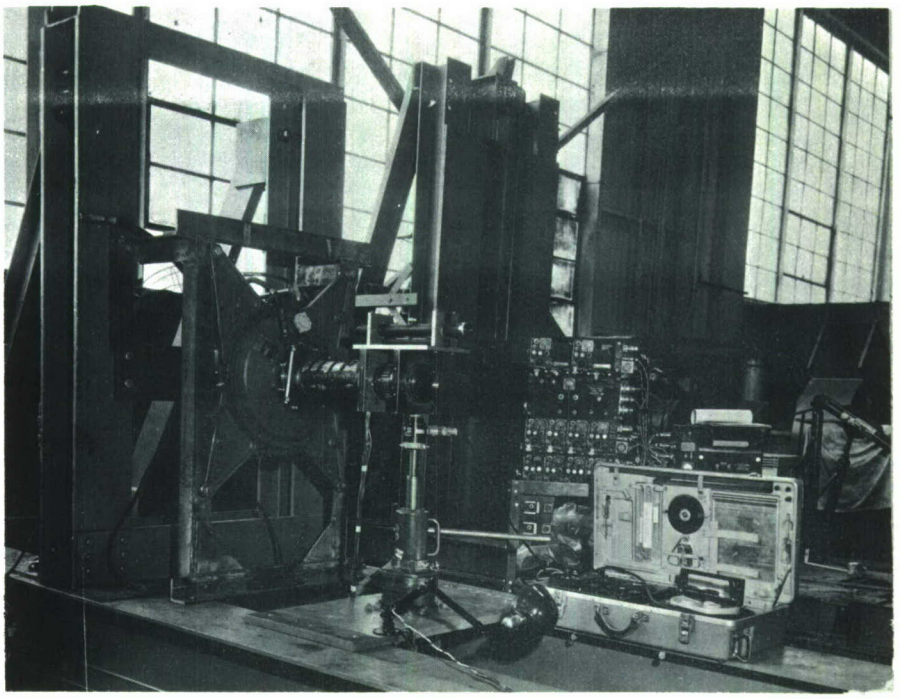

Hydraulic Jack Load System and Load Cell

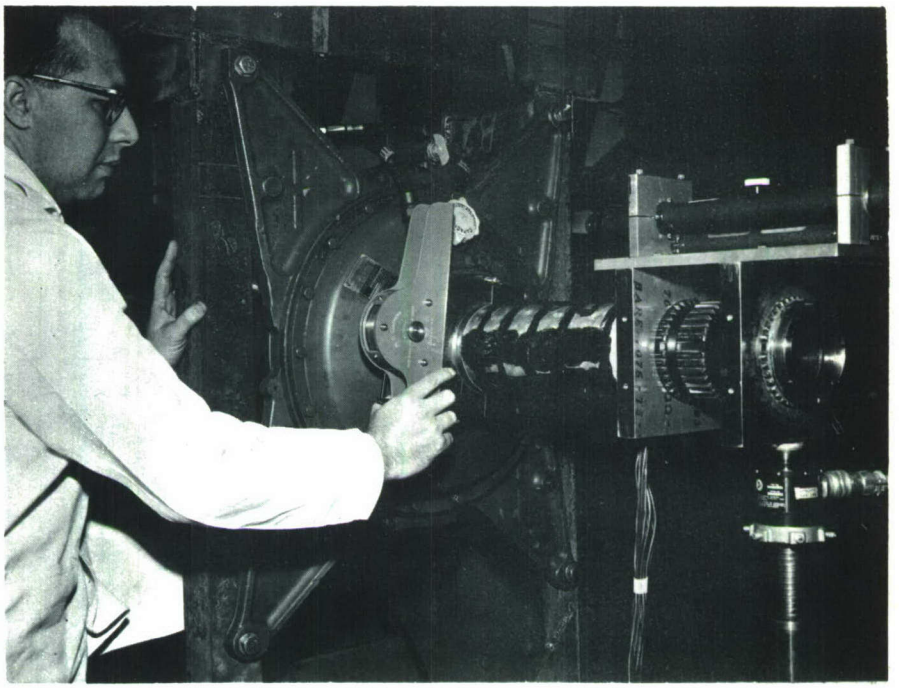

Inclinometer Check

Figure 4 Rotor Shaft Calibration - Shear Loading

TABLE I

Estimation of Accuracy Obtained in Subject Test

Chan. No.	Item	Att. Setting	Trace Calibration Factor	Estimated Reading Accuracy @ ± .02"	Estimated* Overall Accuracy	Specified Accuracy
5	F_x	1	1,000 lb/in.	± 20 lb	± 36 lb	± 35 lb
6	F_y	1	1,115 lb/in.	± 22 lb	± 36 lb	± 35 lb
7	M_y	5	19,290"lb/in.	± 400"lb	± 400"lb	± 100"lb
8	M_x	5	22,050"lb/in.	± 400"lb	± 500"lb	± 100"lb
9	$M_{z_{steady}}$	15	92,500"lb/in.	± 1860"lb	± 2400"lb	-
10	$M_{z_{alt.}}$	2	14,710"lb/in.	± 300"lb	± 100"lb	± 200"lb
11	$F_{z_{steady}}$	1.5	6,050"/in.	± 120 lb	± 360 lb	-
13	$F_{x_{(spare)}}$	1	1,091 lb/in.	± 20 lb	± 60 lb	± 35 lb
14	$F_{z_{alt.}}$	1	721"/in.	± 20 lb	± 30 lb	± 50 lb
15	$F_{y_{(spare)}}$	1	945 lb/in.	± 20 lb	± 36 lb	± 35 lb

*Based on repeated static loadings and readings

B. DATA PROCESSING

Fixed System Loads

In combination with the proper load calibrations, the measured strain data for each shaft yields the rotating system loads shown below:

1. F_x = 0°-180° shear
2. F_y = 90°-270° shear
3. M_x = 0°-180° moment
4. M_y = 90°-270° moment
5. M_z = Torque, Alternating
6. F_z = Axial Load, Alternating
7. F_z = Axial Load, Steady
8. M_z = Torque, Steady

The steady and alternating loads for lift and torque were measured on separate strain gage bridges to permit the use of high sensitivity bridges for the alternating loads. The measured rotating shaft loads are located on the shaft relative to the master spline azimuth as shown.

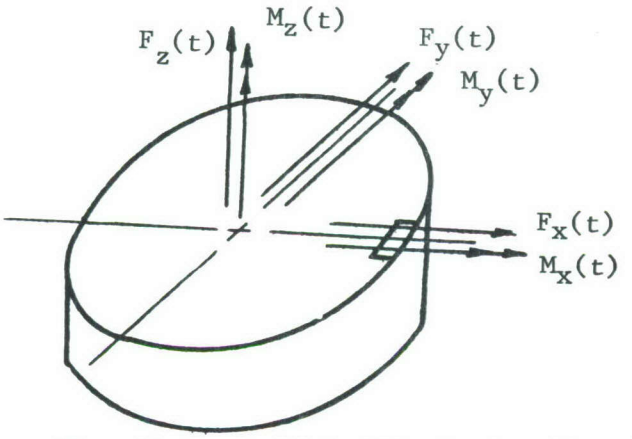

Figure 5 presents a flow diagram which illustrates the steps necessary to convert the measured strain data to the correct Fourier Series coefficients for the steady and first four harmonics of rotating shaft loads. The initial step in processing the oscillograph data after it had been reviewed for general acceptability, was the selection of a typical rotor cycle for each flight condition. Subsequently, this cycle of load and motion traces was subdivided into 24 equal time increments and ordinates from a zero position read at each point using the Benson Lehner Data Reader. The resulting data was then harmonically analyzed, using the method of Reference 3, and programmed on a digital computer to obtain the steady loads and the important harmonics. Following the harmonic analyses, each steady term of the series was adjusted to correct for the difference between the base line from which all the ordinates were measured and the zero load position obtained during the preflight calibration.

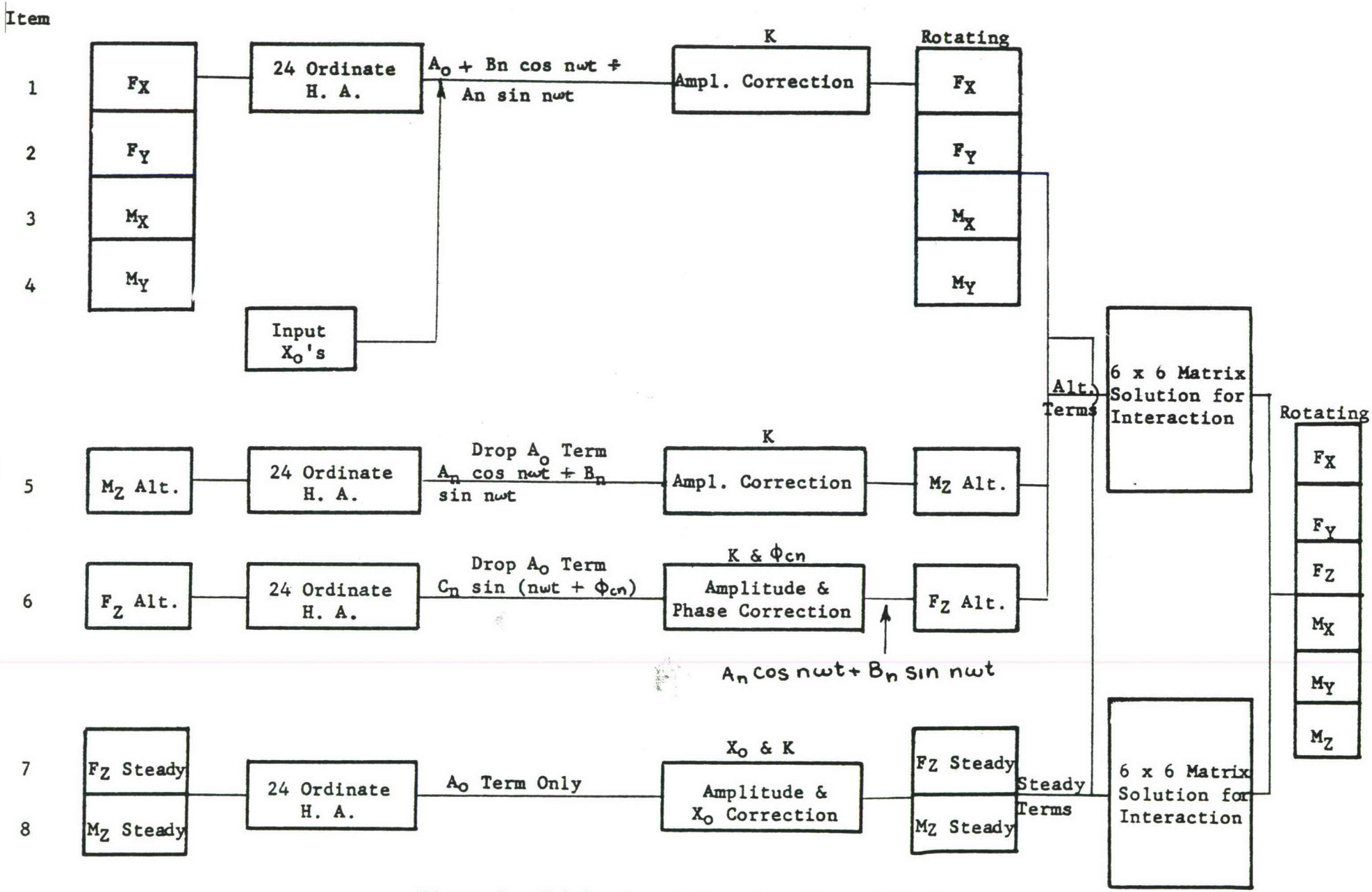

Figure 5 Hub Loads and Moments - Forward Head

Continuing to the right on the flow diagram, the harmonic components are converted to shaft loads by applying the amplitude and, in some cases, phase calibration constants obtained from the load calibration tests and adjusted for pre-flight and post-flight sensitivity checks. Following these corrections, the measured data is regrouped into steady and alternating terms in Items 1-4, alternating terms only in Items 4 and 5, and steady coefficients in Items 7 and 8.

The next step in the processing consists of an interaction correction involving the use of the interaction matrices obtained during the load calibration and shown in Appendix C. These were of the following form for both the alternating and steady loads.

$$\begin{bmatrix} F_x \\ F_y \\ F_z \\ M_\alpha \\ M_\beta \\ M_\gamma \end{bmatrix} = \begin{bmatrix} i_{ax} & i_{ay} & i_{az} & i_{a\alpha} & i_{a\beta} & i_{a\gamma} \\ i_{bx} & i_{by} & i_{bz} & i_{b\alpha} & i_{b\beta} & i_{b\gamma} \\ i_{cx} & i_{cy} & i_{cz} & i_{c\alpha} & i_{c\beta} & i_{c\gamma} \\ i_{d\alpha} & i_{dy} & i_{dz} & i_{d\alpha} & i_{d\beta} & i_{d\gamma} \\ i_{e\beta} & i_{ey} & i_{ez} & i_{e\alpha} & i_{e\beta} & i_{e\gamma} \\ i_{f\gamma} & i_{fy} & i_{fz} & i_{f\alpha} & i_{f\beta} & i_{f\gamma} \end{bmatrix} \begin{bmatrix} F_x \\ F_y \\ F_z \\ M_\alpha \\ M_\beta \\ M_\gamma \end{bmatrix}$$

Measured — Actual

After the inversion of the steady and alternating interaction matrices, the corrected coefficients for steady and alternating loads can be obtained by adjustment of the Fourier Series coefficients using,

$$\begin{bmatrix} F_x \\ F_y \\ F_z \\ M_\alpha \\ M_\beta \\ M_\gamma \end{bmatrix} = \begin{bmatrix} \text{INTERACTION MATRIX} \\ \text{FOR} \\ \text{STEADY LOADS} \\ \text{OR ALTERNATING LOAD} \end{bmatrix}^{-1} \begin{bmatrix} F_x \\ F_y \\ F_z \\ M_\alpha \\ M_\beta \\ M_\gamma \end{bmatrix}$$

Actual — Measured

Regrouping the steady and alternating coefficients, the shaft loads in the rotating axis system are defined in the general form,

$$Q = \bar{A}_o + \sum_{n=1}^{4} \bar{A}_n \cos n\Omega t + \sum_{n=1}^{4} \bar{B}_n \cos n\Omega t$$

Then, the total rotating system loads were obtained by combining the pitch link loads with the rotor shaft loads. Using the Fourier Series representation, the coefficients of like terms were combined using the following equations from Appendix A.

$$F_{z\,RT} = F_{z\,R} + F_{zRP_1} + F_{zRP_2} + F_{zRP_3}$$

$$M_{xRT} = M_{xR} + F_{zRP_1}\,(P_{1y}) + F_{zRP_2}\,(P_{2y}) + F_{zRP_3}\,(P_{3y})$$

$$M_{yRT} = M_{yR} + F_{zRP_1}\,(P_{1x}) + F_{zRP_2}\,(P_{2x}) + F_{zRP_3}\,(P_{3x})$$

Where,

P_{nx}, P_{ny}, Pitch link location in rotating system

F_{zRPn}, Rotating pitch link load

F_{zRT}, Total vertical load rotating system

M_{xRT}, M_{yRT}, Total moment rotating system

Redefining the coefficients, the final rotating loads on the fuselage are represented by again using the same general form

$$Q = A_o + \sum_{n=1}^{4} A_n \cos n\Omega t + \sum_{n=1}^{4} B_n \sin n\Omega t$$

To obtain the fixed system loads, the rotating axis system in the x-y plane is viewed in its displaced position from the fixed axes by the azimuth angle Ωt.

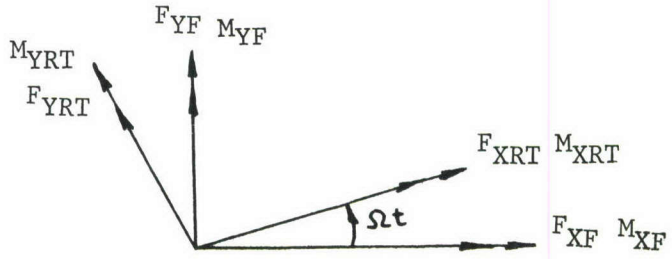

For the forward rotor with a counter-clockwise rotation when viewed from above, the load in the fixed system can be written as,

$$\begin{bmatrix} F_{xF} \\ F_{yF} \\ F_{zF} \\ M_{xF} \\ M_{yF} \\ M_{zF} \end{bmatrix} = \begin{bmatrix} \cos\Omega t & -\sin\Omega t & & & & \\ \sin\Omega t & \cos\Omega t & & & & \\ & & 1 & & & \\ & & & \cos\Omega t & -\sin\Omega t & \\ & & & \sin\Omega t & \cos\Omega t & \\ & & & & & 1 \end{bmatrix} \begin{bmatrix} F_{xRT} \\ F_{yRT} \\ F_{zRT} \\ M_{xRT} \\ M_{yRT} \\ M_{zRT} \end{bmatrix}$$

Appendix A presents the detailed steps necessary in transforming the rotating system loads into an axis system fixed to the helicopter fuselage.

For simplicity in writing the fixed system shaft loads, the rotating system coefficients are defined using a double subscript. The coefficient, together with the first subscript, define the term of the generalized load series expanded for four harmonics.

$$Q = A_0 + A_1 \cos\Omega t + B_1 \sin\Omega t + A_2 \cos 2\Omega t + B_2 \sin 2\Omega t$$
$$+ A_3 \cos 3\Omega t + B_3 \sin 3\Omega t + A_4 \cos 4\Omega t + B_4 \sin 4\Omega t$$

The second subscript denotes the load in the following order:

1. F_{xRT}
2. F_{yRT}
3. F_{zRT}
4. M_{xRT}
5. M_{yRT}
6. M_{zRT}

Using this notation the forward rotor fixed system shaft loads can be written in terms of the rotating coefficients as,

$$F_{xF} = (\tfrac{1}{2}A_{11} - \tfrac{1}{2}B_{12}) + (\tfrac{1}{2}B_{21} - A_{02} + \tfrac{1}{2}A_{22})\sin\Omega t + (A_{01} + \tfrac{1}{2}A_{21} - \tfrac{1}{2}B_{22})\cos\Omega t$$
$$+ (\tfrac{1}{2}B_{11} + \tfrac{1}{2}B_{31} - \tfrac{1}{2}A_{12} + \tfrac{1}{2}A_{32})\sin 2\Omega t + (\tfrac{1}{2}A_{11} + \tfrac{1}{2}A_{31} + \tfrac{1}{2}B_{12} - \tfrac{1}{2}B_{32})\cos 2\Omega t$$
$$+ (\tfrac{1}{2}B_{21} + \tfrac{1}{2}B_{41} - \tfrac{1}{2}A_{22} + \tfrac{1}{2}A_{42})\sin 3\Omega t + (\tfrac{1}{2}A_{21} + \tfrac{1}{2}A_{41} + \tfrac{1}{2}B_{22} - \tfrac{1}{2}B_{42})\cos 3\Omega t$$

$$F_{yF} = \tfrac{1}{2}B_{11} + \tfrac{1}{2}A_{12} + (A_{01} - \tfrac{1}{2}A_{21} + \tfrac{1}{2}B_{22})\sin\Omega t + (A_{02} + \tfrac{1}{2}A_{22} + \tfrac{1}{2}B_{21})\cos\Omega t$$
$$+ (\tfrac{1}{2}A_{11} - \tfrac{1}{2}A_{31} + \tfrac{1}{2}B_{12} + \tfrac{1}{2}B_{32})\sin 2\Omega t + (-\tfrac{1}{2}B_{11} + \tfrac{1}{2}B_{31} + \tfrac{1}{2}A_{12} + \tfrac{1}{2}A_{32})\cos 2\Omega t$$
$$+ (\tfrac{1}{2}A_{21} - \tfrac{1}{2}A_{41} + \tfrac{1}{2}B_{22} + \tfrac{1}{2}B_{42})\sin 3\Omega t + (-\tfrac{1}{2}B_{21} + \tfrac{1}{2}B_{41} + \tfrac{1}{2}A_{22} + \tfrac{1}{2}A_{42})\cos 3\Omega t$$

$$F_{zF} = A_{03} + A_{13}\cos\Omega t + B_{13}\sin\Omega t + A_{23}\cos 2\Omega t + B_{23}\sin 2\Omega t$$
$$+ A_{33}\cos 3\Omega t + B_{33}\sin 3\Omega t$$

$$M_{xF} = \tfrac{1}{2}A_{14} - \tfrac{1}{2}B_{15} + (\tfrac{1}{2}B_{24} - A_{05} + \tfrac{1}{2}A_{25})\sin\Omega t + (A_{04} + \tfrac{1}{2}A_{24} - \tfrac{1}{2}B_{25})\cos\Omega t$$
$$+ (\tfrac{1}{2}B_{14} + \tfrac{1}{2}B_{34} - \tfrac{1}{2}A_{15} + \tfrac{1}{2}A_{35})\sin 2\Omega t + (\tfrac{1}{2}A_{14} + \tfrac{1}{2}A_{34} + \tfrac{1}{2}B_{15} - \tfrac{1}{2}B_{35})\cos 2\Omega t$$
$$+ (\tfrac{1}{2}B_{24} + \tfrac{1}{2}B_{44} - \tfrac{1}{2}A_{25} + \tfrac{1}{2}A_{45})\sin 3\Omega t + (\tfrac{1}{2}A_{24} + \tfrac{1}{2}A_{44} + \tfrac{1}{2}B_{25} - \tfrac{1}{2}B_{45})\cos 3\Omega t$$

$$M_{yF} = \tfrac{1}{2}B_{14} + \tfrac{1}{2}A_{15} + (A_{04} - \tfrac{1}{2}A_{24} + \tfrac{1}{2}B_{25})\sin\Omega t + (\tfrac{1}{2}B_{24} + A_{05} + \tfrac{1}{2}A_{25})\cos\Omega t$$
$$+ (\tfrac{1}{2}A_{14} - \tfrac{1}{2}A_{34} + \tfrac{1}{2}B_{15} + \tfrac{1}{2}B_{35})\sin 2\Omega t + (-\tfrac{1}{2}B_{14} + \tfrac{1}{2}B_{34} + \tfrac{1}{2}A_{15} + \tfrac{1}{2}A_{35})\cos 2\Omega t$$
$$+ (\tfrac{1}{2}A_{24} - \tfrac{1}{2}A_{44} + \tfrac{1}{2}B_{25} + \tfrac{1}{2}B_{45})\sin 3\Omega t + (-\tfrac{1}{2}B_{24} + \tfrac{1}{2}B_{44} + \tfrac{1}{2}A_{25} + \tfrac{1}{2}A_{45})\cos 3\Omega t$$

$$M_{zF} = A_{06} + A_{16}\cos\Omega t + B_{16}\sin\Omega t + A_{26}\cos 2\Omega t$$
$$+ B_{26}\sin 2\Omega t + A_{36}\cos 3\Omega t + B_{36}\sin 3\Omega t$$

Similar expressions for the fixed system shaft loads of the aft rotor are derived in Appendix A using a negative direction of rotation.

Rotor Hub Accelerations

The following plan view of the forward rotor is used in defining the rotor hub accelerations in a plane perpendicular to the shaft.

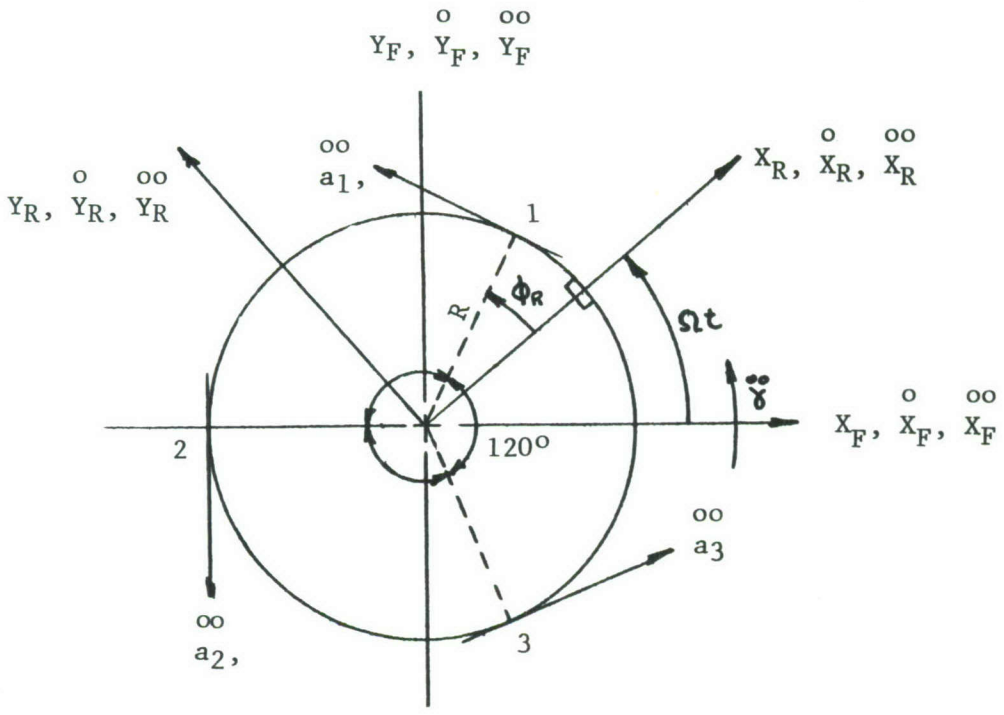

Using the sign convention shown, the measured accelerations are expressed in terms of the linear in-plane accelerations of the hub in the rotating system.

$$\begin{bmatrix} \ddot{a}_1 \\ \ddot{a}_2 \\ \ddot{a}_3 \end{bmatrix} = \begin{bmatrix} -\sin\phi_R & \cos\phi_R & R \\ -\sin(\phi_R + 120^\circ) & \cos(\phi_R + 120^\circ) & R \\ -\sin(\phi_R + 240^\circ) & \cos(\phi_R + 240^\circ) & R \end{bmatrix} \begin{bmatrix} \ddot{X}_R \\ \ddot{Y}_R \\ \ddot{\gamma} \end{bmatrix}$$

Solving the above set of equations for rotating system accelerations by inversion of the matrix yields,

$$\begin{bmatrix} \overset{\infty}{x}_R \\ \overset{\infty}{y}_R \\ \overset{\infty}{\gamma} \end{bmatrix} = \begin{bmatrix} -\frac{2}{3}\sin\Phi_R & -\frac{\sqrt{3}}{3}\cos\Phi_R + \frac{1}{3}\sin\Phi_R & \frac{\sqrt{3}}{3}\cos\Phi_R + \frac{1}{3}\sin\Phi_R \\ \frac{2}{3}\cos\Phi_R & -\frac{\sqrt{3}}{3}\sin\Phi_R - \frac{1}{3}\cos\Phi_R & \frac{\sqrt{3}}{3}\sin\Phi_R - \frac{1}{3}\cos\Phi_R \\ \frac{1}{3R} & \frac{1}{3R} & \frac{1}{3R} \end{bmatrix} \begin{bmatrix} \overset{\infty}{a}_1 \\ \overset{\infty}{a}_2 \\ \overset{\infty}{a}_3 \end{bmatrix}$$

Next, the rotating system acceleration equations shown above are transformed to obtain fixed system in-plane accelerations using the procedure established for the rotating system loads. The forward rotor fixed system acceleration equations at the hub in expanded form can be written as,

$$\overset{\infty}{x}_F = \overset{\infty}{A}_{01F} + \overset{\infty}{A}_{11F}\cos\Omega t + \overset{\infty}{B}_{11F}\sin\Omega t + \overset{\infty}{A}_{21F}\cos 2\Omega t + \overset{\infty}{B}_{21F}\sin 2\Omega t + \overset{\infty}{A}_{31F}\cos 3\Omega t + \overset{\infty}{B}_{31F}\sin 3\Omega t$$

$$\overset{\infty}{y}_F = \overset{\infty}{A}_{02F} + \overset{\infty}{A}_{12F}\cos\Omega t + \overset{\infty}{B}_{12F}\sin\Omega t + \overset{\infty}{A}_{22F}\cos 2\Omega t + \overset{\infty}{B}_{22F}\sin 2\Omega t + \overset{\infty}{A}_{23F}\cos 3\Omega t + \overset{\infty}{B}_{23F}\sin 3\Omega t$$

$$\overset{\infty}{\gamma}_F = \overset{\infty}{A}_{06F} + \overset{\infty}{A}_{16F}\cos\Omega t + \overset{\infty}{B}_{16F}\sin\Omega t + \overset{\infty}{A}_{26F}\cos 2\Omega t + \overset{\infty}{B}_{26F}\sin 2\Omega t + \overset{\infty}{A}_{36F}\cos 3\Omega t + \overset{\infty}{B}_{36F}\sin 3\Omega t$$

The fixed system acceleration coefficients, A_{mnF}, above are defined in Appendix A in terms of the harmonic coefficients of the rotating system accelerations.

Supplementing this accelerometer data, transmission motions were measured and used in combination with the in-plane motions to define the vertical and angular hub accelerations. Six velocity pickups were installed on each transmission, and calibrated such that the recorded trace deflection provided direct acceleration readings. Harmonically analyzing the traces as explained earlier and then, applying the phase and amplitude corrections, the measured data is corrected to transmission accelerations at each pickup location.

Computer Program - The digital program for this contract, initially prepared under Reference 3, integrates into one continuous procedure, the sequence of operations which convert measured trace deflections to fixed system harmonic loads. This program, in conjunction with a Benson-Lehner automatic data reader, permits rapid and accurate conversion of the recorded oscillograph data to measured hub loads. Using the integrated program permits both final and intermediate results to be calculated from one basic set of inputs at each rotor. This input includes 24 ordinate trace deflections for each recording channel, basic calibration data and interaction matrices.

An example of the input is presented in Figure 6 for the forward rotor, Flight C96X124, Run 1. Briefly, input locations from 101 to 194 store the conversion factors, x_o positions and phase corrections for the strain bridges, velocity pickup data and hub accelerometer data. Inputs 200 to 235 store the elements of the interaction matrix for alternating loads; the steady load elements are included as inputs 236 to 271. Transmission inversion elements are inputs 272 to 307. Inputs 310 to 321 provide the basic dimensions of the rotor system. The remainder of the input shown on the same figure are the rotor effective mass and damping adjustments which were omitted in the present program.

Figure 7 illustrates the output format of this program for the forward rotor, Run 1, Flight C96X124. The first printed outputs are the first three harmonics of transmission motions and accelerations presented both in the form of sine and cosine, and resultant and phase. In the next section, the tabulation presents the steady and four harmonics of rotating system loads in combination with and separate from pitch link loads. It is noted that no difference exists in the two tabulations of rotating system loads so the pitch link loads were not available. Next, the tabulation of the steady and three harmonics of the fixed system shaft and pitch link loads is presented. Following these load results, the rotor hub accelerations are shown in the rotating and fixed system.

FLT. NO. C96X124 FWD ROTOR HEAD

ITEM	IDENT	LOC	
Run No.			24
β Shaft Tilt	Print on Output Shaft		7.25
RPM			258
IAS			80
ACC. #1	X_0	101	249
	K_0	102	0
	K_1	103	2.77
	K_2	104	2.72
	K_3	105	2.814
	K_4	106	3.38
	$\phi_c 1$	107	16
	$\phi_c 2$	108	36
	$\phi_c 3$	109	63
ACC. #1	$\phi_c 4$	110	88
ACC. #2	X_0	111	379
	K_0	112	0
	K_1	113	1.978
	K_2	114	1.909
	K_3	115	1.909
	K_4	116	2.344
	$\phi_c 1$	117	15
	$\phi_c 2$	118	32
	$\phi_c 3$	119	60
ACC. #2	$\phi_c 4$	120	88
ACC. #3	X_0	121	341
	K_0	122	0
	K_1	123	2.63
	K_2	124	2.582
	K_3	125	2.582
	K_4	126	3.076
	$\phi_c 1$	127	11
	$\phi_c 2$	128	34
	$\phi_c 3$	129	62
ACC. #3	$\phi_c 4$	130	89
MB #1	K_1	131	.000651
	K_2	132	.000472
	K_3	133	.000465
	$\phi_c 1$	134	-154
	$\phi_c 2$	135	-78
MB #1	$\phi_c 3$	136	-50
MB #2	K_1	137	.000777
	K_2	138	.000505
	K_3	139	.000492
	$\phi_c 1$	140	-156
	$\phi_c 2$	141	-72
MB #2	$\phi_c 3$	142	-48
MB #3	K_1	143	.000539
	K_2	144	.000382
	K_3	145	.000379
	$\phi_c 1$	146	-153
	$\phi_c 2$	147	-84
MB #3	$\phi_c 3$	148	-51

ITEM	IDENT	LOC	24
MB #4	K_1	149	.000707
	K_2	150	.000509
	K_3	151	.000502
	$\phi_c 1$	152	-160
	$\phi_c 2$	153	-80
MB #4	$\phi_c 3$	154	-53
MB #5	K_1	155	.000701
	K_2	156	.000508
	K_3	157	.000500
	$\phi_c 1$	158	-148
	$\phi_c 2$	159	-72
MB #5	$\phi_c 3$	160	-46
MB #6	K_1	161	.000664
	K_2	162	.000452
	K_3	163	.000450
	$\phi_c 1$	164	-139
	$\phi_c 2$	165	-73
MB #6	$\phi_c 3$	166	-46
	ω_1	167	27
	ω_2	168	54
	ω_3	169	81
P/L #1	X_0	170	428
P/L #1	K	171	0
P/L #2	X_0	172	380
P/L #2	K	173	0
P/L #3	X_0	174	528
P/L #3	K	175	0
FX	X_0	176	208
FX	K	177	+12.59
FY	X_0	178	271
FY	K	179	+12.45
MX	X_0	180	392
MX	K	181	+169.8
MY	X_0	182	339
MY	K	183	167.7
MZ Alt	K	184	109.3
FZ Alt	K	185	5.221
FZ Alt	$\phi_c 1$	186	2.1
	$\phi_c 2$	187	4.7
	$\phi_c 3$	188	6.8
FZ Alt	$\phi_c 4$	189	8.5
MZ Mean	X_0	190	430
MZ Mean	K	191	848.5
FZ Mean	X_0	192	583
EZ Mean	K	193	54.27
No. of P/L		194	3
	a_{11}	200	0.91771
	a_{12}	201	-0.05621
	a_{13}	202	+0.00021

ELEMENTS OF INVERSE INTERACTION MATRIX FOR ALTERNATING LOADS

ELEMENTS OF INVERSE INTERACTION MATRIX FOR STEADY LOADS

ITEM	IDENT	LOC	24
	a_{14}	203	+0.00806
	a_{15}	204	+0.00143
	a_{16}	205	+0.00133
	a_{21}	206	+0.00773
	a_{22}	207	+0.93498
	a_{23}	208	-0.00634
	a_{24}	209	+0.00342
	a_{25}	210	-0.00046
	a_{26}	211	-0.00117
	a_{31}	212	+0.64628
	a_{32}	213	+8.9019
	a_{33}	214	+0.93949
	a_{34}	215	+0.41989
	a_{35}	216	-0.00509
	a_{36}	217	+0.00023
	a_{41}	218	-8.6482
	a_{42}	219	+0.41738
	a_{43}	220	-0.01747
	a_{44}	221	+0.92403
	a_{45}	222	-0.02062
	a_{46}	223	-0.10091
	a_{51}	224	-0.24957
	a_{52}	225	+0.15950
	a_{53}	226	+0.02728
	a_{54}	227	+0.04493
	a_{55}	228	+0.99907
	a_{56}	229	+0.02996
	a_{61}	230	+0.01889
	a_{62}	231	-0.04882
	a_{63}	232	+0.00559
	a_{64}	233	-0.00886
	a_{65}	234	-0.00278
	a_{66}	235	+1.00084
	b_{11}	236	0.91791
	b_{12}	237	-0.05615
	b_{13}	238	+0.00019
	b_{14}	239	+0.00804
	b_{15}	240	+0.00146
	b_{16}	241	+0.00129
	b_{21}	242	+0.07719
	b_{22}	243	+0.93497
	b_{23}	244	-0.00633
	b_{24}	245	+0.00342
	b_{25}	246	-0.00048
	b_{26}	247	-0.00116
	b_{31}	248	+0.64602
	b_{32}	249	+8.9016
	b_{33}	250	+0.93953
	b_{34}	251	+0.04205
	b_{35}	252	-0.00508
	b_{36}	253	+0.00037
	b_{41}	254	-8.6581
	b_{42}	255	+0.41706
	b_{43}	256	-0.01666
	b_{44}	257	+0.92419
	b_{45}	258	-0.02245
	b_{46}	259	-0.10038
	b_{51}	260	-0.19275

ELEMENTS OF INVERSE MATRIX FOR ENGINE MOTION

ITEM	IDENT	LOC	24
	b_{52}	261	+0.20456
	b_{53}	262	+0.01863
	b_{54}	263	+0.03214
	b_{55}	264	+0.99938
	b_{56}	265	+0.00359
	b_{61}	266	+0.10649
	b_{62}	267	-0.05508
	b_{63}	268	-0.00071
	b_{64}	269	-0.00783
	b_{65}	270	+0.01538
	b_{66}	271	1.00107
	c_{11}	272	0
	c_{12}	273	0
	c_{13}	274	-0.0477
	c_{14}	275	1.048
	c_{15}	276	0
	c_{16}	277	0
	c_{21}	278	0
	c_{22}	279	-.0688
	c_{23}	280	0
	c_{24}	281	0
	c_{25}	282	.0229
	c_{26}	283	1.0458
	c_{31}	284	1.0
	c_{32}	285	0
	c_{33}	286	-0.201
	c_{34}	287	+0.201
	c_{35}	288	0
	c_{36}	289	0
	c_{41}	290	0
	c_{42}	291	0.0509
	c_{43}	292	0
	c_{44}	293	0
	c_{45}	294	-0.0170
	c_{46}	295	-0.0340
	c_{51}	296	0
	c_{52}	297	0
	c_{53}	298	-0.0503
	c_{54}	299	-0.0503
	c_{55}	300	0
	c_{56}	301	0
	c_{61}	302	0
	c_{62}	303	0.0017
	c_{63}	304	0
	c_{64}	305	0
	c_{65}	306	0.0828
	c_{66}	307	-0.0845
	P_1X	310	5.1
	P_1Y	311	8.63
	P_2X	312	10.02
	P_2Y	313	0.11
	P_3X	314	4.92
	P_3Y	315	8.73
	ϕR	316	0
	ρ	317	7.25
	g	318	386.4
	χ	319	19.7
	Ω	320	27.0
	R	321	4.50

ITEM	IDENT	LOC	24
	Mex_0	751	1.636
	Mex_1	752	3.2334
	Mex_2	753	0.94964
	Mex_3	754	1.3763
	Cex_1	755	0
	Cex_2	756	0
	Cex_3	757	0
	Mey_0	758	1.636
	Mey_1	759	3.2334
	Mey_2	760	0.94964
	Mey_3	761	1.3763
	Cey_1	762	0
	Cey_2	763	0
	Cey_3	764	0
	Mez_0	765	1.4608
	Mez_1	766	0.59288
	Mez_2	767	1.11327
	Mez_3	768	0.58689
	Cez_1	769	16.305
	Cez_2	770	14.167
	Cez_3	771	33.639
	$Ie\alpha_0$	772	0
	$Ie\alpha_1$	773	-484.89
	$Ie\alpha_2$	774	-289.35
	$Ie\alpha_3$	775	-258.45
	$Ce\alpha_1$	776	0
	$Ce\alpha_2$	777	0
	$Ce\alpha_3$	778	0
	$Ie\beta_0$	779	0
	$Ie\beta_1$	780	-484.89
	$Ie\beta_2$	781	-289.35
	$Ie\beta_3$	782	-258.45
	$Ce\beta_1$	783	0
	$Ce\alpha_2$	784	0
	$Ce\beta_3$	785	0
	$Ie\delta_0$	786	16037
	$Ie\gamma_1$	787	-994.60
	$Ie\gamma_2$	788	233.57
	$Ie\gamma_3$	789	477.89
	$Ce\gamma_1$	790	0
	$Ce\gamma_2$	791	0
	$Ce\gamma_3$	792	0

Figure 6 Computer Input Sample

HUB LOAD CALCULATIONS

JOB# 5592 JUNE 19,1961 C96X124-FWD

RUN	B	RPM	IAS
24	7.25	258	80

TRANS. DISPLACEMENTS -INCHES-

X	Y	Z	ALPHA	BETA	GAMMA
47425765 48	27421312 48	56920830 48	-23461873 47	-43189358 47	16789420 46
27909460 47	-79218076 47	-44077674 48	25016119 47	75625114 46	15098101 47
-79238515 47	-91175542 47	-21084176 48	61144559 46	71282738 46	19037534 46
90247673 47	92311554 47	62568117 47	-44133036 46	-84008374 46	28409890 45
-15302368 48	28306510 48	32653685 48	-12775991 47	-21604219 47	-12309776 47
62591793 48	59557184 48	95844420 47	-56447140 46	-44651979 47	-17765640 46

X	RESUL	PHASE	X	RESUL	PHASE
10000000 51	47507816 48	86632102 52	20000000 51	12009739 48	31871649 53
30000000 51	64435201 48	34626187 53	40000000 51		
Y	RESUL	PHASE	Y	RESUL	PHASE
10000000 51	28542659 48	10611360 53	20000000 51	12974746 48	31535473 53
30000000 51	65941767 48	25420942 52	40000000 51		
Z	RESUL	PHASE	Z	RESUL	PHASE
10000000 51	71991820 48	12775306 53	20000000 51	21992957 48	28652846 53
30000000 51	34031230 48	73642088 52	40000000 51		
ALPHA	RESUL	PHASE	ALPHA	RESUL	PHASE
10000000 51	34296730 47	31683632 53	20000000 51	75408103 46	12582107 53
30000000 51	13967417 47	24616310 53	40000000 51		
BETA	RESUL	PHASE	BETA	RESUL	PHASE
10000000 51	43846462 47	27993188 53	20000000 51	11017548 47	13968475 53
30000000 51	49603846 47	20581935 53	40000000 51		
GAMMA	RESUL	PHASE	GAMMA	RESUL	PHASE
10000000 51	15191165 47	63453472 51	20000000 51	19248348 46	81512334 52
30000000 51	12437313 47	26178770 53	40000000 51		

TRANS. ACCELERATIONS IN/SEC

XDDOT	YDDOT	ZDDOT	ADDOT	BDDOT	GDDOT
-34573383 51	-19990136 51	-41495285 51	17103705 50	31485042 50	-12239487 49
-20345996 50	57749977 50	32132624 51	-18236751 50	-55130708 49	-11006516 50
23105951 51	26586788 51	61481457 51	-17829753 50	-20786046 50	-55513449 49
-26316221 51	-26918049 51	-18244863 51	12869193 50	24496842 50	-82843239 48
10039884 52	-18571901 52	-21424083 52	83823277 50	14174528 51	80764440 50
-41066475 52	-39075468 52	-62883524 51	37034969 50	29296163 51	11656036 50

XDDOT	RESUL	PHASE	XDDOT	RESUL	PHASE
10000000 51	34633198 51	26663210 53	20000000 51	35020402 51	13871649 53
30000000 51	42275935 52	16626187 53	40000000 51		
YDDOT	RESUL	PHASE	YDDOT	RESUL	PHASE
10000000 51	20807598 51	28611360 53	20000000 51	37834359 51	13535473 53
30000000 51	43264393 52	20542094 53	40000000 51		
ZDDOT	RESUL	PHASE	ZDDOT	RESUL	PHASE
10000000 51	52482037 51	30775306 53	20000000 51	64131464 51	10652846 53
30000000 51	22327891 52	25364209 53	40000000 51		
ADDOT	RESUL	PHASE	ADDOT	RESUL	PHASE
10000000 51	25002316 50	13683632 53	20000000 51	21989002 50	30582107 53
30000000 51	91640224 50	66163104 52	40000000 51		
BDDOT	RESUL	PHASE	BDDOT	RESUL	PHASE
10000000 51	31964071 50	99931880 52	20000000 51	32127169 50	31968475 53
30000000 51	32545083 51	25819353 52	40000000 51		
GDDOT	RESUL	PHASE	GDDOT	RESUL	PHASE
10000000 51	11074359 50	18634535 53	20000000 51	56128184 49	26151233 53
30000000 51	81601213 50	81787698 52	40000000 51		

ROTATING SHAFT LOADS

FX	FY	FZ	MX	MY	MZ
94647574 52	-96737951 52	40115999 54	-78631087 54	18919943 54	-58080983 55
72907318 53	13700754 53	-82479900 51	37684520 53	16315686 55	-30054004 53
20835158 53	-70592994 53	67798949 52	20368924 55	78046081 54	-67716899 53
-10000020 53	-42281517 52	66400105 52	-89922942 53	14777135 53	-42010378 53
50685307 52	-13231501 53	-27362480 51	-60544639 52	-45963240 53	-88465889 53
10284080 52	-54990941 51	-17391180 52	-12236080 53	-96980239 52	-22885259 54
39968920 52	43294581 50	-84053846 52	-53136607 52	-18731708 53	-46226578 53
-98774859 52	71675563 52	33832394 52	20228765 52	25056883 53	39865501 53
70595559 52	11521190 53	-52862386 52	14043755 53	-56069463 53	-13818395 53

FX	RESUL	PHASE	FX	RESUL	PHASE
10000000 51	75825990 53	74051335 52	20000000 51	11211173 53	29687827 53
30000000 51	41270776 52	14429322 52	40000000 51	12140925 53	30555384 53
FY	RESUL	PHASE	FY	RESUL	PHASE
10000000 51	71910232 53	16901653 53	20000000 51	13890640 53	19772138 53
30000000 51	55161108 51	27450163 53	40000000 51	13568776 53	31886547 52
FZ	RESUL	PHASE	FZ	RESUL	PHASE
10000000 51	68298805 52	35306384 53	20000000 51	66456459 52	92359740 52
30000000 51	85834154 52	19168985 53	40000000 51	62761954 52	14738040 53
MX	RESUL	PHASE	MX	RESUL	PHASE
10000000 51	20372409 55	10599076 51	20000000 51	90126533 53	26614812 53
30000000 51	13340039 53	24652654 53	40000000 51	14188695 53	81965647 51
MY	RESUL	PHASE	MY	RESUL	PHASE
10000000 51	18086280 55	64435877 52	20000000 51	48280256 53	16217745 53
30000000 51	21093329 53	20737210 53	40000000 51	61413615 53	15592061 53
MZ	RESUL	PHASE	MZ	RESUL	PHASE
10000000 51	74086582 53	20393253 53	20000000 51	97934087 53	20540195 53
30000000 51	23347463 54	25858032 53	40000000 51	42192490 53	10911761 53

ROT. SHAFT & PITCH LINK LOADS

FX	FY	FZ	MX	MY	MZ
94647574 52	-96737951 52	40115999 54	-78631087 54	18919943 54	-58080983 55
72907318 53	13700754 53	-82479900 51	37684520 53	16315686 55	-30054004 53
20835158 53	-70592994 53	67798949 52	20368924 55	78046081 54	-67716899 53
-10000020 53	-42281517 52	66400105 52	-89922942 53	14777135 53	-42010378 53
50685307 52	-13231501 53	-27362480 51	-60544639 52	-45963240 53	-88465889 53
10284080 52	-54990941 51	-17391180 52	-12236080 53	-96980239 52	-22885259 54
39968920 52	43294581 50	-84053846 52	-53136607 52	-18731708 53	-46226578 53
-98774859 52	71675563 52	33832394 52	20228765 52	25056883 53	39865501 53
70595559 52	11521190 53	-52862386 52	14043755 53	-56069463 53	-13818395 53

FX	RESUL	PHASE	FX	RESUL	PHASE
10000000 51	75825990 53	74051335 52	20000000 51	11211173 53	29687827 53
30000000 51	41270776 52	14429322 52	40000000 51	12140925 53	30555384 53
FY	RESUL	PHASE	FY	RESUL	PHASE
10000000 51	71910232 53	16901653 53	20000000 51	13890640 53	19772138 53
30000000 51	55161108 51	27450163 53	40000000 51	13568776 53	31886547 52
FZ	RESUL	PHASE	FZ	RESUL	PHASE
10000000 51	68298805 52	35306384 53	20000000 51	66456459 52	92359740 52
30000000 51	85834154 52	19168985 53	40000000 51	62761954 52	14738040 53

MX	RESUL	PHASE	MX	RESUL	PHASE
10000000 51	20372409 55	10599076 51	20000000 51	90126533 53	26614812 53
30000000 51	13340039 53	24652654 53	40000000 51	14188695 53	81965647 51
MY	RESUL	PHASE	MY	RESUL	PHASE
10000000 51	18086280 55	64435877 52	20000000 51	48280256 53	16217745 53
30000000 51	21093329 53	20737210 53	40000000 51	61413615 53	15592061 53
MZ	RESUL	PHASE	MZ	RESUL	PHASE
10000000 51	74086582 53	20393253 53	20000000 51	97934087 53	20540195 53
30000000 51	23347463 54	25858032 53	40000000 51	42192490 53	10911761 53

FIXED SYS. SHAFT & P.L. LOADS

FX	FY	FZ	MX	MY	MZ
71750155 53	17267956 53	40115999 54	-37138815 54	18342305 55	-58080983 55
11080498 53	-92536056 52	-82479900 51	-80829072 54	19356077 54	-30054004 53
10093985 53	78490169 52	67798949 52	-18483809 54	-76433102 54	-67716899 53
16497187 52	-18437107 52	66400105 52	41232048 54	-21016774 54	-42010378 53
52906933 52	66460530 51	-27362480 51	19515606 54	40582486 54	-88465889 53
-22315099 53	24652148 52	-17391180 52	-38896920 53	29966119 53	-22885259 54
11761897 53	-91642300 51	-84053846 52	91345190 52	-96989260 53	-46226578 53

FX	RESUL	PHASE	FX	RESUL	PHASE
10000000 51	14988861 53	47667465 52	20000000 51	55419318 52	17318274 52
30000000 51	25225103 53	29779293 53			
FY	RESUL	PHASE			
10000000 51	12134095 53	31030500 53	20000000 51	19598391 52	28982279 53
30000000 51	26300409 52	11039220 53			
FZ	RESUL	PHASE			
10000000 51	68298805 52	35306384 53	20000000 51	66456459 52	92359740 52
30000000 51	85834154 52	19168985 53			
MX	RESUL	PHASE			
10000000 51	82915560 54	25711921 53	20000000 51	45617329 54	64671259 52
30000000 51	39955098 53	28321582 53			
MY	RESUL	PHASE			
10000000 51	78845905 54	16578906 53	20000000 51	45701674 54	33262136 53
30000000 51	10151298 54	16283077 53			
MZ	RESUL	PHASE			
10000000 51	74086582 53	20393253 53	20000000 51	97934087 53	20540195 53
30000000 51	23347463 54	25858032 53			

ROTATING SYSTEM ACCELERATIONS

X	Y	GAMMA
26743874 52	-16847615 52	-50134259 50
-10326795 52	-24845060 52	27187051 50
-15469249 52	10890180 51	-48024407 50
-79635530 50	-19549359 52	77491051 49
-53064916 51	66642600 49	-64097826 50
21950500 50	-27266670 50	-87169488 50
-33656493 52	78068020 51	14222733 50
66172650 50	38838256 52	12991672 51

X	RESUL	PHASE	X	RESUL	PHASE
10000000 51	28668405 52	11111341 53	20000000 51	15489733 52	26705302 53
30000000 51	53110296 51	27236871 53	40000000 51	33662998 52	27112636 53
Y	RESUL	PHASE	Y	RESUL	PHASE
10000000 51	30018646 52	21414148 53	20000000 51	19579668 52	17681157 53
30000000 51	28069265 50	16626557 53	40000000 51	39615102 52	11365458 52
GAMMA	RESUL	PHASE	GAMMA	RESUL	PHASE
10000000 51	57031391 50	29847031 53	20000000 51	48645578 50	27916611 53
30000000 51	10819912 51	21632794 53	40000000 51	13069292 51	62476201 51

HUB FIXED SYS. ACCELERATIONS

X	Y	Z	ALPHA	BETA	GAMMA
25794667 52	-13587205 52		68970584 50	13093638 51	
20400550 51	14633135 50	-41495285 51	-10890076 50	27905550 50	-50134259 50
14633135 50	-20400550 51	32132624 51	13287080 50	17755904 49	27187051 50
-15675055 51	-31173362 51	61481457 51	29319873 50	-19685790 50	-48024407 50
34034838 51	34663195 51	-18244863 51	-31259515 50	30635055 50	77491051 49
-53756679 52	51769510 51	-21424083 52	-12055255 51	-32384042 51	-64097826 50
32915777 51	18738071 52	-62883524 51	-29346974 51	22516778 51	-87169488 50

X	RESUL	PHASE	X	RESUL	PHASE
10000000 51	20452964 51	85897249 52	20000000 51	37471024 51	33527113 53
30000000 51	53857358 52	27350391 53			
Y	RESUL	PHASE	Y	RESUL	PHASE
10000000 51	20452964 51	17589725 53	20000000 51	46618833 51	31803427 53
30000000 51	19440064 52	15444403 52			
Z	RESUL	PHASE	Z	RESUL	PHASE
10000000 51	52482037 51	30775306 53	20000000 51	64131464 51	10652846 53
30000000 51	22327891 52	25364209 53			
ALPHA	RESUL	PHASE	ALPHA	RESUL	PHASE
10000000 51	17179646 50	32066199 53	20000000 51	42858047 50	136833888 53
30000000 51	31726552 51	20233205 53			
BETA	RESUL	PHASE	BETA	RESUL	PHASE
10000000 51	27961982 50	86359259 52	20000000 51	36414790 50	32727559 53
30000000 51	39442762 51	30481107 53			
GAMMA	RESUL	PHASE	GAMMA	RESUL	PHASE
10000000 51	57031391 50	29847031 53	20000000 51	48645578 50	27916611 53
30000000 51	10819912 51	21632794 53			

FIXED SYSTEM AERODYNAMIC LOADS

FX	FY	FZ	MX	MY	MZ
75970130 53	15045089 53	40115999 54	-37138815 54	18342305 55	-58080983 55
11740129 53	-92062908 52	-12648616 52	-80301023 54	18002965 54	19809530 53
10141300 53	71893855 52	67198174 52	-19128086 54	-76519199 54	-94757140 53
15008621 52	-21397454 52	73723309 52	40383677 54	-20447166 54	-53227434 53
56139017 52	99378086 51	-31544165 51	20420100 54	39696061 54	-86655931 53
-29713631 53	31777186 52	-27353231 52	-77401130 52	11366268 54	-25948430 54
12214917 53	16624977 52	-96641760 52	84981773 53	-15518387 54	-87884005 53

FX	RESUL	PHASE	FX	RESUL	PHASE
10000000 51	15513755 53	49179048 52	20000000 51	58110652 52	14967826 52
30000000 51	32126377 53	29234698 53			
FY	RESUL	PHASE	FY	RESUL	PHASE
10000000 51	11680884 53	30798702 53	20000000 51	23592606 52	29491194 53
30000000 51	35863345 52	62382637 52			
FZ	RESUL	PHASE	FZ	RESUL	PHASE
10000000 51	68378228 52	34934002 53	20000000 51	73790762 52	92450040 52
30000000 51	10043818 53	19580350 53			
MX	RESUL	PHASE	MX	RESUL	PHASE
10000000 51	82547792 54	25660156 53	20000000 51	45252866 54	63176453 52
30000000 51	85333528 53	35479588 53			
MY	RESUL	PHASE	MY	RESUL	PHASE
10000000 51	78608489 54	16676058 53	20000000 51	44652703 54	33274732 53
30000000 51	19235706 54	14377951 53			
MZ	RESUL	PHASE	MZ	RESUL	PHASE
10000000 51	96805646 53	16819204 53	20000000 51	10169764 54	21155986 53
30000000 51	27396295 54	25128942 53			

Figure 7 Computer Output Sample

SECTION III

FLIGHT PROGRAM

A. Description of the Aircraft

The flight test program was conducted using an H-21 helicopter S/N 55-4141 (Vertol Designation C-96) as the test vehicle. As described in the previous section, the aircraft was extensively instrumented for the test flights and the configurations were as shown below for each phase of the program. Since the normal gross weight flight with wood blades from Reference 4 is used herein for comparison, this configuration is included as part of the flight program.

In-flight Shaft Loads with Wood and Metal Blades

Basic Configuration	Takeoff gross weight of 13,500 lbs including 1,800 lbs of fuel.
Flight Number	
C96X121 (Flight from Reference 4)	Standard unweighted H-21 wood blades; horizontal center of gravity 19 inches forward of center line between rotors.
C96X124	Standard turned root end unweighted metal blades aft, weighted (20 lbs cabled at 50% R) turned root end metal blade forward; horizontal center of gravity 20 inches forward of center line between rotors.

In-flight Shaft Loads with Variations of Differential Longitudinal Cyclic Trim

Basic Configuration:	Takeoff gross weight of 13,500 lbs including 1,800 lbs of fuel; standard turned root end unweighted metal blades aft, weighted (20 lbs cabled at 50% R) turned rotor end metal blades forward.
Flight Number	
C96X125	Horizontal center of gravity 20 inches forward of center line between rotors; forward longitudinal cyclic locked at 2.22° forward with aft cyclic trim varying between 5.45° forward and 3.19° aft.
C96X128	Horizontal center of gravity 19 inches forward of center line between rotors; forward longitudinal cyclic locked at 4.98° forward with aft cyclic trim varying between 5.45° forward and 3.19° aft.
C96X129	Horizontal center of gravity 19 inches forward of center line between rotors; forward longitudinal cyclic locked at 3.19° aft with aft cyclic trim varying between 5.45° forward and 3.19° aft.

Performance with Variations of Differential Longitudinal Cyclic Trim

Basic Configuration: Takeoff gross weight of 13,500 lbs including 1,800 lbs fuel; standard turned root end unweighted metal blades aft, weighted (20 lbs at 50% R) turned root end metal blades forward.

Flight Number

C96X126 Horizontal center of gravity 19 inches forward of center line between rotors; forward longitudinal cyclic locked at 2.22° forward with aft cyclic trim varying between 5.45° forward and 3.19° aft.

C96X127 Horizontal center of gravity 19 inches forward of center line between rotors; forward longitudinal cyclic locked at 4.98° forward with aft cyclic trim varying between 5.45° forward and 3.19° aft.

C96X132 Horizontal center of gravity 19 inches forward of center line between rotors; forward longitudinal cyclic locked at 3.19° aft with aft cyclic trim varying between 5.45° forward and 3.19° aft.

B. Flight Conditions

Data was recorded and analyzed for the flight conditions as shown below:

In-flight Shaft Loads with Wood and Metal Blades

C96X121

Indicated Air Speed Knots	Rotor rpm	Maneuver
0	258	Hover in Ground Effect
20	258	Level Flight at Pressure Altitude of 2500 feet
40	240	Level Flight at Pressure Altitude of 2500 feet
40	250	Level Flight at Pressure Altitude of 2500 feet
40	258	Level Flight at Pressure Altitude of 2500 feet
40	268	Level Flight at Pressure Altitude of 2500 feet
40	278	Level Flight at Pressure Altitude of 2500 feet
60	258	Level Flight at Pressure Altitude of 2500 feet
80	258	Level Flight at Pressure Altitude of 2500 feet
90	240	Level Flight at Pressure Altitude of 2500 feet
90	250	Level Flight at Pressure Altitude of 2500 feet
90	258	Level Flight at Pressure Altitude of 2500 feet
90	268	Level Flight at Pressure Altitude of 2500 feet
90	278	Level Flight at Pressure Altitude of 2500 feet
105	258	Level Flight at Pressure Altitude of 2500 feet

C96X124

Indicated Air Speed Knots	Rotor rpm	Maneuver
0	258	Hover in Ground Effect
20	258	Level Flight at Pressure Altitude of 2000 feet
40	240	Level Flight at Pressure Altitude of 2000 feet
40	250	Level Flight at Pressure Altitude of 2000 feet
40	258	Level Flight at Pressure Altitude of 2000 feet
40	268	Level Flight at Pressure Altitude of 2000 feet
40	278	Level Flight at Pressure Altitude of 2000 feet
60	258	Level Flight at Pressure Altitude of 2000 feet
80	258	Level Flight at Pressure Altitude of 2000 feet
85	240	Level Flight at Pressure Altitude of 2000 feet
90	250	Level Flight at Pressure Altitude of 2000 feet
90	258	Level Flight at Pressure Altitude of 2000 feet
90	268	Level Flight at Pressure Altitude of 2000 feet
90	278	Level Flight at Pressure Altitude of 2000 feet
110	258	Level Flight at Pressure Altitude of 2000 feet

In-flight Shaft Loads with Variations of Differential Longitudinal Cyclic Trim

C96X125

Indicated Air Speed Knots	Rotor rpm	Forward Long. Cyclic	Aft Long. Cyclic	Maneuver
20	258	2.22°F	3.19°A	Level Flight at Pressure
20	258	2.22°F	1.0°A	Altitude of 2000 feet
20	258	2.22°F	2.0°F	
40	258	2.22°F	3.19°A	
40	258	2.22°F	1.0°A	
40	258	2.22°F	2.0°F	
40	258	2.22°F	4.0°F	
40	258	2.22°F	5.45°F	
60	258	2.22°F	3.19°A	
60	258	2.22°F	1.0°A	
60	258	2.22°F	2.0°F	
60	258	2.22°F	4.0°F	
60	258	2.22°F	5.45°F	
80	258	2.22°F	3.19°A	
80	258	2.22°F	1.0°A	
80	258	2.22°F	2.0°F	
80	258	2.22°F	4.0°F	
80	258	2.22°F	5.45°F	
100	258	2.22°F	1.0°A	
100	258	2.22°F	2.0°F	
100	258	2.22°F	4.0°F	Level Flight at Pressure
100	258	2.22°F	5.45°F	Altitude of 2000 feet

C96X128

Indicated Air Speed Knots	Rotor rpm	Forward Long. Cyclic	Aft Long. Cyclic	Maneuver
20	258	4.98°F	3.19°A	Level Flight at Pressure
20	258	4.98°F	1.0°A	Altitude of 1600 feet
20	258	4.98°F	2.0°F	
40	258	4.98°F	3.19°A	
40	258	4.98°F	1.0°A	
40	258	4.98°F	2.0°F	
40	258	4.98°F	4.0°F	
40	258	4.98°F	5.45°F	
60	258	4.98°F	3.19°A	
60	258	4.98°F	1.0°A	
60	258	4.98°F	2.0°F	
60	258	4.98°F	4.0°F	
60	258	4.98°F	5.45°F	
80	258	4.98°F	3.19°A	
80	258	4.98°F	1.0°A	
80	258	4.98°F	2.0°F	
80	258	4.98°F	4.0°F	
80	258	4.98°F	5.45°F	
100	258	4.98°F	4.00°F	Level Flight at Pressure
100	258	4.98°F	5.45°F	Altitude of 1600 feet

C96X129

Indicated Air Speed Knots	Rotor rpm	Forward Long. Cyclic	Aft Long. Cyclic	Maneuver
20	258	3.19°A	3.19°A	Level Flight at Pressure
40	258	3.19°A	3.19°A	Altitude of 1500 feet
40	258	3.19°A	1.00°A	
40	258	3.19°A	2.0°F	
40	258	3.19°A	4.0°F	
40	258	3.19°A	5.45°F	
60	258	3.19°A	3.19°A	
60	258	3.19°A	1.00°A	
60	258	3.19°A	2.0°F	
60	258	3.19°A	4.0°F	
60	258	3.19°A	5.45°F	
80	258	3.19°A	3.19°A	
80	258	3.19°A	1.0°A	
80	258	3.19°A	2.0°F	
80	258	3.19°A	4.0°F	
80	258	3.19°A	5.45°F	
100	258	3.19°A	3.19°A	
100	258	3.19°A	1.00°A	
100	258	3.19°A	2.0°F	
100	258	3.19°A	4.0°F	Level Flight at Pressure
100	258	3.19°A	5.45°F	Altitude of 1500 feet

Performance with Variations of Differential Longitudinal Cyclic Trim

C96X126

Indicated Air Speed Knots	Rotor rpm	Forward Long. Cyclic	Aft Long. Cyclic	Pressure Altitude Feet	Maneuver
60	258	2.22°F	3.19°A	2890	Level Flight
60	258	2.22°F	1.0°A	2700	Level Flight
60	258	2.22°F	+2.0°F	2380	Level Flight
60	258	2.22°F	+4.0°F	2190	Level Flight
60	258	2.22°F	+5.45°F	2360	Level Flight
80	258	2.22°F	3.19°A	3520	Level Flight
80	258	2.22°F	1.0°A	3360	Level Flight
80	258	2.22°F	+2.0°F	3300	Level Flight
80	258	2.22°F	+4.0°F	3300	Level Flight
80	258	2.22°F	+5.45°F	3060	Level Flight

C96X127

Indicated Air Speed Knots	Rotor rpm	Forward Long. Cyclic	Aft Long. Cyclic	Pressure Altitude Feet	Maneuver
60	258	4.98°F	3.19°A	6220	Level Flight
60	258	4.98°F	1.0°A	6000	Level Flight
60	258	4.98°F	2.0°F	5520	Level Flight
60	258	4.98°F	4.0°F	5720	Level Flight
60	258	4.98°F	5.45°F	4920	Level Flight
80	258	4.98°F	5.45°F	2900	Level Flight

C96X132

Indicated Air Speed Knots	Rotor rpm	Forward Long. Cyclic	Aft Long. Cyclic	Pressure Altitude Feet	Maneuver
60	258	3.19°A	3.19°A	1440	Level Flight
60	258	3.19°A	1.0°A	1280	Level Flight
60	258	3.19°A	2.0°A	1240	Level Flight
60	258	3.19°A	4.0°F	1120	Level Flight
60	258	3.19°A	5.45°F	1190	Level Flight
80	258	3.19°A	3.19°A	1440	Level Flight
80	258	3.19°A	1.0°A	1580	Level Flight
80	258	3.19°A	2.0°A	1660	Level Flight
80	258	3.19°A	4.0°F	1720	Level Flight
80	258	3.19°A	5.45°F	1800	Level Flight

SECTION IV

DISCUSSION OF RESULTS

The results of this program are presented in two major categories; (1) in-flight vibratory load and motion comparisons for wood and metal blades and (2) in-flight vibratory loads and motions under combinations of differential longitudinal cyclic trim (DLCT). Measured shaft loads in the fixed and rotating system are presented using the positions and sign conventions of the sketch below.

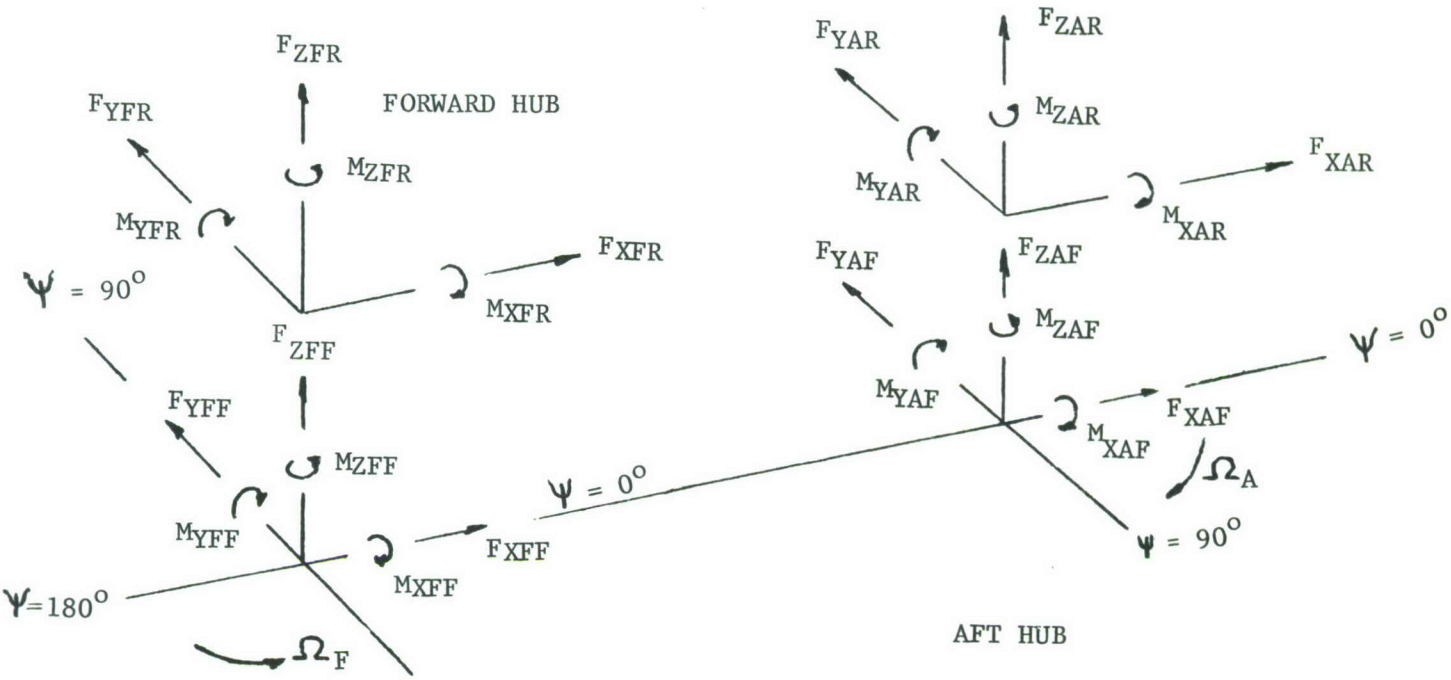

Load comparisons are made for the significant third harmonic since with a three bladed rotor this is usually the dominant portion of the vibration environment. Corresponding second and fourth harmonic loads are presented as necessary for an understanding of the results. Each load plot consists of six directional loads and moments as sine and cosine components and their resultants. Forces and moments at each rotor include: Longitudinal force F_x, Lateral force F_y, Vertical force F_z, Roll Moment M_x, Pitch Moment M_y, and Yaw Moment (Torque) M_z. The absolute time reference for the sine and cosine components is when the red blade is in the trail position.

Fixed system third harmonic loads are presented for wood and metal blades at a gross weight of 13,500 lb. Comparisons include; (1) an airspeed sweep at normal 258 rpm, (2) a rotor speed sweep at 40 knots and (3) a rotor speed sweep at 90 knots. Second and fourth harmonic inplane rotating forces are given to define the contribution of each to the fixed system third harmonic loads.

In-flight fixed system third harmonic loads are given for each DLCT configuration. Comparison curves present the forward and aft rotor loads at normal 258 rpm for a five increment airspeed sweep from 20 to 100 knots. Corresponding fuselage vibration levels are provided for all harmonics. Performance data for each condition consists of total horsepower and its distribution between rotors.

A. Comparison of Wood and Metal Blade Loads and Vibration Levels
Third Harmonic Fixed System Loads

Shaft Forces Figures 8 through 16 illustrate the third harmonic fixed system loads and the related second and fourth harmonic rotating loads for wood and metal blades.

	FIGURE NO.		
Harmonic	Airspeed Sweep	40 knot rpm Sweep	90 knot rpm Sweep
3Ω Fixed System	8	9	10
2Ω Rotating System	11	12	12
4Ω Rotating System	13	14	14

Loads for wood blades are shown on the left and metal blades on the right. The force scales are ± 2,000 lb for the sine and cosine components and + 2,000 lb for the resultants; moment scales are ± 10,000 in. lb for the components and + 20,000 in. lb for the resultants. The scatter of repeated data points are represented by the spread between two solid line plots for the forward rotor, and two dashed line plots for the aft rotor. Generally the measured loads show good repeatability, but in a few instances, there is greater than normal scatter spread between the two lines with differences of 300 lb of force and 5,000 in. lb of moment. The forward rotor, operating in an undisturbed flow field, shows less data scatter than the aft rotor. Resultants have less scatter than components, indicating that the scatter often reflects a phase shift rather than a magnitude change.

The airspeed sweeps show the 3Ω fixed system resultant magnitudes average,

	F_x lb Longitudinal		F_y lb Lateral		F_z lb Vertical	
ROTOR	Wood	Metal	Wood	Metal	Wood	Metal
Forward	800	400	250	100	200	150
Aft	1300	500	500	200	400	250

All metal blade rotor loads are smaller than wood blade loads. Metal blade resultants for the aft rotor are only slightly larger than forward rotor resultants, while with wood blades the aft rotor resultants are much larger than the forward rotor resultants. With either wood or metal blades, the forward rotor longitudinal resultants generally correspond with the pattern of measured vibration data for the H-21, low in hover, high at 20 knots transition, low near 80 knots cruise, and then a continuing increase with forward speed. Lateral resultants are much smaller than the longitudinals and display little trend with airspeed, particularly with metal blades. Vertical wood blade resultants are small for the forward rotor but increase with airspeed; the aft rotor resultant peaks at 60 knots and then drops with increasing airspeed. Metal blade vertical loads are less sensitive to airspeed, except for the aft rotor increase at 100 knots.

G.W. 13,500 lb
C.G. 19 in. fwd

Flt. H21C-96 X121
3rd Harmonic

Fwd Rotor ——
Aft Rotor - - -

Wood Blades

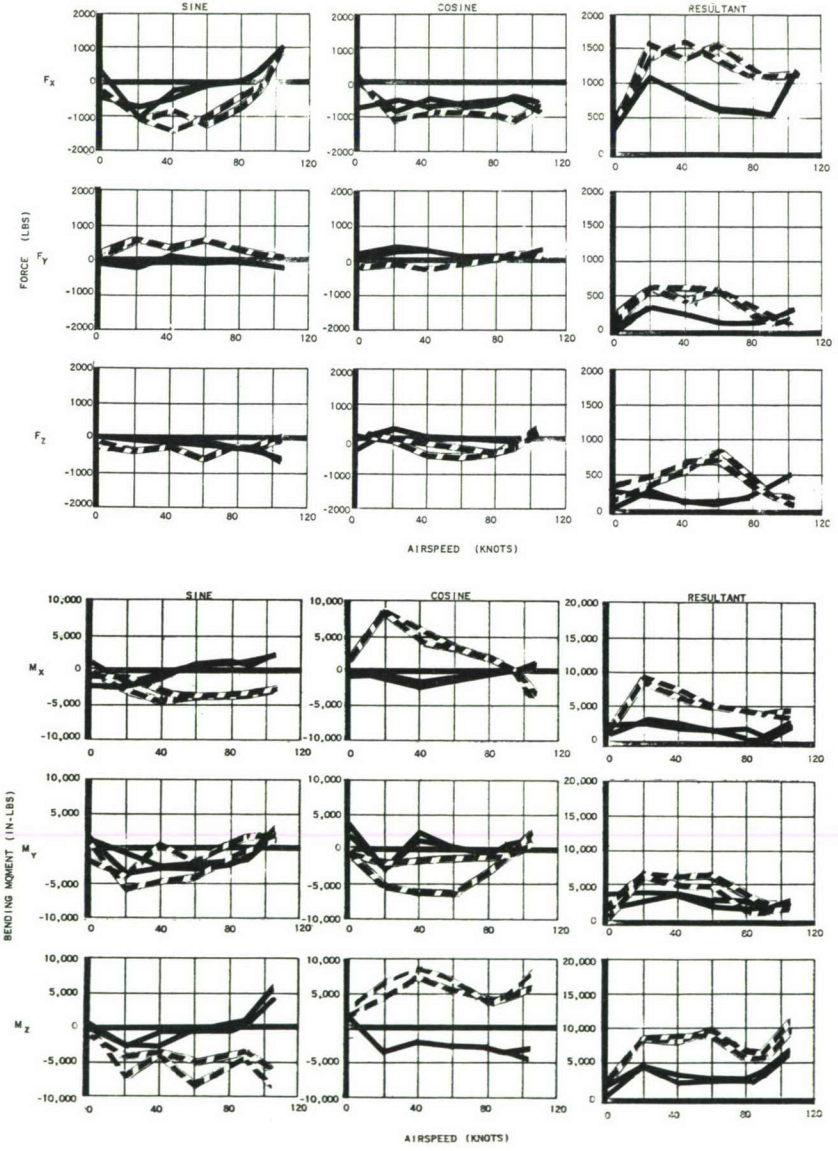

G.W. 13,500 lb.
C.G. 20 in. fwd

Flt. H21C-96 X124
3rd Harmonic

Fwd Rotor ——
Aft Rotor - - -

Metal Blades

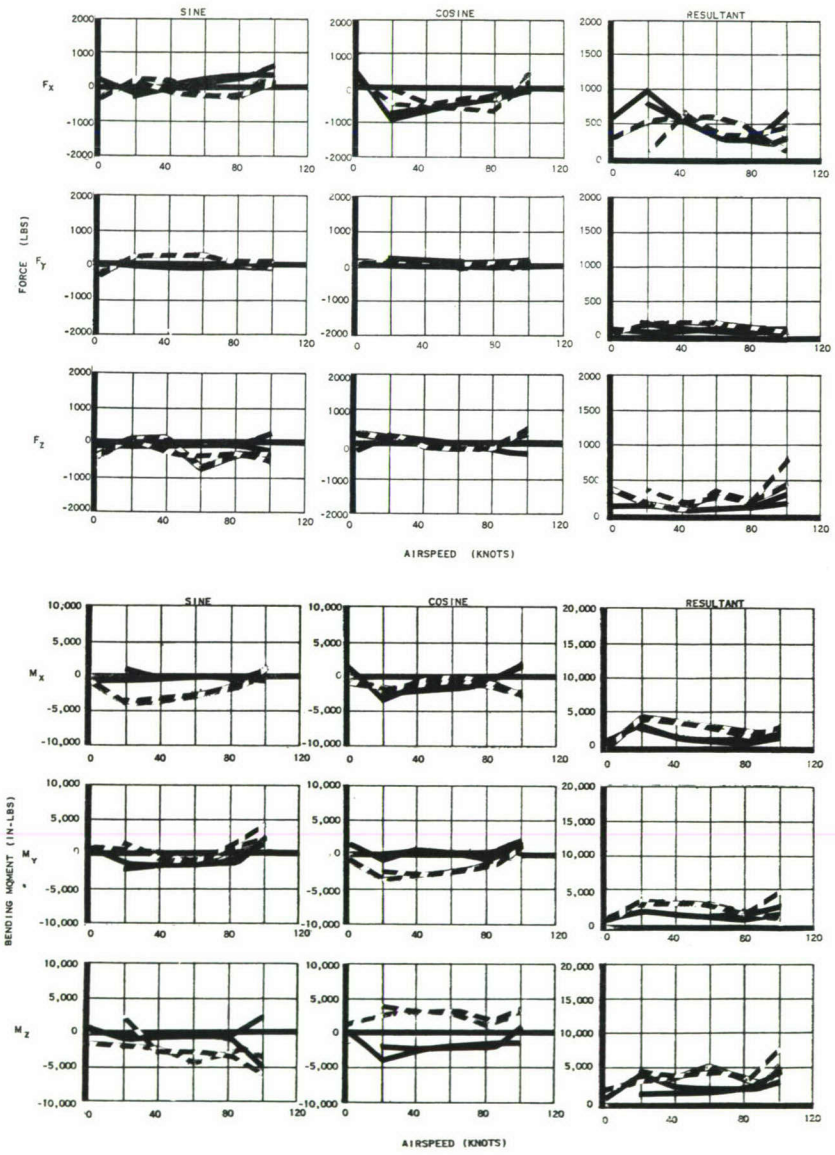

Figure 8 Fixed System Third Harmonic Loads
Airspeed Sweep at 258 RPM

RPM speeps, Figures 9 and 10, show longitudinal resultants increasing with rotor speed, with metal blade maximums much lower than with wood blades. Sine component trends appear similar, increasing with rpm, but the extremely sharp increase with rotor speed is reduced with metal blades. Maximums for 3Ω fixed system loads are,

			40 KNOT SWEEP			
	F_x lb		F_y lb		F_z lb	
ROTOR	Wood	Metal	Wood	Metal	Wood	Metal
Forward	1200	1000	300	150	200	150
Aft	2800	2000	700	500	1100	500
			90 KNOT SWEEP			
Forward	1000	300	250	150	400	250
Aft	2200	800	500	150	700	600

In the 40 knot sweep comparisons, aft rotor lateral resultants increase with rotor speed; forward rotor resultants remain constant with rpm. Further, the significant aft rotor vertical resultant increases with rpm at 40 and 90 knots only for wood blades.

Third harmonic vertical loads arise from direct addition of third harmonic blade root vertical shears. Third harmonic in-plane loads come from second and fourth harmonic blade root horizontal shears. The blade root loads combine in the rotating system to form the shaft loads which were measured by the strain gages. These rotating F_x and F_y loads are then combined as follows to form third harmonic fixed system loads.

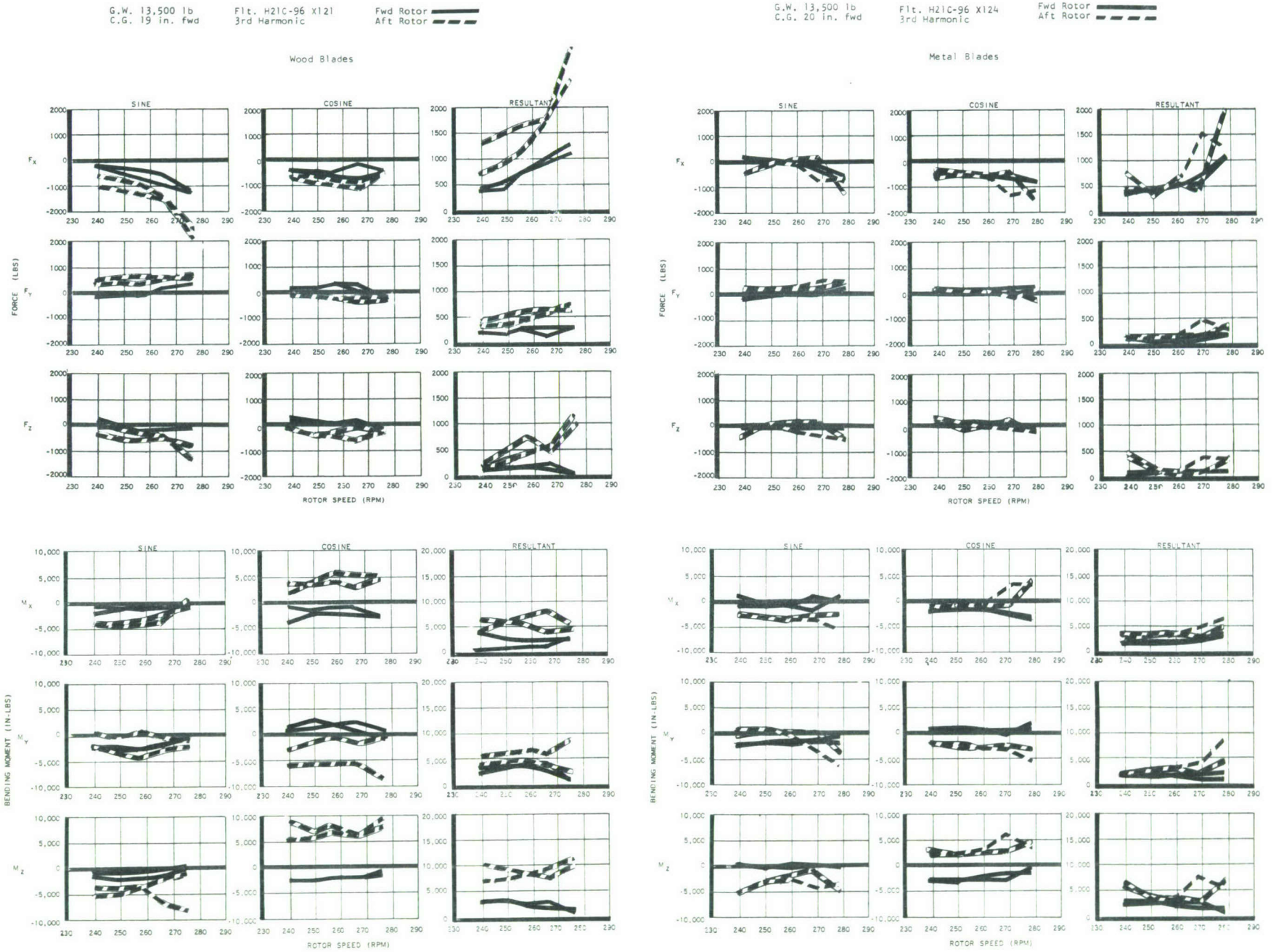

Figure 9 Fixed System Third Harmonic Loads
RPM Sweep at 40 Knots

G.W. 13,500 lb
C.G. 19 in. fwd

Flt. H21C-96 X121
3rd Harmonic

Fwd Rotor ——
Aft Rotor - - -

Wood Blades

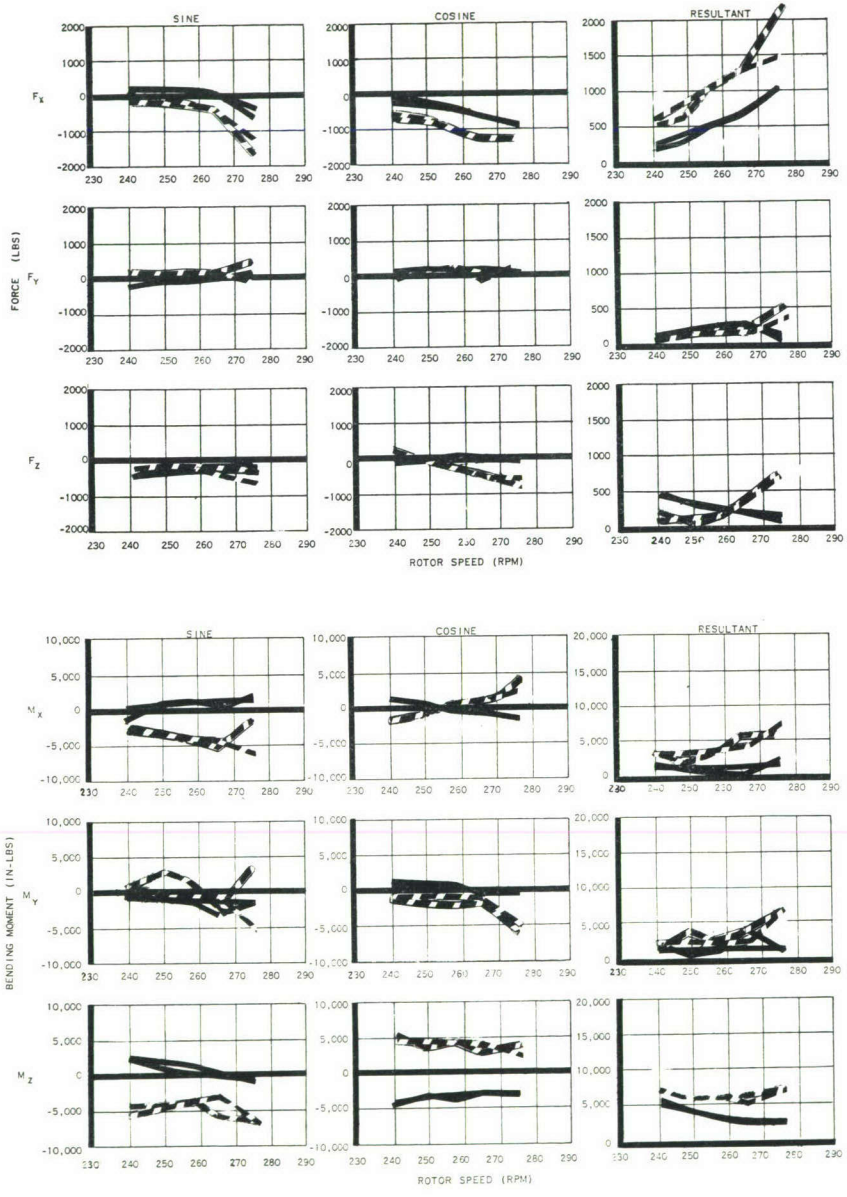

G.W. 13,500 lb.
C.G. 20 in. fwd

Flt. H21C-96 X124
3rd Harmonic

Fwd Rotor ——
Aft Rotor - - -

Metal Blades

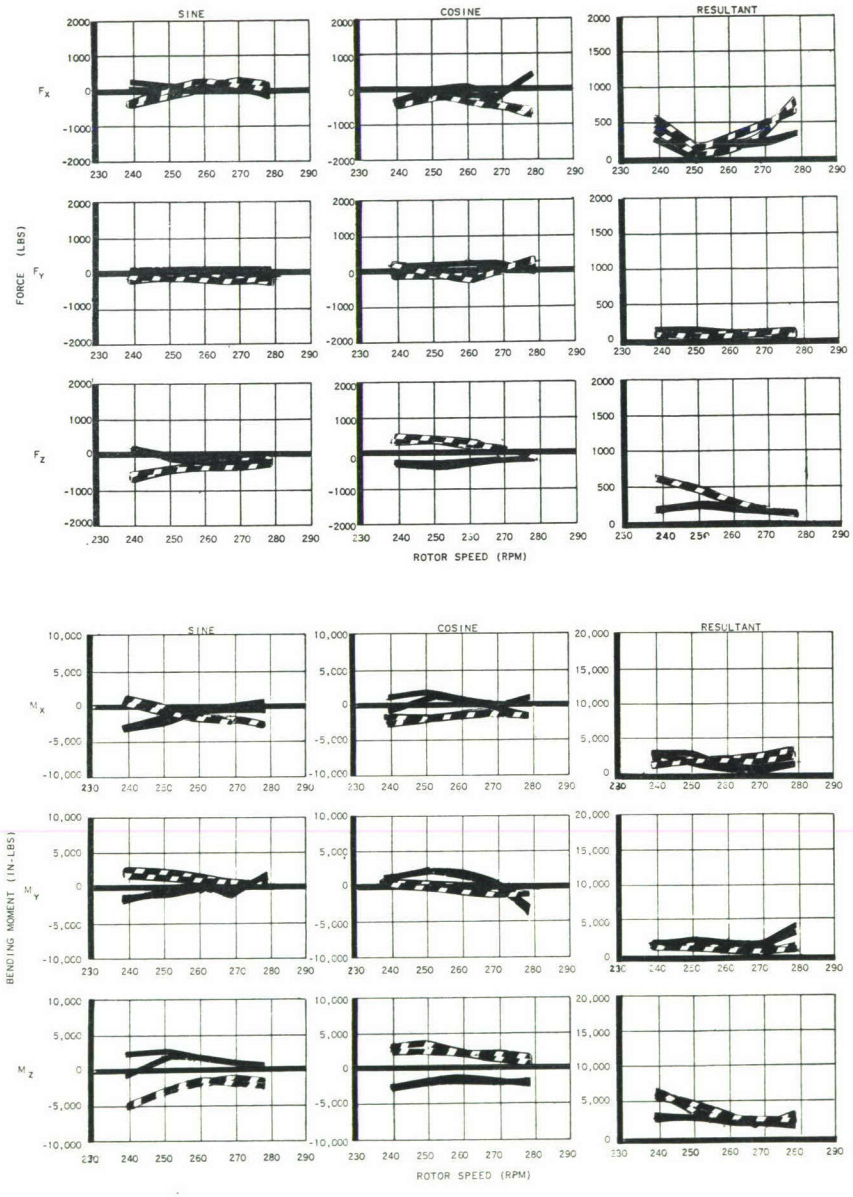

Figure 10 Fixed System Third Harmonic Loads
RPM Sweep at 90 Knots

$$F_{x3} = 1/2\ (F_{x2c} + F_{y2s} + F_{y4s}) \cos 3\Omega t$$
$$+ 1/2\ (-F_{y2c} + F_{x2s} + F_{y4c} + F_{x4s}) \sin 3\Omega t$$

$$F_{y3} = 1/2\ (F_{y2c} - F_{x2s} + F_{y4c} + F_{x4s}) \cos 3\Omega t$$
$$+ 1/2\ (F_{x2c} + F_{y2s} - F_{x4c} + F_{y4s}) \sin 3\Omega t$$

where

F_{x3}, F_{y3} = third harmonic fixed system longitudinal and lateral loads.

F_{x2s}, F_{x2c}, F_{x4s}, F_{x4c} = second and fourth harmonic rotating sine and cosine in-plane loads acting in the direction of the red blade trail position.

F_{y2s}, F_{y2c}, F_{y4s}, F_{y4c} = second and fourth harmonic rotating sine and cosine in-plane loads acting 90^{o} from the direction of the red blade trail position.

Second and fourth harmonic rotating shaft forces are presented in Figures 11 through 14. At each load, similarities exist among the rotating system harmonic components, for both the wood and metal blades. In the second harmonic, the F_x sine curve for the forward rotor loads closely resembles the negative of the F_y cosine curve and the F_y sine curve is similar to the F_x cosine curve. Similar trends are evident at the aft rotor. However, the pattern differs in sign relation because of the opposite direction of shaft rotation. Fourth harmonic in-plane load curves follow another fixed pattern. The load patterns of the curves for all harmonics are shown below.

Second Harmonic		Fourth Harmonic	
Forward	Aft	Forward	Aft
$F_x(\sin) = -F_y(\cos)$	$F_x(\sin) = F_y(\cos)$	$F_x(\sin) = F_y(\cos)$	$F_y(\sin) = -F_y(\cos)$
$F_x(\cos) = F_y(\sin)$	$F_x(\cos) = -F_y(\sin)$	$F_x(\cos) = -F_y(\sin)$	$F_x(\cos) = F_y(\sin)$

Adding the components vectorially with the above identities gives similar in-plane resultants for each harmonic in mutually perpendicular directions.

Figures 11 and 12 present the rotating second harmonic forces. Second harmonic airspeed plots for both wood and metal blades show a tendency toward the low hover, high transition, and low cruise force characteristic at the forward rotor but not at the aft rotor. The most significant differences between wood and metal blades occur at the aft rotor as reflected by the following peaks. Note that "in-plane Force" represents the rotating resultant, either F_x or F_y since they are the same.

	In-plane Force, lb	
ROTOR	Wood	Metal
Forward	750	500
Aft	900	400

In-plane resultants during the 40 knot rpm sweep increase with rotor speed for both wood and metal blades. Resultant forward rotor forces show little change between wood and metal blades, but the aft rotor in-plane resultants indicate significant reduction from the metal blade values. In the 90 knot sweep, the wood blade in-plane resultants exhibit a significant increase with rotor speed, but the metal blades do not show this rpm trend. Rotating second harmonic load reductions with metal blades are typified by the amplitude peaks from the rpm curves which show,

	In-plane Force, lb			
	40 Knot Sweep		90 Knot Sweep	
ROTOR	Wood	Metal	Wood	Metal
Forward	600	500	500	200
Aft	1650	1000	1000	300

Rotating fourth harmonic force comparisons are presented in Figures 13 and 14. The airspeed sweep shows that in-plane resultant shaft forces average,

	In-plane Force, lb	
ROTOR	Wood	Metal
Forward	400	300
Aft	600	200

The rotating fourth harmonic resultants for metal blades are significantly less than the corresponding wood blade resultants. Both the airspeed sweep at 258 rpm and the rpm sweeps at 40 and 90 knots display this trend. Again, as in the second harmonic rotating forces, the aft rotor showed the greater force reduction. The metal blades show no significant force increase during the rpm sweep at 90 knots as did the wood blades.

G.W. 13,500 lb
C.G. 19 in. fwd

Flt. H21C-96 X121
2nd Harmonic

Fwd Rotor
Aft Rotor

Wood Blades

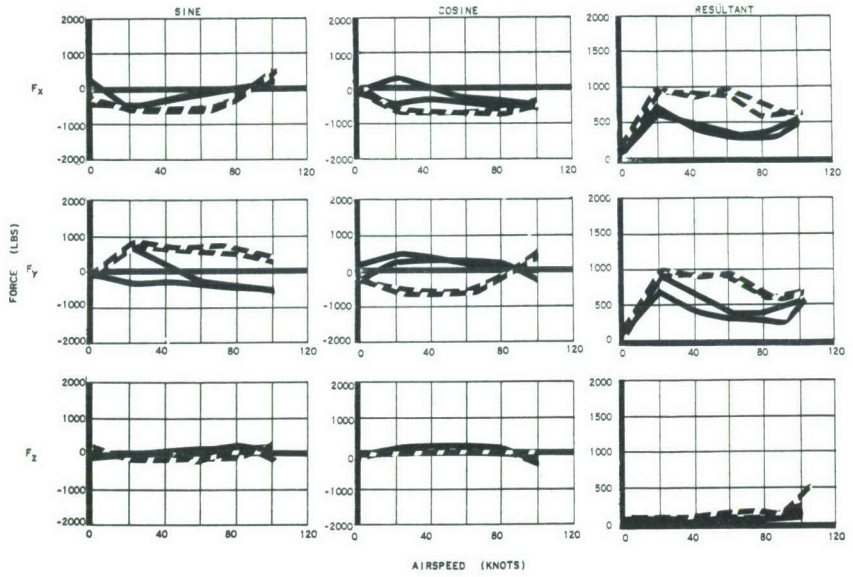

G.W. 13,500 lb.
C.G. 20 in. fwd

Flt. H21C-96 X124
2nd Harmonic

Fwd Rotor
Aft Rotor

Metal Blades

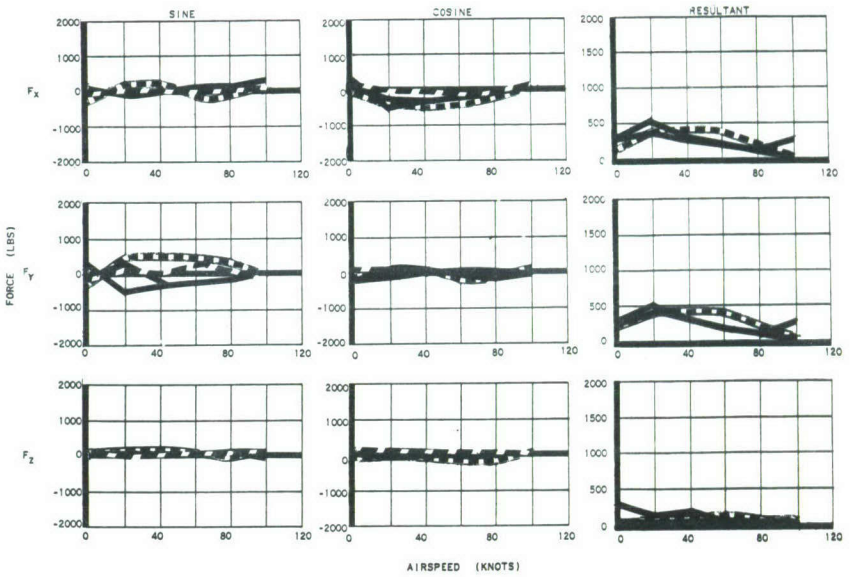

Figure 11 Rotating System Second Harmonic Loads
Airspeed Sweep at 258 RPM

G.W. 13,500 lb
C.G. 19 in. fwd

Flt. H21C-96 X121
2nd Harmonic

Fwd Rotor ——
Aft Rotor – – –

Wood Blades

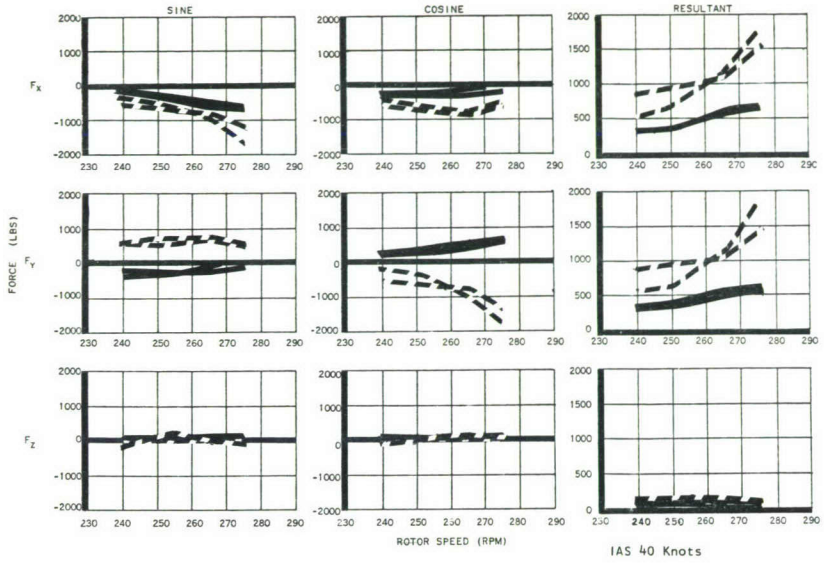

IAS 40 Knots

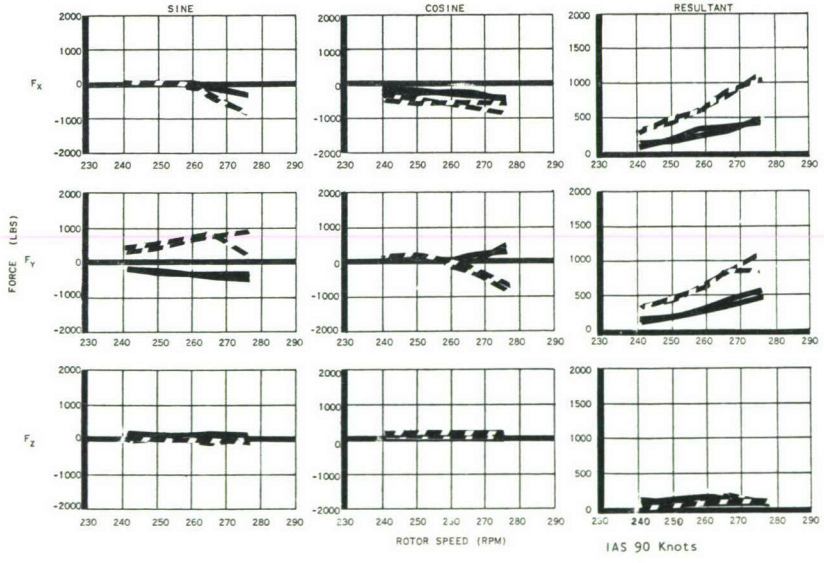

IAS 90 Knots

G.W. 13,500 lb
C.G. 20 in. fwd

Flt. H21C-96 X124
2nd Harmonic

Fwd Rotor ——
Aft Rotor – – –

Metal Blades

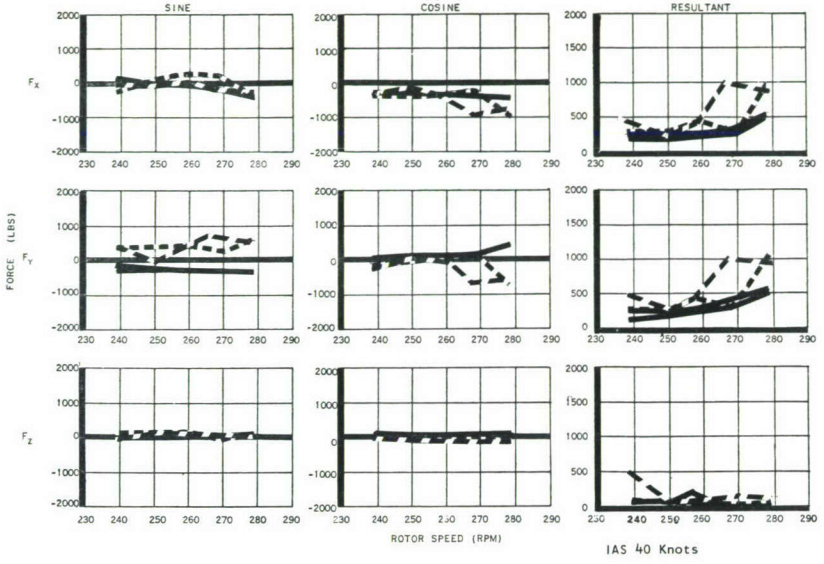

IAS 40 Knots

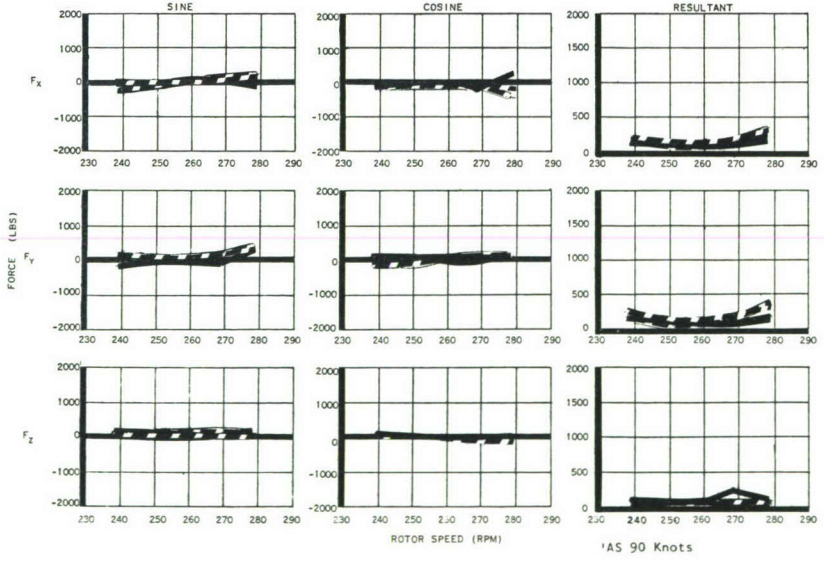

IAS 90 Knots

Figure 12 Rotating System Second Harmonic Loads
RPM Sweeps at 40 Knots and 90 Knots

G.W. 13,500 lb.
C.G. 19 in. fwd

Flt. H21C-96 X121
4th Harmonic

Fwd Rotor
Aft Rotor

Wood Blades

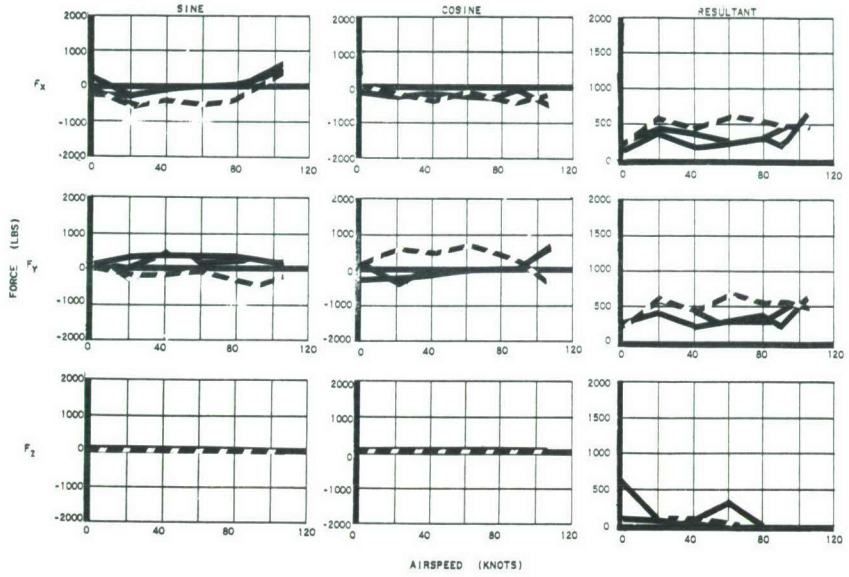

G.W. 13,500 lb
C.G. 20 in. fwd

Flt. H21C-96 X124
4th Harmonic

Fwd Rotor
Aft Rotor

Metal Blades

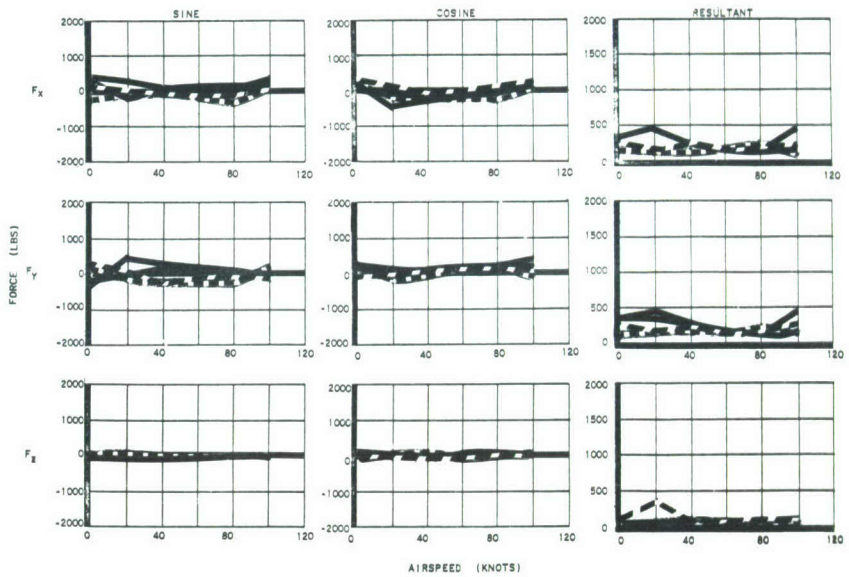

Figure 13 Rotating System Fourth Harmonic Loads
Airspeed Sweep at 258 RPM

G.W. 13,500 lb
C.G. 19 in. fwd

Flt. H21C-96 X121
4th Harmonic

Fwd Rotor ——
Aft Rotor - - -

Wood Blades

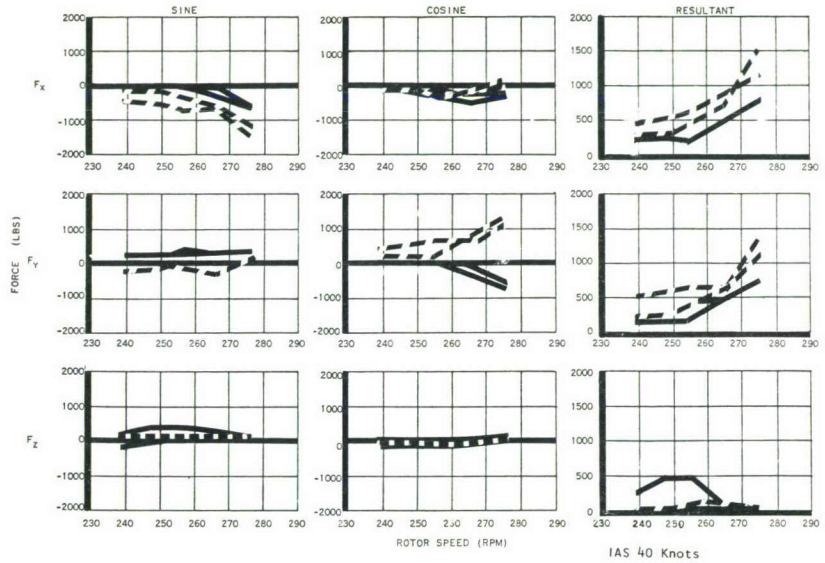

IAS 40 Knots

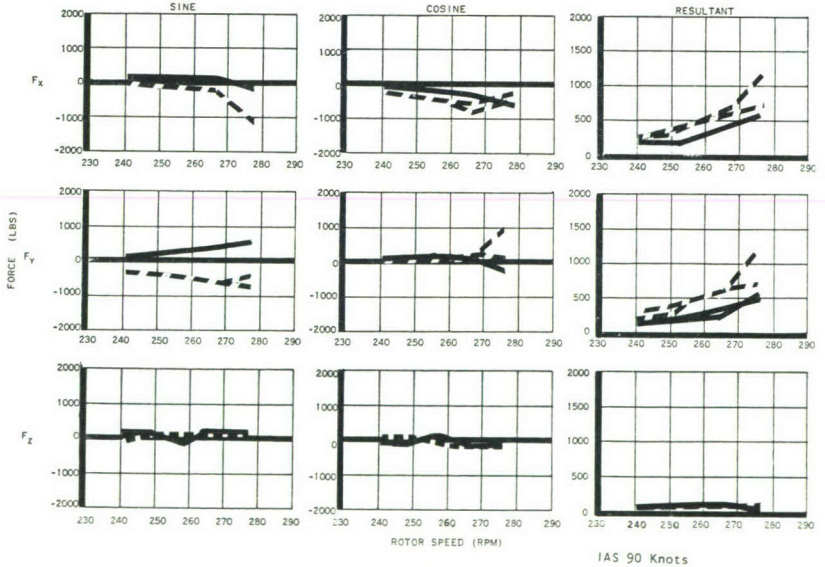

IAS 90 Knots

G.W. 13,500 lb.
C.G. 20 in. fwd

Flt. H21C-96 X124
4th Harmonic

Fwd Rotor ——
Aft Rotor - - -

Metal Blades

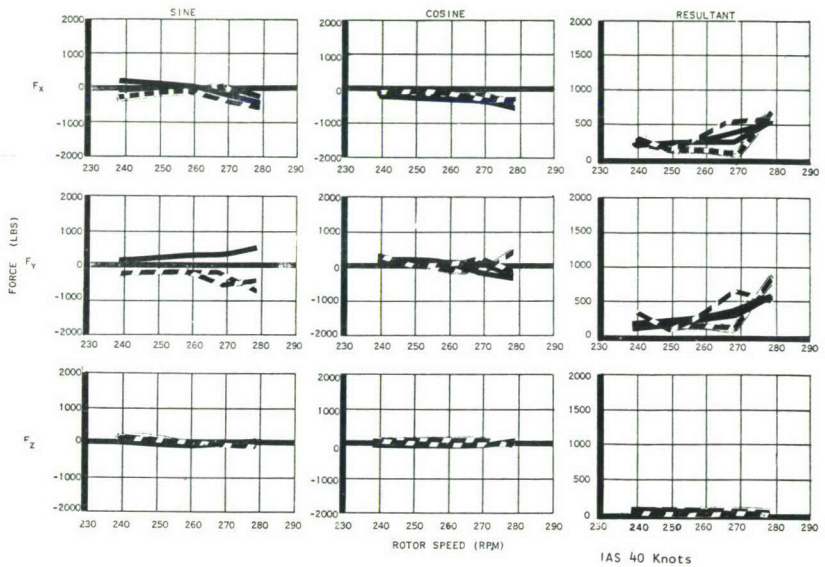

IAS 40 Knots

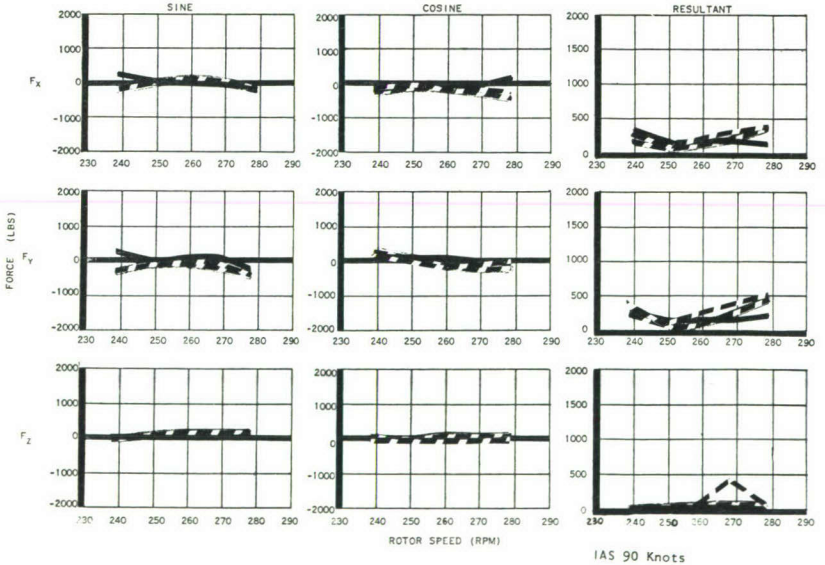

IAS 90 Knots

Figure 14 Rotating System Fourth Harmonic Loads
RPM Sweeps at 40 Knots and 90 Knots

Shaft Moments - Comparisons of the third harmonic fixed system moments are shown in Figures 8, 9 and 10. These in-plane moments originate from the second and fourth harmonics rotating system rolling and pitching moments which in turn result from vertical shears at the blade roots in the corresponding harmonics. In detail, the third harmonic comparison for wood and metal blades are presented as,

	Figure No.
Airspeed Sweep at 258 rpm	8
rpm Sweep at 40 knots	9
rpm Sweep at 90 knots	10

Airspeed trends for both wood and metal blades are similar, but the metal blade resultants are generally smaller. Showing the largest change, the aft rotor resultants with metal blades are usually half the comparable wood blade values; the forward rotor moments decrease slightly. Resultant maximums during the airspeed sweep are,

	Rolling Moment M_x, in. lb		Pitching Moment M_y, in. lb		Yawing Moment M_z, in. lb	
ROTOR	Wood	Metal	Wood	Metal	Wood	Metal
Forward	2500	2500	3500	2000	6,000	4500
Aft	8500	4000	6500	4000	10,000	7500

Aft rotor pitching and yawing metal blade resultants have a tendency to decrease with rotor speed at 40 knots whereas the wood blade curves show no variation. This trend reverses at 90 knots with wood blade resultants increasing with rotor speed. In general, the rpm sweeps show large moment reductions at the aft rotor with metal blades, and resultant maximums below those of the airspeed sweep.

Blade Frequency Correlation - As illustrated in Figures 8 through 14, metal and wood blade load comparisons show that metal blade shaft loads are smaller than similar wood blade loads. In order to study the effect of blades on the shaft loads, Figure 15 presents the blade natural frequency spectra for both wood and metal blades. Rotor speed is plotted along the abscissa with the ordinate axis as natural frequency. For example, projecting a vertical line upward from 260 rpm to its first wood blade intersection shows the first flap bending mode to be 10.5 cps. Diagonal straight lines are shown for the integer rotor orders. Note that in these flights the aircraft was equipped with either unweighted wood blades forward and aft, or with metal weighted blades forward and metal unweighted blades aft.

For a three bladed rotor, it is generally considered that the blade first flap bending natural frequency should be located as far as possible from 3Ω so as to minimize magnification of the 3Ω root shears which directly result in 3Ω vertical shaft loads. Of the three blades flown in the program, the unweighted aft rotor metal blade is closest to 3Ω, the wood blade used on both rotors is farther away, and the weighted forward rotor metal blade is farthest away. At the forward rotor the 20 lb weighted metal blade vertical loads are smaller than the wood blade loads and therefore correlate with the calculated natural frequency relations. At the aft rotor there is disagreement because the unweighted metal blade vertical loads are again smaller than the wood blade loads, but the metal blade natural frequency is closer to 3Ω. However, all of the natural frequencies are less than 2.5Ω, and it has been shown analytically that the question of resonance is important when the blades are quite close to 3Ω, but below about 2.5Ω other characteristics such as coupled blade-fuselage natural frequencies can be more important.

A similar relation between natural frequency and load is generally considered to exist for the in-plane fourth harmonic rotating loads which contribute to third harmonic longitudinal and lateral fixed system loads. It is considered desirable here that the first lag bending natural frequency be as far as possible from 4Ω resonance. Figure 15 shows that wood blade first lag bending lies between 4 and 5Ω, while the lag bending frequencies for both the metal blades are remote from 4Ω, being actually above 5Ω. This does show some correlation with 4Ω rotating loads in Figure 14 where wood blade loads are higher than metal blade loads. Note also that the wood blade natural frequency moves closer to 4Ω with increasing rotor rpm in Figure 15 and that correspondingly, 4Ω wood blade rotating loads increase markedly with rotor rpm in Figure 14.

The second flap bending natural frequency of the wood blade is about 10% lower than the metal blades and closer to 4Ω excitation. However, since this mode is not located in the chordwise direction, the frequency location is not directly related to the rotating fourth harmonic loads.

Leone-Myklestad Method

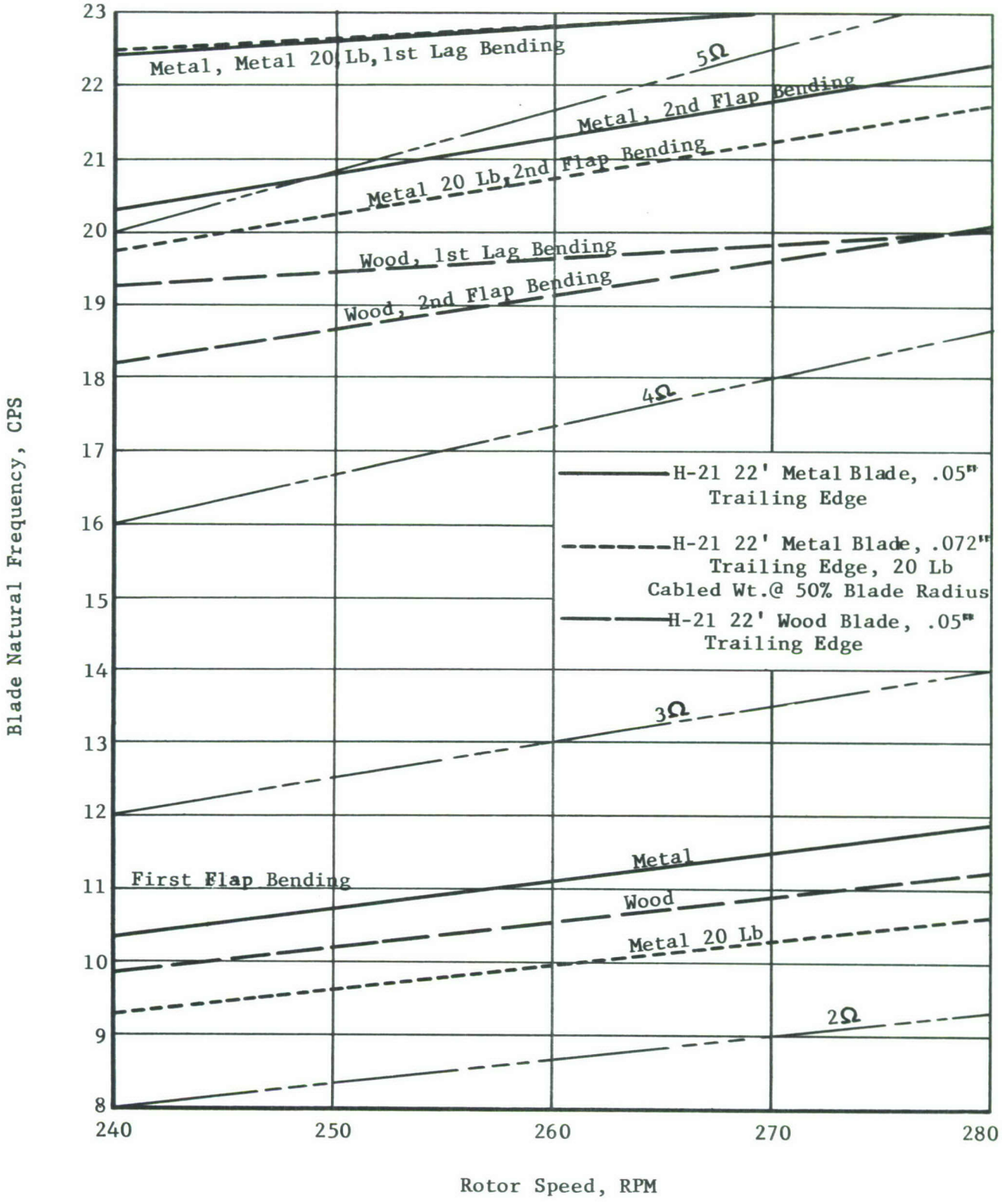

Figure 15 Blade Frequency Spectra

Cockpit Floor Response with Wood and Metal Blades - Figure 16 presents comparable cockpit floor vibratory motion for wood and metal blades at the first three rotor harmonics. Motion plots at each harmonic include (1) an airspeed sweep at 258 rpm, (2) rpm sweep at 40 knots and (3) rpm sweep at 90 knots.

Cockpit floor first and second harmonic amplitudes average,

FIRST HARMONIC

Condition	Vertical		Lateral	
	Wood Blades	Metal Blades	Wood Blades	Metal Blades
Airspeed Sweep at 258 rpm	±.008"	±.005"	±.005"	±.008"
rpm Sweep at 40 Knots	±.009"	±.004"	±.004"	±.005"
rpm Sweep at 90 Knots	±.009"	±.004"	±.006"	±.009"

SECOND HARMONIC

Condition	Vertical		Lateral	
	Wood Blades	Metal Blades	Wood Blades	Metal Blades
Airspeed Sweep at 258 rpm	±.009"	±.004"	±.003"	±.002"
rpm Sweep at 40 Knots	±.010"	±.006"	±.003"	±.001"
rpm Sweep at 90 Knots	±.006"	±.003"	±.002"	±.003"

In the vertical direction for both first and second harmonics, cockpit floor amplitudes with metal blades average one half the wood blade amplitudes. Lateral amplitude generally increases with metal blades in the first harmonic, but in the second harmonic the trend reverses with a decrease at all conditions except the 90 knot rpm sweep.

Cockpit floor vertical motion in the third harmonic with metal blades is approximately one half the response with wood blades for all airspeed and rpm combinations with the exception of 90 knots. RPM curves at 90 knots show nearly equal cockpit floor vertical motion for a rotor speed of 265 rpm and below, but at 278 rpm wood blade values are twice those for metal blades. Vertical motion rpm trends for wood and metal blades at 40 knots follow the same trend, increasing with rpm. Lateral motion of the cockpit floor shows no significant variation with blade configuration. However, at 90 knots some amplitude reduction with metal blades appears for 240 and 250 rpm.

In general, the cockpit floor motion trends with wood and metal blades are defined by average values as follows:

THIRD HARMONIC

Condition	Vertical		Lateral	
	Wood Blades	Metal Blades	Wood Blades	Metal Blades
Airspeed Sweep at 258 rpm	±.016"	±.009"	±.011"	±.009"
rpm Sweep at 40 Knots	±.015"	±.008"	±.010"	±.010"
rpm Sweep at 90 Knots	±.016"	±.013"	±.009"	±.007"

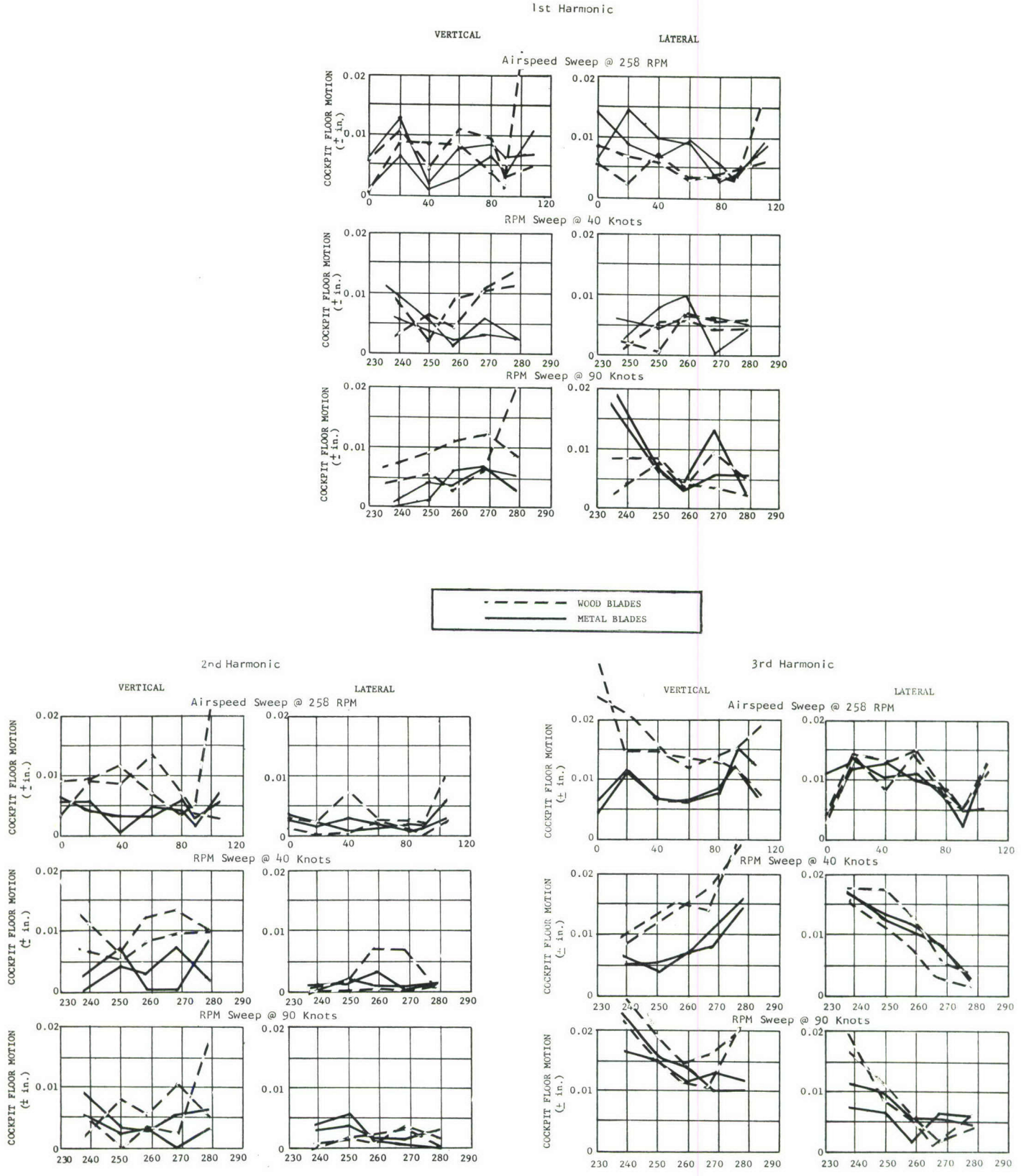

Figure 16 Comparison of Cockpit Floor Motions

B. Effect of Differential Longitudinal Cyclic

General - Normal flight control for the H2-1 Helicopter includes both longitudinal cyclic and differential collective swashplate motions. Inasmuch as this program was to evaluate Differential Longitudinal Cyclic Trim, the test vehicle controls were modified to provide longitudinal control by differential collective only. The longitudinal cyclic controls were modified to permit a preset position at the forward head and a five position in-flight variation at the aft rotor. Figure 17 illustrates the mechanical control motions which introduce longitudinal cyclic control i.e., forward or aft tilting of the tip path plane and its perpendicular thrust vector.

Consider the method of tilting the aft rotor tip path plane forward, for example. One rotating blade pitch link is shown instantaneously at 330° azimuth in the Aft Swashplate illustration. This is the same azimuth at which the nonrotating longitudinal control link is located. The blade itself follows its pitch link by 60°, so that the corresponding blade is instantaneously at 270° azimuth. An upward position of the stationary longitudinal link places the swashplate in a raised position, forcing the rotating blade pitch link to a maximum up position at 330°, and pitching the 270° blade upward about its mechanical pitch axis. The increased angle of attack here causes the blade lift to increase and it flaps up, reaching a maximum at 0° azimuth. Assuming zero lateral control, the events are repeated in the opposite direction so that the same blade reaches flap full down at 180° azimuth. All blades go through the same pattern, so that the net effect is to tilt the tip path plane forward. Lateral control is imposed in a similar manner. The forward swashplate arrangement is also shown in Figure 17. Photographs of the aft rotor controls are presented in Figure 18.

Third Harmonic Fixed System Loads - Figures 19 to 21 present fixed system third harmonic loads for longitudinal cyclic combinations of the forward and aft rotor. Airspeed plots are shown for each cyclic combination with the forward rotor loads on the left and aft rotor loads on the right. Each load set contains rotor shaft forces and moments as sine and cosine components and their resultants. Five aft cyclic positions, 3.19°A, 1.0°A, 2.0°F, 4.0°F and 5.45°F are plotted on each set of curves for a fixed forward cyclic position. In detail, the third harmonic loads during an airspeed sweep are shown as follows:

Forward Rotor Longitudinal Cyclic Position	Aft Rotor Longitudinal Cyclic Position	Figure No.
4.98° Fwd	3.19°A, 1.0°A, 2.0°F 4.0°F, 5.45°F	19
2.22° Fwd	3.19°A, 1.0°A, 2.0°F 4.0°F, 5.45°F	20
3.19° Aft	3.19°A, 1.0°A, 2.0°F 4.0°F, 5.45°F	21

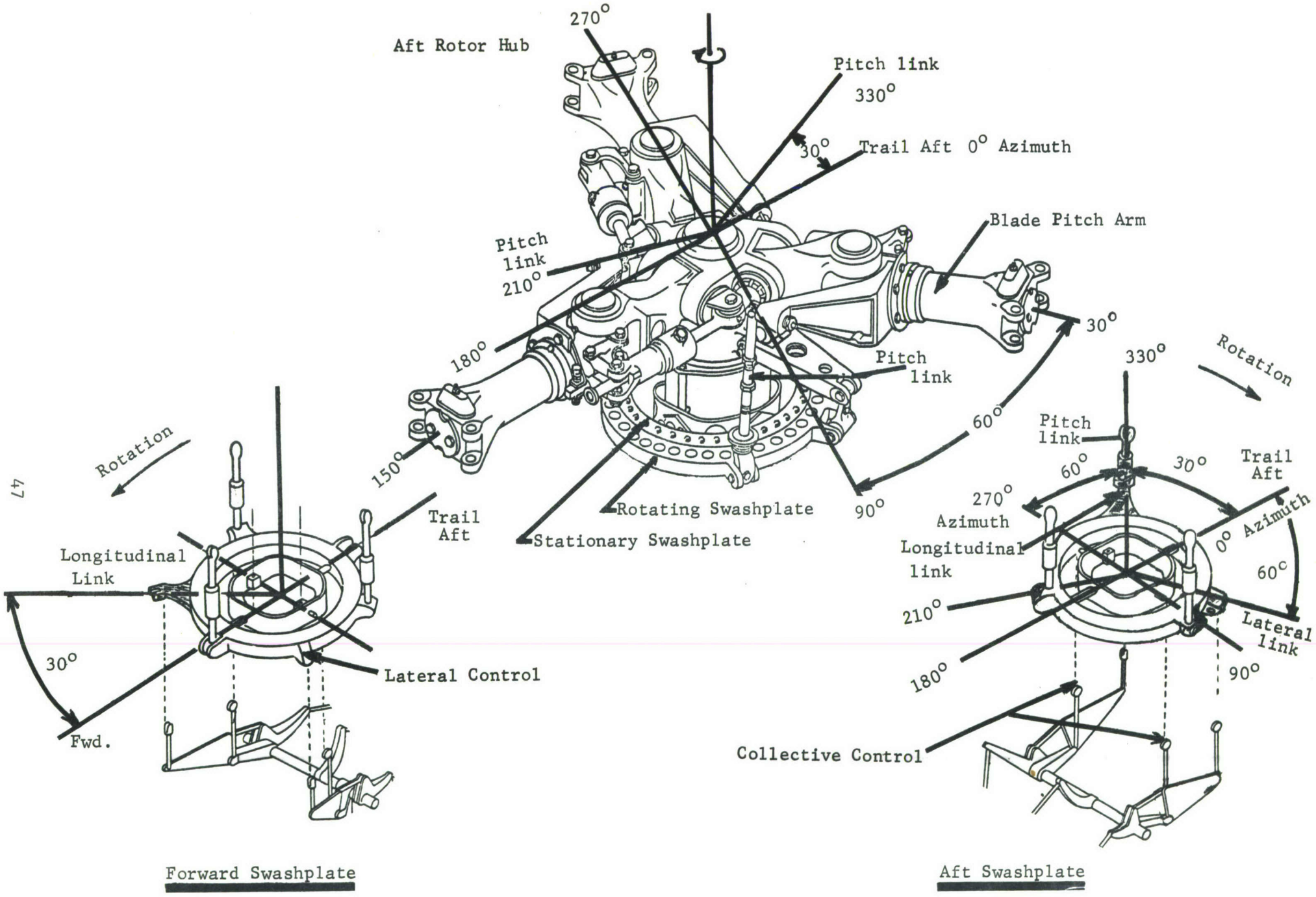

Figure 17 Control System Schematic

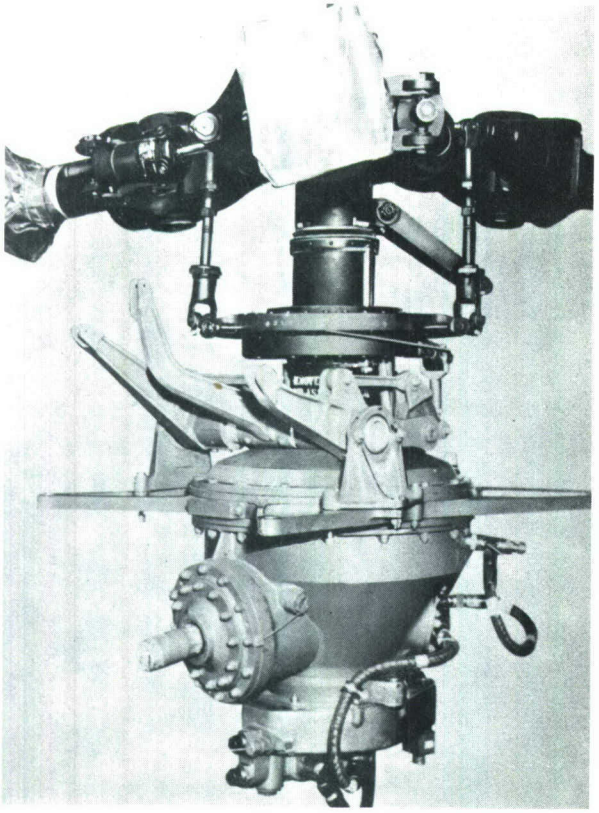

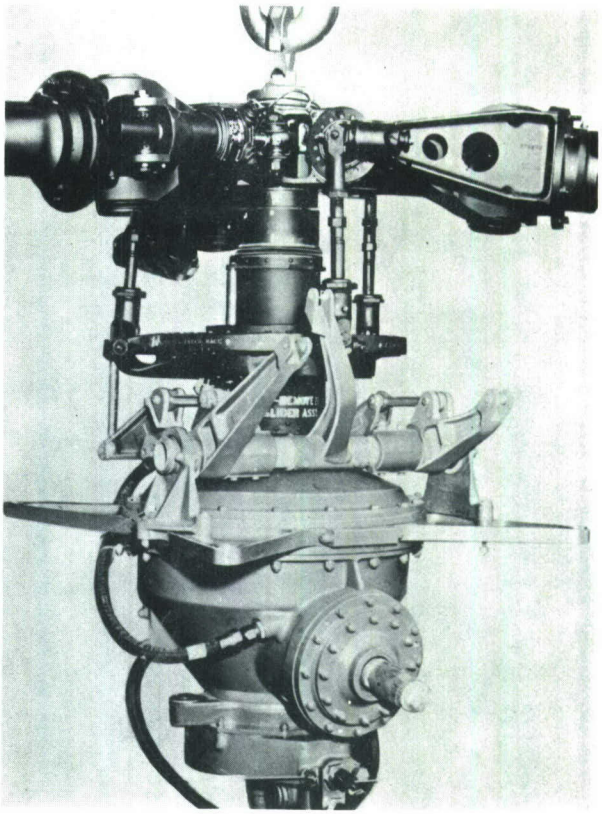

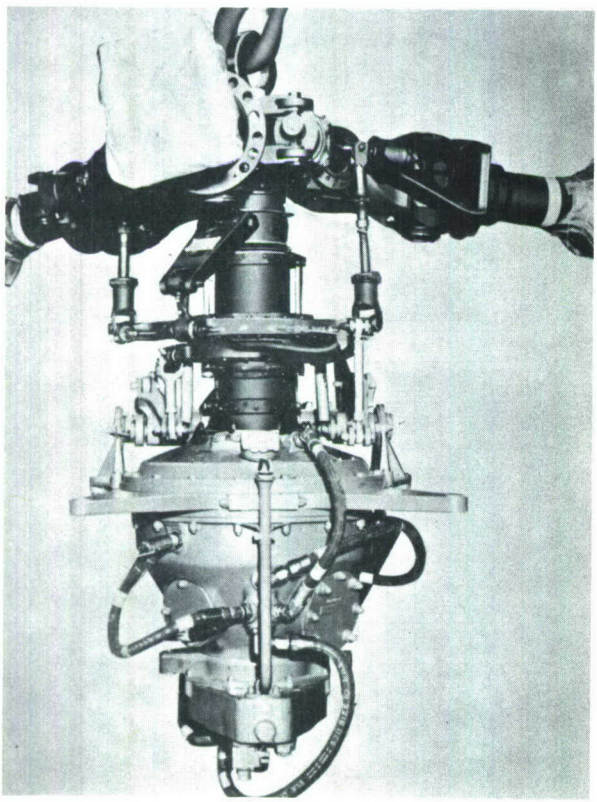

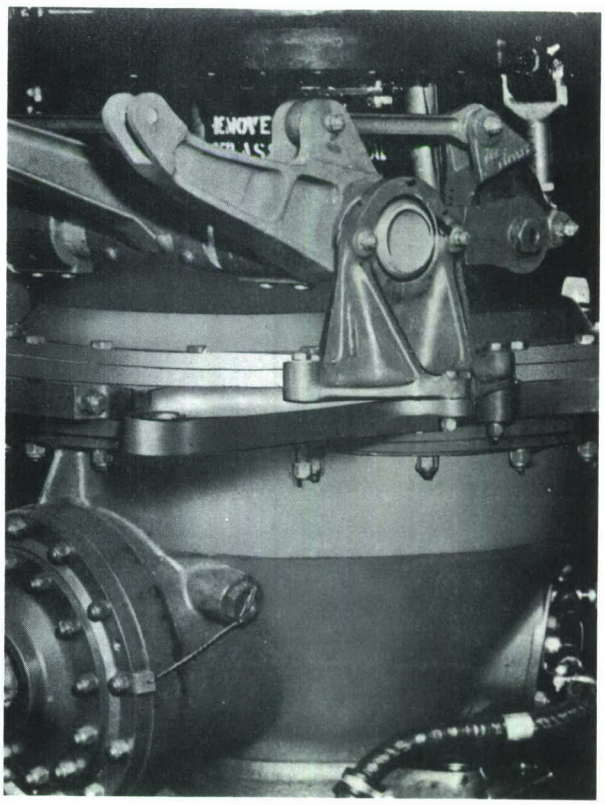

Figure 18 Aft Rotor Controls

Third harmonic fixed system forces with forward rotor cyclic at 4.98° forward usually follow trends with only small variations induced by aft cyclic settings. Components and resultants of the forward rotor forces generally follow the trends shown in Figure 8 for standard flight controls. Aft inplane forces similarly follow the trends of the flight with standard controls, but for an aft cyclic setting of 1.0° aft the longitudinal forces appear erratic with airspeed. In particular, for 60 knots the resultant increases to 750 lb, nearly three times corresponding resultants for other aft cyclic positions. Compared to the standard controls, the peak forces are shown below:

FORCES

	LONGITUDINAL		LATERAL		VERTICAL	
ROTOR	F_x, lb		F_y, lb		F_z, lb	
	Standard Controls	Fwd Cyclic 4.98° Fwd	Standard Controls	Fwd Cyclic 4.98° Fwd	Standard Controls	Fwd Cyclic 4.98° Fwd
Forward	950	800	200	150	200	200
Aft	600	750	250	250	800	500

Moment M_x and M_y curves at the same forward cyclic position show large scatter with aft cyclic position. However, for all positions of aft cyclic, the forward rotor torque (M_z) is consistent, with little scatter of the components or resultants. Maximum loads during the airspeed sweep are compared below to the standard control flight.

MOMENTS

	ROLLING		PITCHING		YAWING	
ROTOR	M_x, In. lb		M_y, In. lb		M_z, In. lb	
	Standard Controls	Fwd Cyclic 4.98° Fwd	Standard Controls	Fwd Cyclic 4.98° Fwd	Standard Controls	Fwd Cyclic 4.98° Fwd
Forward	4500	4000	4500	4300	4000	4000
Aft	4000	4000	4500	3500	7000	6000

No significant variation of the forward rotor peak moments results from a 4.98° forward setting of the forward cyclic, but at the aft rotor, pitching moment and torque peaks are reduced.

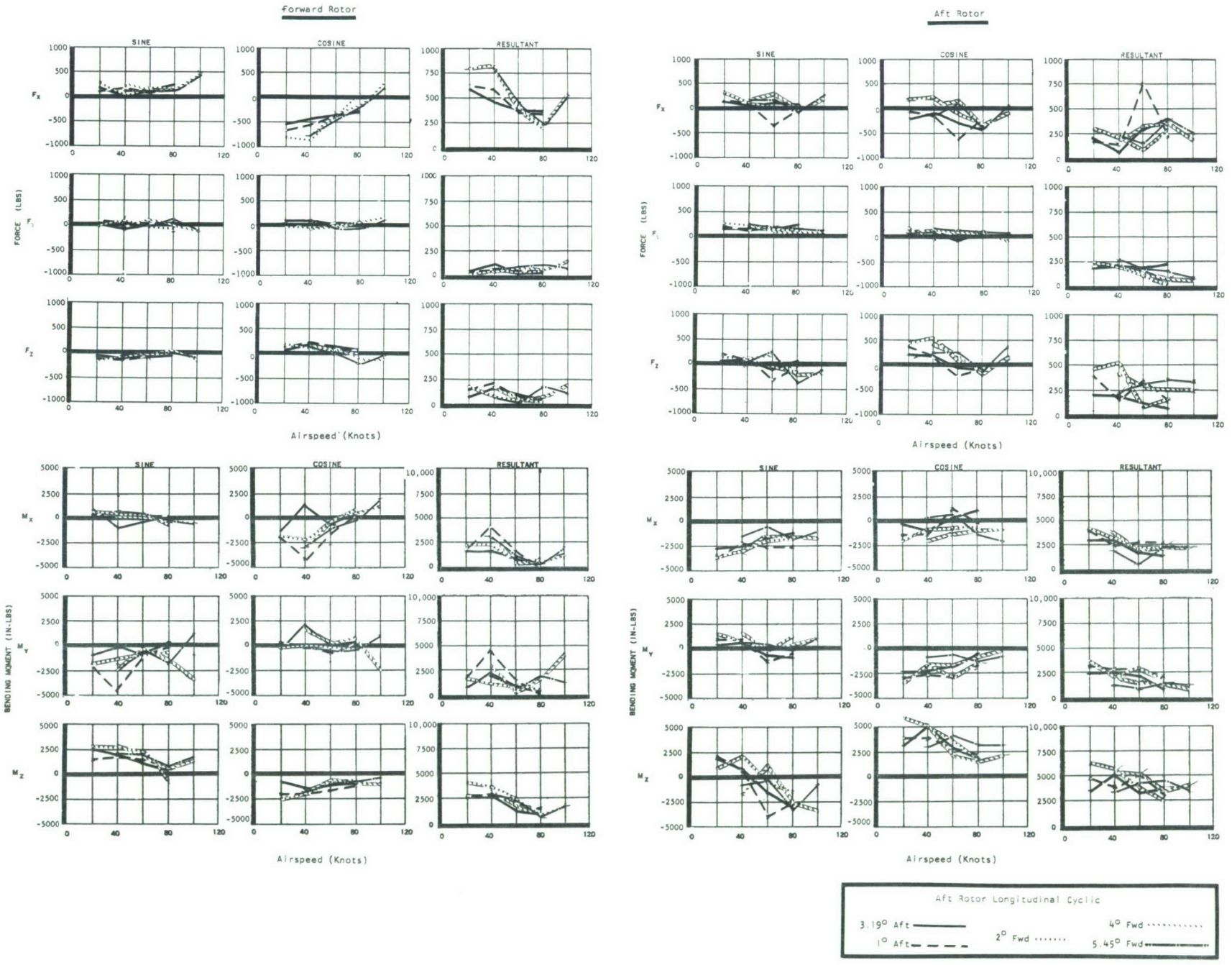

Figure 19 Fixed System Third Harmonic Loads with DLCT
Forward Rotor Longitudinal Cyclic at 4.98° Fwd

Curves for the fixed system loads show only small variations with aft cyclic setting when the forward cyclic position is fixed at 2.22° forward. Both forces and moments at the aft cyclic settings, 2.0° forward and 4.0° forward, appear nearly identical with the metal blade loads for the standard controls as shown in Figure 8. Some load variations with cyclic appear at the aft rotor which would be expected since the plotted cyclic setting is at the aft rotor. Resultant peaks with the fixed cyclic arrangement generally decrease, but without an apparent pattern as shown below:

FORCES

	LONGITUDINAL		LATERAL		VERTICAL	
ROTOR	F_x, lb		F_y, lb		F_z, lb	
	Standard Controls	Fwd Cyclic 2.22° Fwd	Standard Controls	Fwd Cyclic 2.22° Fwd	Standard Controls	Fwd Cyclic 2.22° Fwd
Forward	950	700	200	100	200	200
Aft	600	550	250	250	800	450

MOMENTS

	ROLLING		PITCHING		YAWING	
ROTOR	M_x, In. lb		M_y, In. lb		M_z, In. lb	
	Standard Controls	Fwd Cyclic 2.22° Fwd	Standard Controls	Fwd Cyclic 2.22° Fwd	Standard Controls	Fwd Cyclic 2.22° Fwd
Forward	4500	2500	4500	3000	4000	3000
Aft	4000	4000	4500	3500	7000	3500

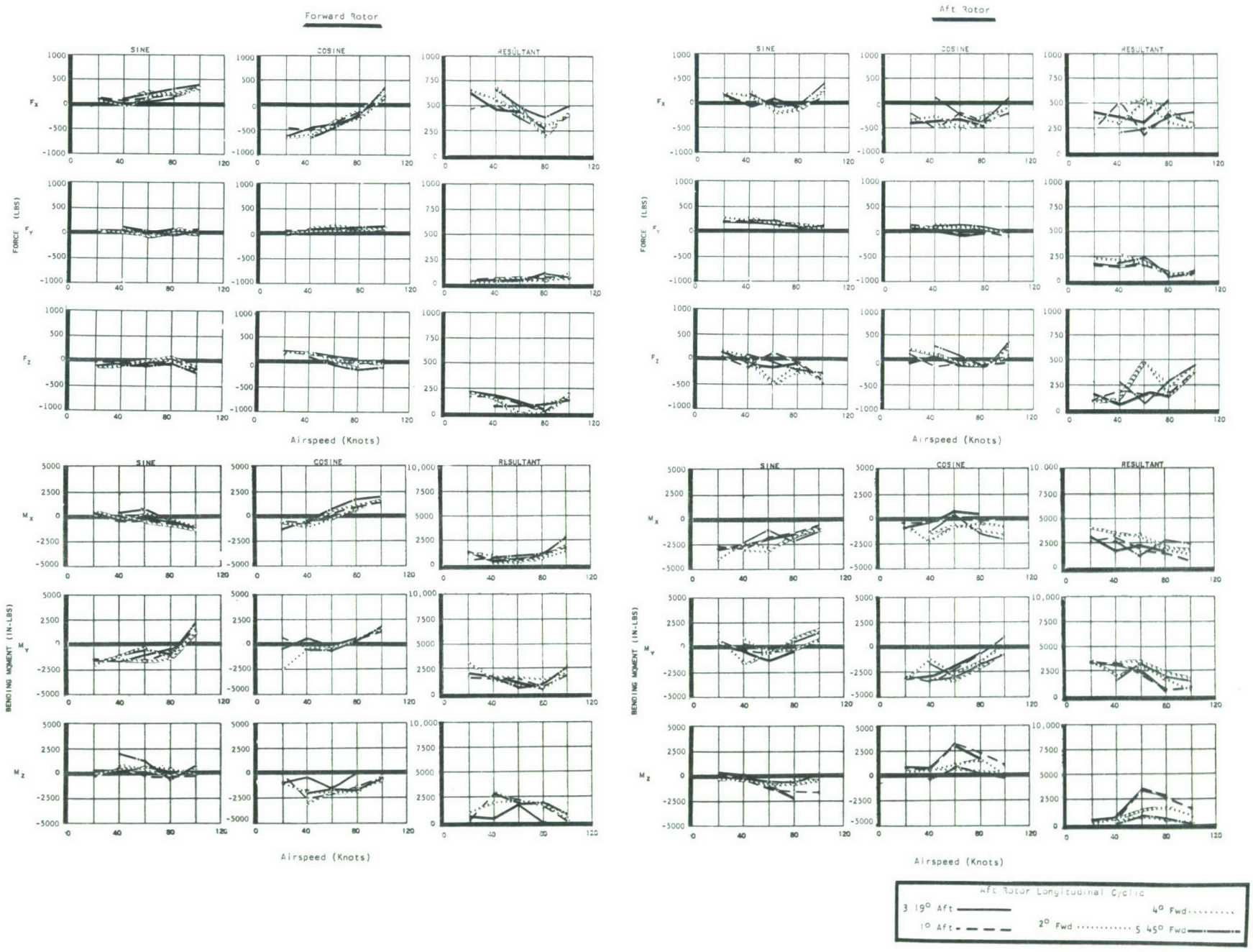

Figure 20 Fixed System Third Harmonic Loads with DLCT Forward Rotor Longitudinal Cyclic at 2.22° Fwd

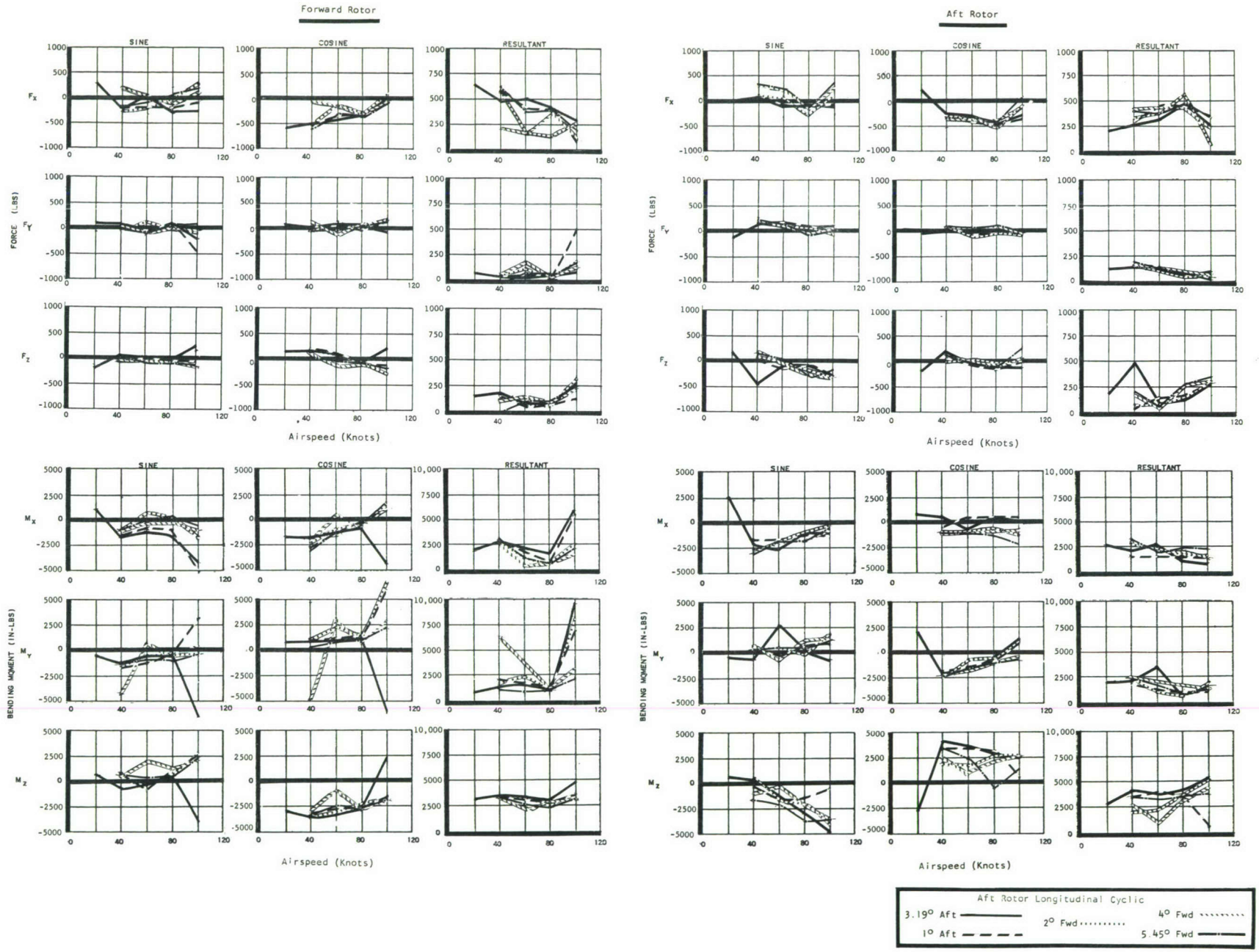

Figure 21 Fixed System Third Harmonic Loads with DLCT
Forward Rotor Longitudinal Cyclic at 3.19° Aft

Fixed system third harmonic forces with forward rotor longitudinal cyclic fixed at 3.19° aft show several significant variations for aft settings of longitudinal cyclic. Forward longitudinal resultants show erratic load changes with aft cyclic settings; localized variations are shown for the forward rotor lateral force at 100 knots and the aft rotor vertical force at 40 knots. Reversing the trend shown in Figures 18 and 19, forward lateral and vertical peak force resultants increase with the forward longitudinal cyclic set at 3.19° aft with reference to standard longitudinal cyclic control. Peak forces from the load plots show:

FORCES

	LONGITUDINAL		LATERAL		VERTICAL	
ROTOR	F_x, lb		F_y, lb		F_z, lb	
	Standard Controls	Fwd Cyclic 3.19° Aft	Standard Controls	Fwd Cyclic 3.19° Aft	Standard Controls	Fwd Cyclic 3.19° Aft
Forward	950	700	200	500	200	300
Aft	600	550	250	250	800	450

Forward longitudinal cyclic locked at 3.19°A tends to produce significant variations of fixed third harmonic moments at both the forward and aft rotors. Typified by large phase and resultant load changes between (1) airspeed data points and (2) aft longitudinal cyclic positions, these moment plots show some of the most significant changes that occur from Differential Longitudinal Cyclic Trim. Forward rotor pitching and yawing moments, and shaft torque generally decrease with airspeed to 80 knots and then increase to a maximum peak at 100 knots. Maximum forward rotor resultants appear with the aft rotor longitudinal cyclic at a maximum position of 3.19° aft. Maximum resultants compared to the metal blade flight with standard controls show:

MOMENTS

	ROLLING		PITCHING		YAWING	
ROTOR	M_x, In. lb		M_y, In. lb		M_z, In. lb.	
	Standard Controls	Fwd Cyclic 3.19° Aft	Standard Controls	Fwd Cyclic 3.19° Aft	Standard Controls	Fwd Cyclic 3.19° Aft
Forward	4500	6000	4500	9500	4000	4500
Aft	4000	3000	4500	3500	7000	5500

Forward rotor third harmonic moments increase between 10% and 110%; aft rotor moments decrease between 20% and 25%.

Third Harmonic Vibratory Response - Velocity pickups in the cockpit area provided data which were reduced to vibratory motions of the cockpit floor in the vertical, lateral and longitudinal directions. Recorded simultaneously with hub loads, this data were recorded to study the forced response characteristics of the fuselage with fixed cyclic settings for each airspeed sweep. With a three bladed rotor the predominant portion of the vibration environment is at the third rotor harmonic. Thus correlation of forces and motions is made at this harmonic.

Figure 22 presents plots of third harmonic cockpit floor motion. The figure is divided, horizontally, into three sections, corresponding to the forward rotor cyclic settings. Vertically the columns present vertical, lateral and longitudinal motion.

During airspeed sweeps with forward longitudinal cyclic at 2.22° forward, vertical motions generally increase with airspeed. The aft cyclic setting of 3.19° aft shows minimum amplitudes with no definite airspeed trends. Vertical amplitudes increase and define an increasing trend with airspeed as the aft rotor longitudinal cyclic varies through the incremental settings of 1.0° aft, 2.0° forward, 4.0° forward and 5.45° forward. Vertical amplitude peaks at ±.015" corresponding to a forward speed of 100 knots with the aft cyclic setting at 5.45° forward. Longitudinal motion peaks at ±.006" for all positions of the aft cyclic with the forward longitudinal cyclic at 2.22° forward. Amplitudes at 60 knots show that the forward settings of aft cyclic are more critical with longitudinal amplitudes four times those for aft settings.

Vertical amplitude plots corresponding to a forward cyclic position of 4.98° forward usually decrease with airspeed, omitting the data points at 20 knots. Again, forward setting of aft cyclic shows maximum vertical amplitudes. Similar to vertical motion with aft cyclic setting, lateral amplitudes tend to decrease with airspeed. Cockpit floor longitudinal amplitudes are below ±.003" for all longitudinal cyclic positions of the aft rotor.

At a forward longitudinal cyclic position of 3.19° aft, vertical amplitude increases rapidly with airspeed for all cyclic settings of the aft rotor. Vertical amplitude curves with aft positions of 1.0° aft show an average minimum of ±.007" for 40 knots increasing rapidly with airspeed to unacceptable maximum amplitudes of ±.040" for 80 knots. Forward settings of aft cyclic show similar unacceptable vertical amplitudes of ±.050" for 100 knots, but at 80 knots amplitudes are only ±.015". Lateral cockpit floor motion decreases with airspeed and with aft cyclic settings, but with forward positions of 4.0° forward and 5.45° forward the curves peak at 80 knots with an amplitude of ±.010". Curves of cockpit floor longitudinal motion are similar for all aft cyclic positions with a peak amplitude of ±.005" for 80 knots forward speed.

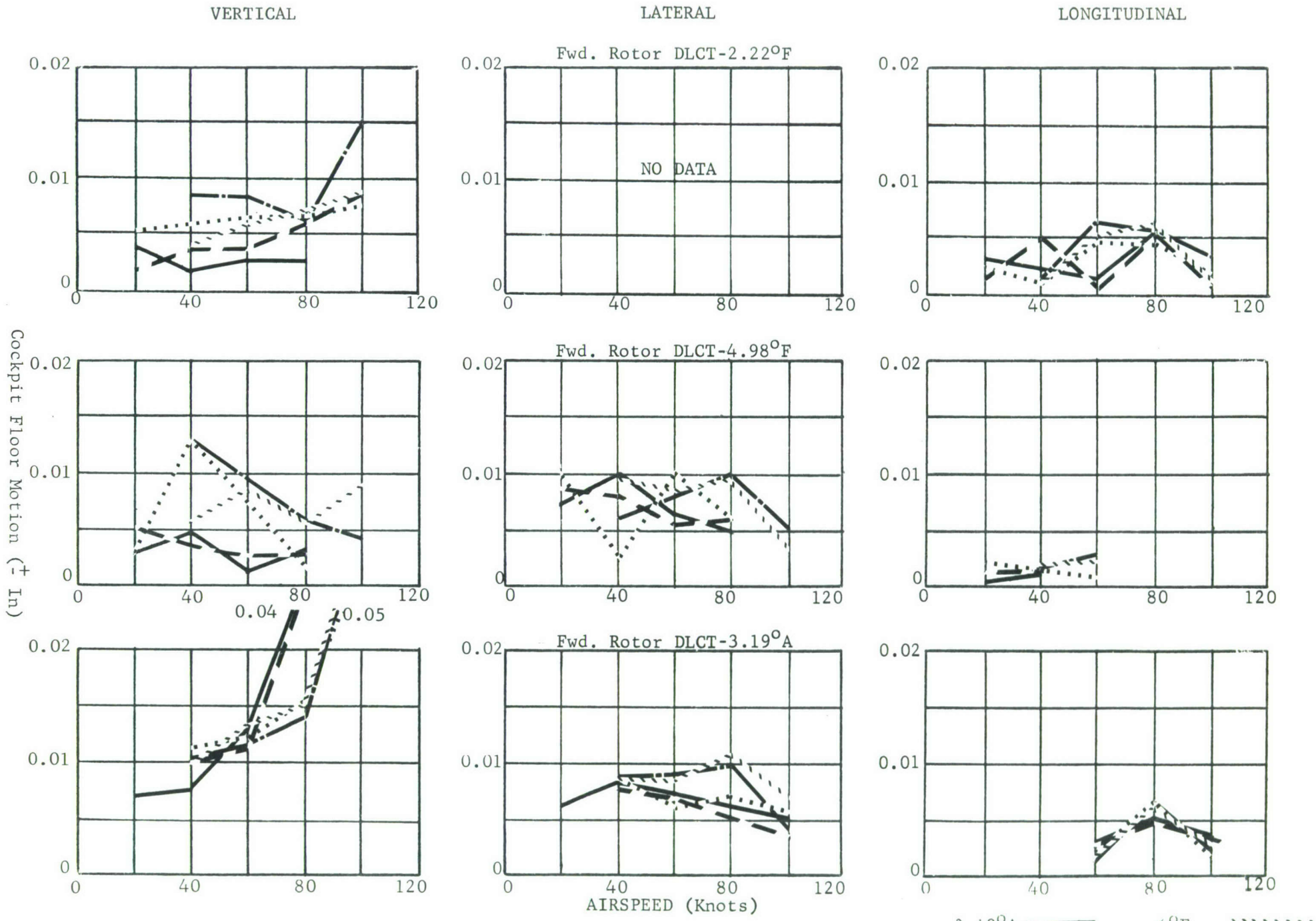

Figure 22 3rd Harmonic Cockpit Floor Motion with DLCT

Correlation of Hub Loads and Cockpit Floor Vibration Level - As shown in Figure 22 the most significant 3 Ω cockpit motion trends appear for vertical motion at forward speeds of 60 and 80 knots. Since these trends are outstanding, the load-motion correlation herein considers only cyclic variations for these airspeeds, but notes that similar explanations are valid for the lesser trends. Cockpit floor vertical response apparently fluctuates with longitudinal cyclic combinations as a result of cancellation between forced responses due to phase changes in the forces. Consider first, results from the wood blade hub load measurement program, Reference 3.

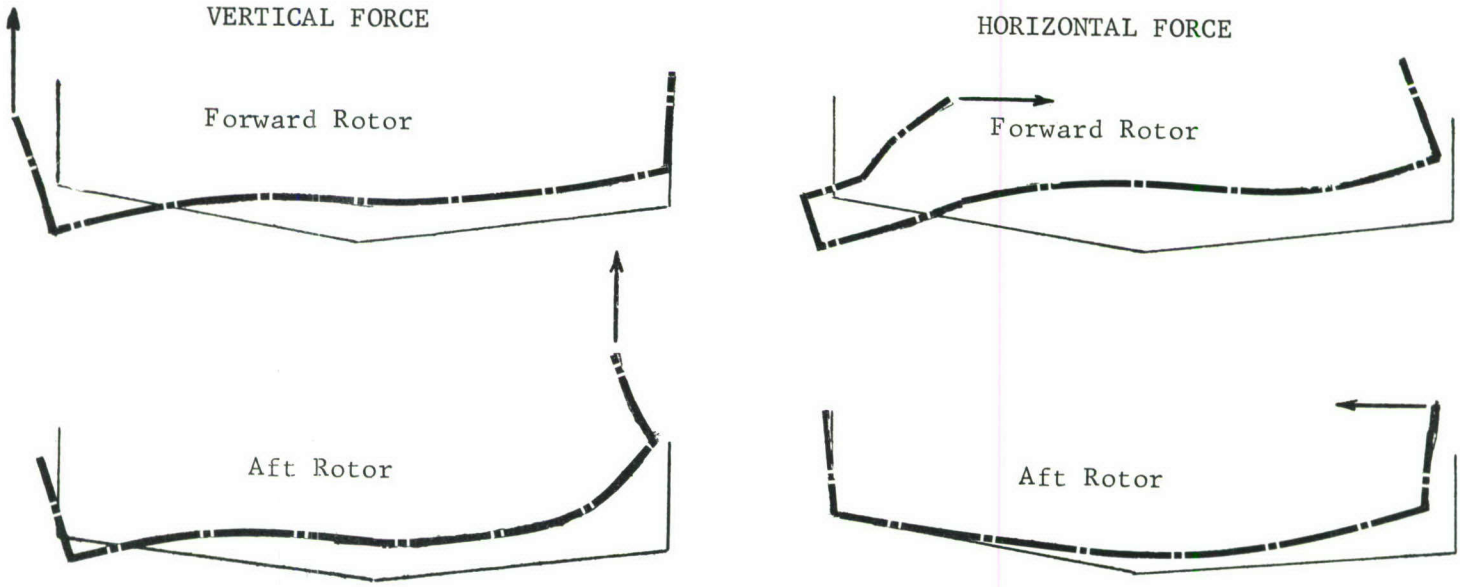

Vertical forward rotor 3 Ω force viewed at the instant the load is acting upward produces down and forward cockpit floor motion; up vertical 3Ω force at the aft rotor produces down and aft cockpit floor motion. Longitudinal forward rotor 3Ω force produces down and forward cockpit floor motion; the same load at the aft rotor produces little response at the cockpit floor.

Figures 23 and 24 review, at 60 and 80 knots respectively, the position of the longitudinal forward rotor load vector and the vertical forward and aft rotor load vectors with respect to time for each longitudinal cyclic combination. As an example of the method of presentation, note the forward rotor longitudinal load vectors at 60 knots with aft cyclic at 3.19° aft and forward rotor cyclic positions as shown for each vector.

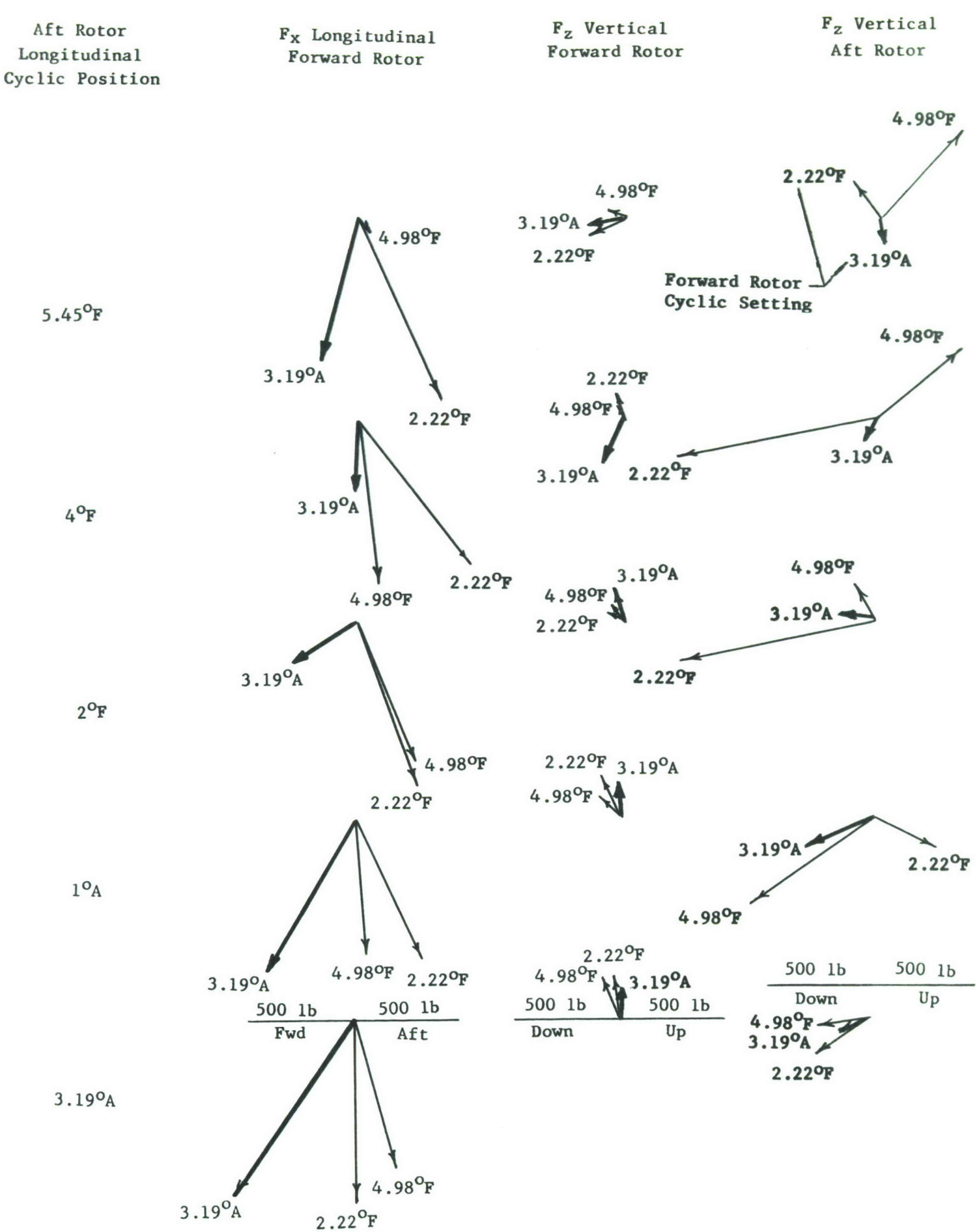

Figure 23 Longitudinal And Vertical Load Resultants With Respect To Time At 60 Knots

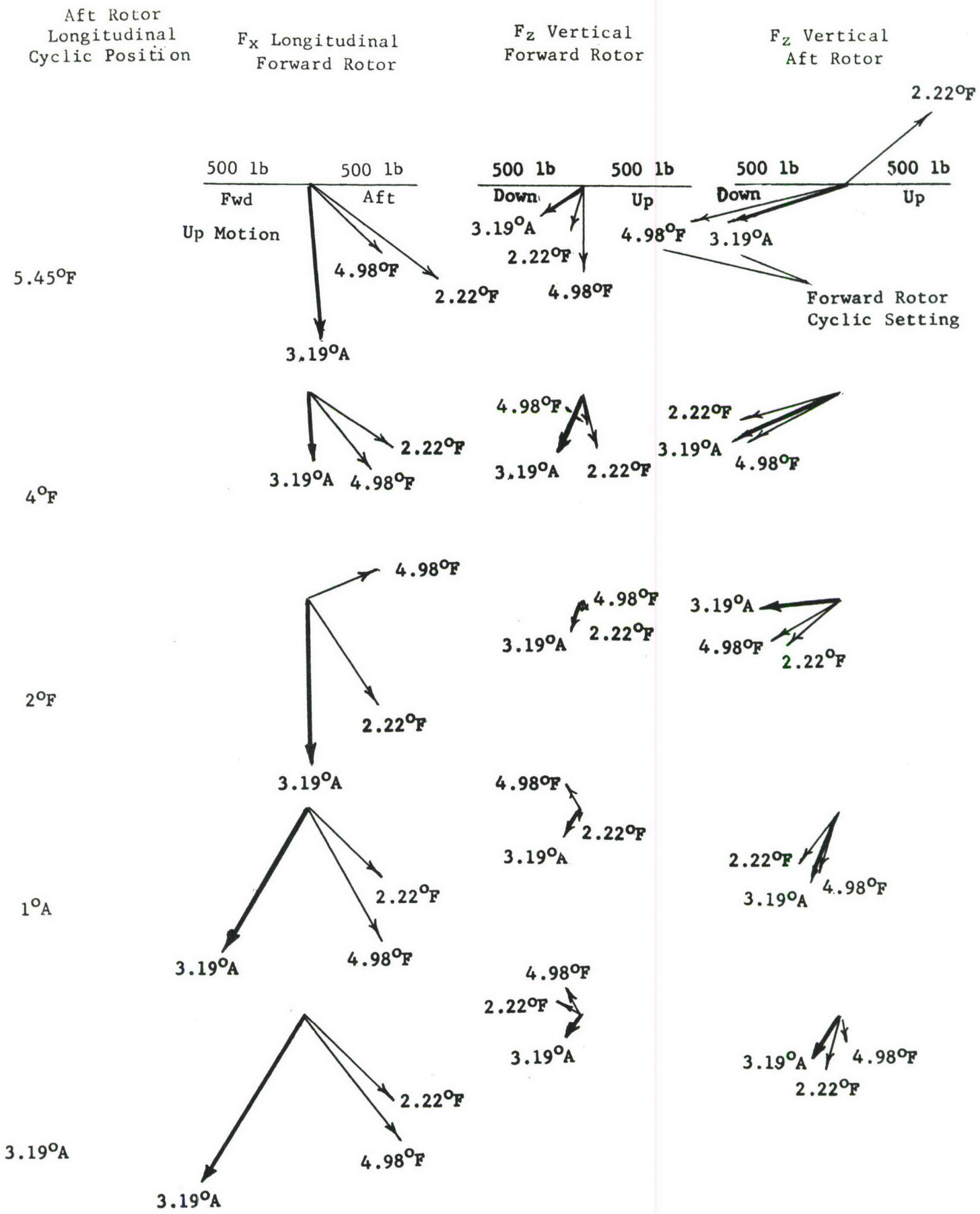

Figure 24 Longitudinal and Vertical Load Resultants with Respect to Time at 80 Knots

Fx Longitudinal Forward Rotor

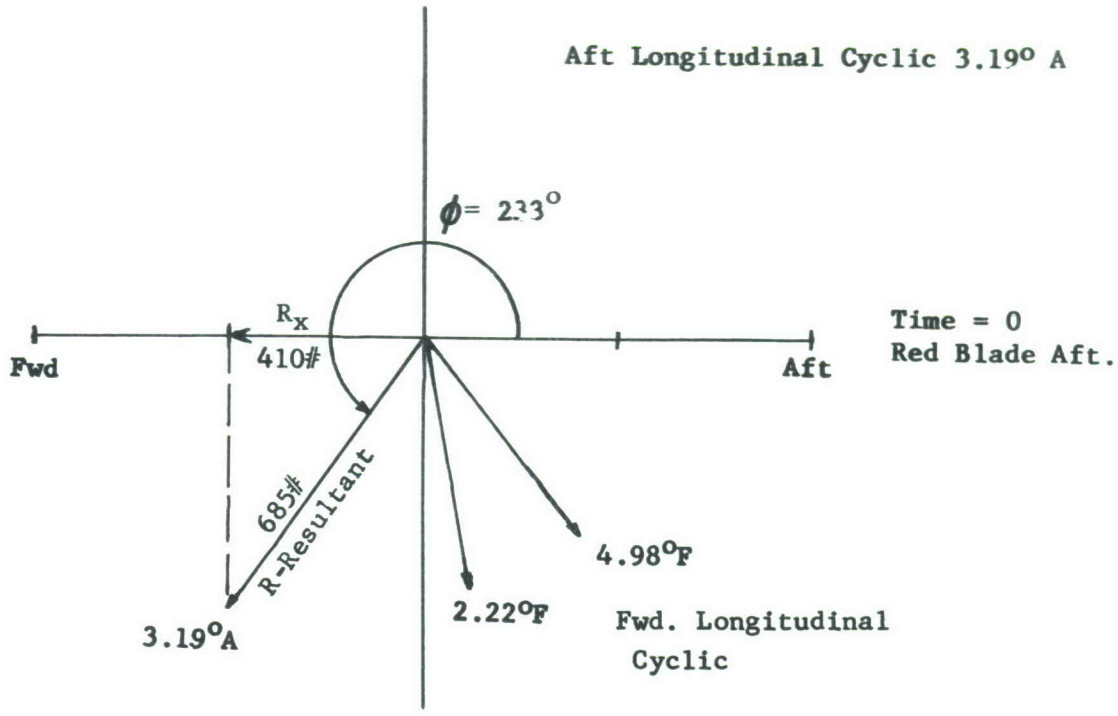

To illustrate the method of presentation, consider "R", the resultant force corresponding to an aft rotor cyclic setting of 3.19° aft, as a typical 3Ω maximum amplitude or magnitude vector of the longitudinal force. The instant pictured is reference time zero, when the red blade is in its zero azimuth, trail position over the fuselage. The projection "R_x" on the horizontal axis is the instantaneous physical magnitude and direction of the longitudinal force. In the sample, it is 410 lb forward at the instant the red blade is at trail aft. One complete revolution of "R" takes a 3Ω period, that is, the time required for the red blade to advance 120° of its 360° rotation. Thus, as "R" rotates, its projection R_x describes the harmonic oscillation of the longitudinal force. ϕ is one way to describe the phase angle of the resultant vector.

Figure 24 illustrates longitudinal loads at the forward rotor and vertical loads at both rotors as they vary with longitudinal cyclic position at an airspeed of 80 knots. Aft longitudinal load is not shown because the response to it at the cockpit floor in the mode shape above is quite small.

The horizontal axis of each load figure indicates the direction of the load and the corresponding direction of cockpit floor motion. For example, longitudinal forward rotor load acting forward produces up cockpit floor motion, just opposite that shown on Page 57. The rows in Figure 24 are the aft rotor longitudinal cyclic settings. Within each row, the vectors are labeled with the forward rotor cyclic settings.

Now consider the 3.19°A forward rotor settings, the heavy lines. With the aft rotor at 5.45°F, the vectors are not in phase; that is, F_x is nearly straight

down or a nearly zero instantaneous load, F_z forward and F_z aft are both indicating down load or cockpit-floor up motion. This arbitrary phasing is true in the first three rows of Figure 24, for aft cyclic settings of 5.45°F, 4.°F and 2°F. Then in the last two rows at aft cyclic settings of 1°A and 3.19°A, this phasing changes, F_x exhibits a forward load-up cockpit floor motion while the F_z vectors are in about the same direction, thus lining up all the vectors in phase.

The vibration data, Figure 22, Page 56, last row for the forward rotor 3.19°A setting corresponding to the heavy lines on Figure 24, shows that at 80 knots the vibration level of the aft rotor cyclics 5.45°F, 4°F and 2°F are relatively moderate at about ±0.015". The 1°A and 3.19° aft rotor cyclics result in much larger vibration levels in the order of ±0.025". Note that relative to the load phasing in Figure 24, the low vibration occurs when the load phasing is mixed, the high vibration when the load phasing is together.

The other forward cyclic settings in Figure 24 do not show this in-phase condition at any of the conditions flown. Figure 22 then shows no particularly severe vibration levels at 80 knots in the first two rows, 2.22°F and 4.98°F, forward rotor cyclic.

Figure 23 presents the same load information at 60 knots. Here again there is no particular phase agreement and in Figure 22 at 60 knots, there are no outstandingly severe vibration levels.

Figure 25 is a three dimensional presentation of rotor loads and vibration. The horizontal axes of each plot are forward swashplate tilt (longitudinal cyclic)in the plane of the paper and aft swashplate tilt coming out of the paper. The vertical axes are given either as rotor load or vibration. Rotor load magnitude variations are not particularly significant. However, the vertical cockpit floor vibration level plot clearly shows that forward cyclic at both rotors results in low vibration, while aft cyclic at both rotors results in high vibration levels. As an intermediate condition, with aft cyclic near zero, movement of the forward rotor cyclic causes a large vibration increase as the swashplate is tilted aft.

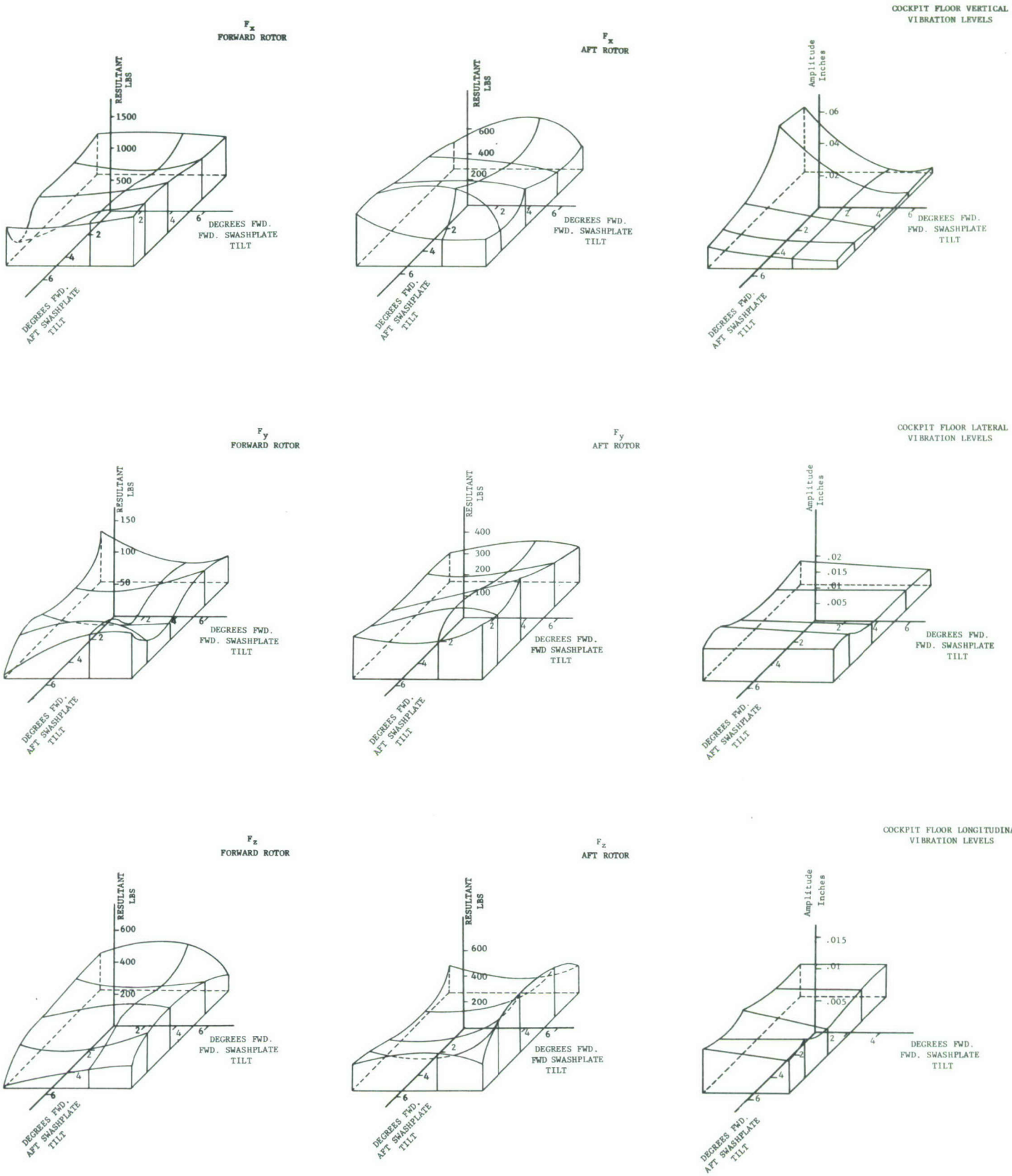

Figure 25 Resultant Loads and Motions with DLCT

M_x
FORWARD ROTOR

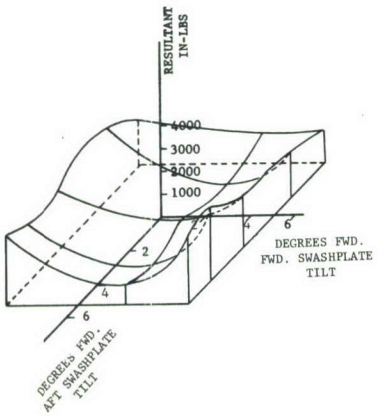

M_x
AFT ROTOR

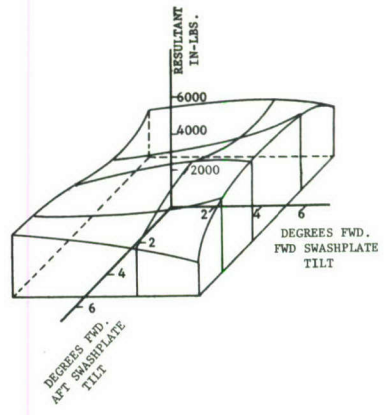

M_y
FORWARD ROTOR

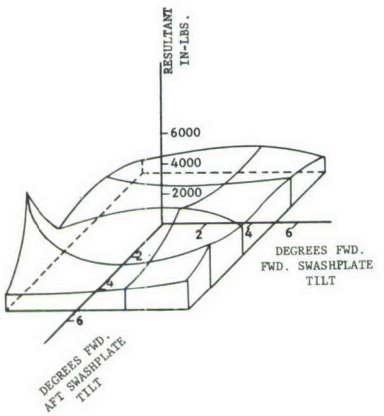

M_y
AFT ROTOR

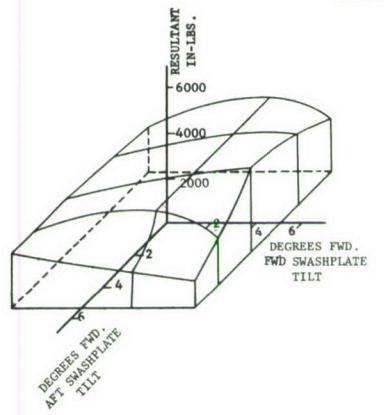

M_z
FORWARD ROTOR

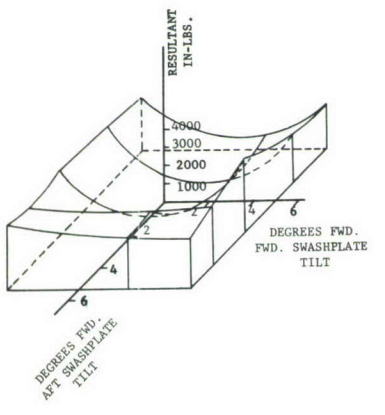

M_z
AFT ROTOR

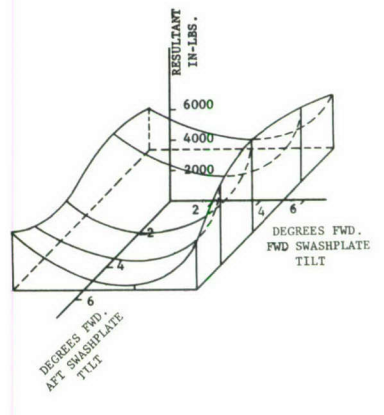

Figure 25 Cont'd. Resultant Loads and Motions with DLCT

Steady Torque - Figure 26 presents steady torque and horsepower curves for the forward and aft synchronizing shafts with various longitudinal cyclic combinations between rotors. The figure is divided into three columns for the Forward Synchronizing Shaft, Aft Synchronizing Shaft, and Total Power. The row divisions are for three forward rotor longitudinal cyclic settings, 4.98°F, 2.22°F and 3.19°A. Each small figure has aft rotor longitudinal cyclic as abscissa from 3.19°A to 5.45°F, the left ordinate is shaft torque and the right ordinate is horsepower. For the first row of data, 4.98°F data is available only at 60 knots; the 2.22°F and 3.19°A rows contain both 60 and 80 knot data.

The total power curves are relatively flat, with only small changes resulting from aft rotor cyclic variations. Forward cyclic changes have more effect on power, with 4.98°F averaging 950 hp, 2.22°F - 900 hp, and 3.19°A - 850 hp. At 3.19°A there is a 50 hp spread between 60 and 80 knots forward speed.

Power distribution between forward and aft rotors can be studied in the first two columns. Aft rotor power is always larger than forward rotor power, but the specific ratios vary with cyclic. Average power distributions for forward cyclic changes at 60 knots are as follows.

Fwd Rotor	Fwd Power	Aft Power	Total Power	Fwd %	Aft %
4.98°F	425	525	950	45	55
2.22°F	350	550	900	39	61
3.19°A	275	575	850	32	68

Thus as forward rotor cyclic setting moves aftward total power decreases and the power proportion to the aft rotor increases.

Within the 4.98°F forward rotor setting, the effect of aft rotor cyclic change is to require higher power to to the aft rotor at 3.19°A, nearly equal power to the two rotors at 2°F, and the highest aft rotor power at 5.45°F. At the other two forward cyclics, 2.22°F and 3.19°A, aft rotor cyclic causes a linear change increasing aft rotor power and decreasing forward rotor power, and reaching a maximum aft rotor power value at the most forward setting of 5.45°F.

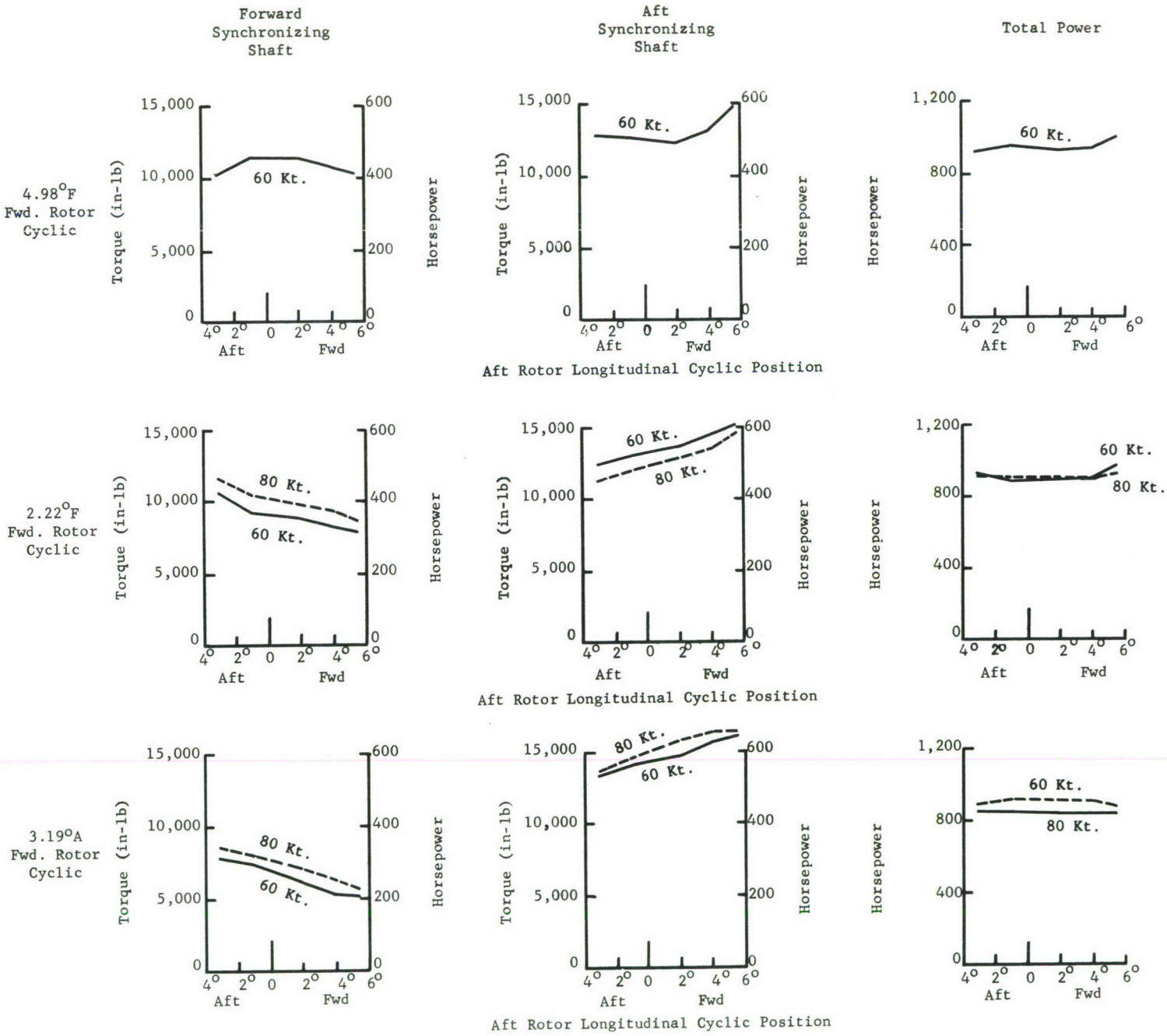

Figure 26 Steady Torque Distribution

SECTION V

CONCLUSIONS

A rotor shaft load measurement program has been conducted on the H-21 helicopter equipped with metal blades, providing rotor shaft loads for two basic configurations. The flight program included (1) standard flight controls and (2) modified flight controls with fixed longitudinal cyclic combinations. Cockpit floor motions were measured concurrently to permit correlation of load and vibration data. The helicopter was flown at 13,500 lb, normal gross weight, through an airspeed sweep and two rotor speed sweeps to obtain vibratory load and motion data. Investigation of the longitudinal cyclic loads included flights at the same gross weight with an airspeed sweep at normal rotor speed for each condition. The data was processed to obtain rotating and fixed coordinate system shaft loads and cockpit floor vibratory response. Forward and aft synchronizing shaft torques were measured on the performance flight to provide the torque distribution between rotors and the power required. A comparison of rotor loads with wood and metal blades is also made.

Specific conclusions relating to the effect of differential longitudinal cyclic control are as follows:

1. With forward rotor cyclic fixed at 4.98° forward and aft rotor cyclic varied from 5.45° forward to 3.19° aft, measured 3Ω rotor loads differ only moderately. Forward rotor longitudinal 3Ω loads are smaller with aft cyclic in the aft rotor; forward rotor lateral and vertical loads indicate little difference. Aft rotor longitudinal and vertical loads have large scatter with no particularly favored aft rotor cyclic setting. In most cases the load peaks are less than with standard H-21 controls.

2. With forward rotor cyclic fixed at 2.22° forward and aft rotor cyclic varied from 5.45° forward to 3.19° aft, forward rotor loads show small scatter with a tendency for aft cyclic in the aft rotor to produce smaller loads. Aft rotor longitudinal and vertical loads again have large scatter. There is a similar tendency for aft cyclic to produce smaller aft rotor loads.

3. With forward rotor cyclic fixed at 3.19° aft and aft rotor cyclic varied from 5.45° forward to 3.19° aft there is a larger scatter than previously, with a tendency for aft rotor cyclic at mid-setting to produce the smallest longitudinal loads. Aft rotor loads display less scatter, but no particular aft setting produces minimum loads. At high speed, aft cyclic settings of the aft rotor result in large increases of forward rotor 3Ω rolling and pitching moments.

4. Vertical cockpit floor vibration is significantly affected by forward rotor cyclic changes, with forward tilts generally reducing vibration levels. At high speed the lowest vibration levels occur when the forward rotor is set at the most forward 4.98° cyclic position. Less forward rotor cyclic, 2.22° forward, results in a 50 to 100% increase in vibration. Forward rotor cyclic set 3.19° aft results in a better than five fold increase in vertical vibration.

5. Aft cyclic settings of the aft rotor tend to reduce vibration when the forward rotor settings are forward. When the forward rotor setting is aft, this trend reverses and forward cyclic settings of the aft rotor tend to delay the onset of high vibration levels.

6. Lateral and longitudinal vibration levels are not varied in any regular pattern by the cyclic changes.

7. Overall, forward cyclic at both rotors produces moderate vibration levels, aft cyclic at both rotors produces a large increase in vibration.

8. Vibration changes are traceable to phase relation changes between vertical and longitudinal rotor forces, with little actual magnitude change due to the cyclic variations.

9. Total aircraft power decreases linearly for aftward settings of the forward rotor cyclic. At the same time the proportion of power to the aft rotor increases, and that to the forward rotor decreases. In general, moving the aft rotor cyclic forward linearly increases the power to the aft rotor and linearly decreases the power to the forward rotor.

Specific conclusions relating to the differences between wood and metal blades are as follows:

1. All metal blade rotor loads are smaller than wood blade loads.

2. Although with wood blades the aft rotor loads are as much as twice the forward rotor loads, with metal blades the difference is generally smaller.

3. With either wood or metal blades, the forward rotor longitudinal loads, more than any others, generally correspond with the pattern of measured vibration levels, low in hover, high in transition, low in cruise and then increasing with forward speed.

4. Lateral rotor loads are generally one-third of the longitudinal loads and display little definite trend with airspeed.

5. Vertical rotor loads are also generally one-third of the longitudinal loads and display little definite trend with airspeed.

6. With either wood or metal blades, longitudinal loads at both rotors increase with rotor speed; the trend is more pronounced at the aft rotor.

7. Lateral metal blade loads show little variation with rotor speed; lateral wood blade loads show a small increase with rotor speed for the aft rotor only.

8. Vertical metal blade loads show little variation with rotor speed; vertical wood blade loads show a significant increase with rotor speed for the aft rotor only.

9. Rotating second harmonic in-plane loads at the forward rotor show the same airspeed trend as the longitudinal fixed system third harmonic loads, low in hover, high in transition, low in cruise and then increasing with forward speed. This corresponds with articulated rotor theory from which it is known that rotating second and fourth harmonic in-plane loads add to produce fixed system third harmonic longitudinals, and subtract to produce fixed system third harmonic laterals.

10. In-plane second harmonic metal blade loads are about 20% smaller than the wood blade loads at the forward rotor over the airspeed range, but are nearly 50% smaller at the aft rotor.

11. In-plane fourth harmonic loads average about two-thirds of the second harmonic in-plane loads, and display similar airspeed and rpm trends.

12. There is some correlation between blade natural frequencies and loads. At the forward rotor the metal blade first lag bending natural frequency is farther from 3Ω than that of the wood blade and the metal blade vertical loads are lower. At the aft rotor there is no such correlation.

13. The first lag bending natural frequency of the wood blade is closer to 4Ω than the metal blade and the wood blade rotating 4Ω loads are much higher than those of the metal blade. Increasing rotor rpm moves the wood blade closer to 4Ω resonance than the metal blade and rotating 4Ω wood blade loads do increase markedly with rotor rpm.

14. Cockpit floor vibration levels generally correlate with the load trends. Vibration is generally lower with metal blades than with wood blades.

REFERENCES

1. Air Force Contract AF33(616)7292, "Data Analysis of H-21C Vibration Incorporating Longitudinal Cyclic Trim", October 11, 1960.

2. Air Force Contract AF33(616)5240, "Theoretical Analysis and Calculations for a Method of Computing the Response of Tandem Rotor Helicopters to Rotor Induced Vibratory Forces", May 27, 1957.

3. Scarborough, J. B., "Numerical Mathematical Analysis", The John Hopkins Press, London, Fourth Edition, 1958.

4. Yntema, Robert T.; Gabel, Richard; Ricks, Robert G., "A Study of Tandem Helicopter Fuselage Vibration; Phase III, In-flight Measurement of Steady and Oscillatory Rotor Shaft Loads", Boeing-Vertol Report R-239, February 1961.

5. Yntema, Robert T.; Gabel, Richard; Ricks, Robert G., "A Study of Tandem Helicopter Fuselage Vibration; Phase IIC and IV, A Method for the Prediction of Coupled Vertical-Lateral Natural and Forced Modes," Boeing-Vertol Report R-246, February 1961.

APPENDIX A

ROTOR SHAFT LOADS IN THE

FIXED SYSTEM ACTING ON THE HELICOPTER FORWARD ROTOR

ROTOR SHAFT LOADS IN THE FIXED SYSTEM
ACTING ON THE HELICOPTER FORWARD ROTOR

The forces and moments in the rotating system acting on the helicopter below the rotor are obtained by combining the pitch link loads and the rotor shaft loads. The forward rotor system is represented by the following schematic diagram which shows the pitch link locations relative to the rotating axis system and the fixed axis system.

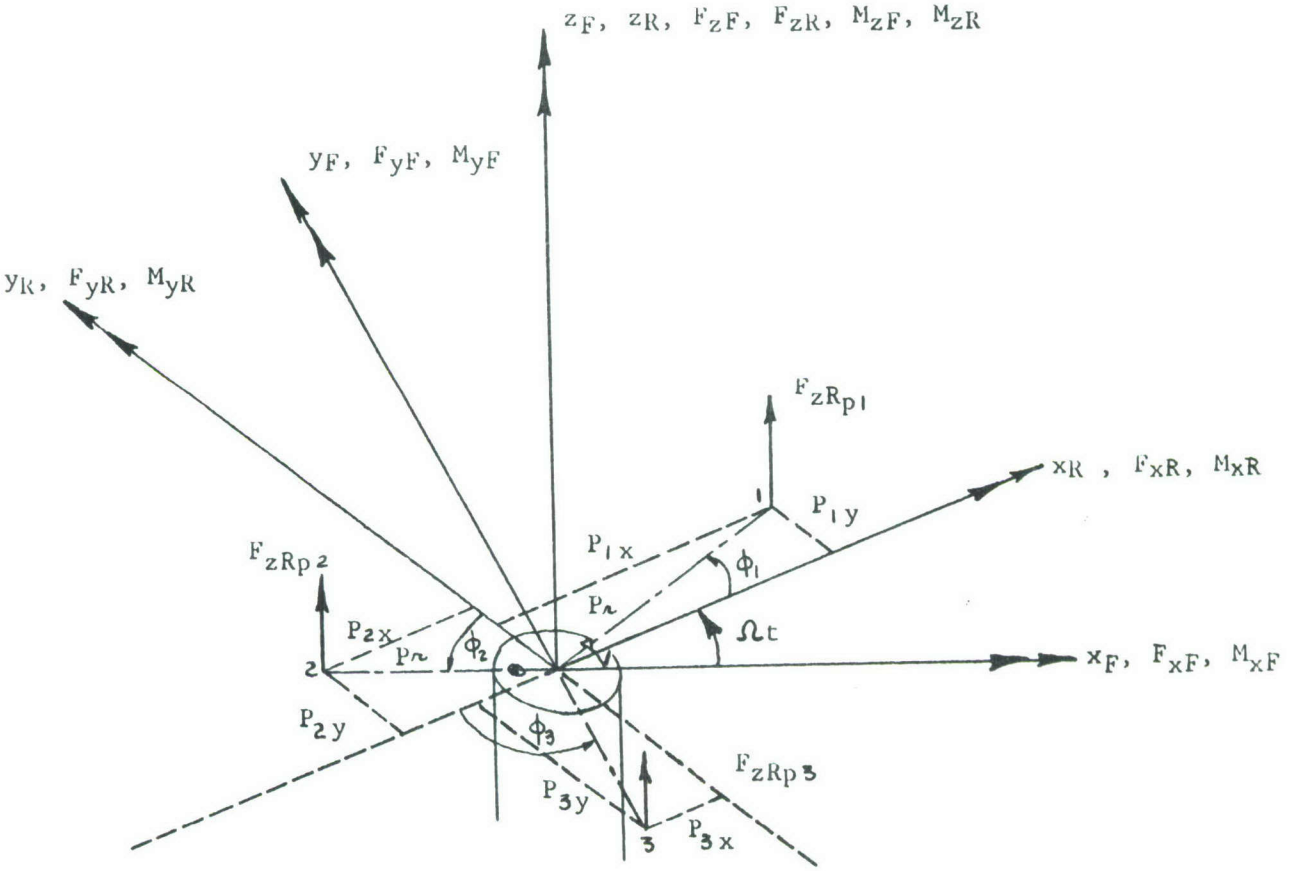

The pitch links are located in the rotating system by the radial arm, p_r and the angles ϕ_1, ϕ_2, ϕ_3. These quantities can be defined in terms of the location of pitch link No. 1 relative to the azimuth position, $\psi = 0$.

$$p_r = \left(\overline{p_{1x}}^2 + \overline{p_{1y}}^2\right)^{\frac{1}{2}}$$

$$\phi_1 = \tan^{-1} \frac{p_{1y}}{p_{1x}}$$

$$\phi_2 = 120^\circ + \phi_1 - 90^\circ = 30^\circ + \tan^{-1} \frac{p_{1y}}{p_{1x}}$$

$$\phi_3 = 240^\circ + \phi_1 - 180^\circ = 60^\circ + \tan^{-1} \frac{p_{1y}}{p_{1x}}$$

Then,

$$p_{2x} = p_r \sin\left(30^\circ + \tan^{-1} \frac{p_{1y}}{p_{1x}}\right)$$

$$p_{2y} = p_r \cos\left(30^\circ + \tan^{-1} \frac{p_{1y}}{p_{1x}}\right)$$

$$p_{3x} = p_r \cos\left(60^\circ + \tan^{-1} \frac{p_{1y}}{p_{1x}}\right)$$

$$p_{3y} = p_r \sin\left(60^\circ + \tan^{-1} \frac{p_{1y}}{p_{1x}}\right)$$

Combining the loads in the pitch link and shaft

$$F_{zRT} = F_{zR} + F_{zRp_1} + F_{zRp_2} + F_{zRp_3}$$

$$F_{xRT} = F_{xR}$$

$$F_{yRT} = F_{yR}$$

$$M_{xRT} = M_{xR} + F_{zRp_1}\,(p_{1y}) + F_{zRp_2}\,(p_{2y}) - F_{zRp_3}\,(p_{3y})$$

$$M_{yRT} = M_{yR} - F_{zRP_1}\,(p_{1x}) + F_{zRp_2}\,(p_{2x}) + F_{zRp_3}\,(p_{3x})$$

$$M_{zRT} = M_{zR}$$

Rewriting in matrix forms,

$$\begin{vmatrix} F_{xRT} \\ F_{yRT} \\ F_{zRT} \\ M_{xRT} \\ M_{yRT} \\ M_{zRT} \\ \text{Total} \\ \text{Loads} \end{vmatrix} = \begin{vmatrix} 1 & & & & & & & & \\ & 1 & & & & & & & \\ & & 1 & & & 1 & 1 & 1 & \\ & & & 1 & & p_1 y & p_2 y & -p_3 y & \\ & & & & 1 & -p_1 x & p_2 x & p_3 x & \\ & & & & & 1 & & & \end{vmatrix} \begin{vmatrix} F_{xR} \\ F_{yR} \\ F_{zR} \\ M_{xR} \\ M_{yR} \\ M_{zR} \\ F_{zRp_1} \\ F_{zRp_2} \\ F_{zRp_3} \end{vmatrix}$$

The above procedure can be applied to each Fourier Series coefficient, to obtain the coefficients of the series which represents the combined pitch links and rotor shaft loads.

The fixed system loads can be written as trigonometric functions of the relative angle, Ωt between the rotating axis system and the fixed axis system. For the forward rotor, the loads in the fixed system can be written as,

$$\begin{vmatrix} F_{xF} \\ F_{yF} \\ F_{zF} \\ M_{xF} \\ M_{yF} \\ M_{zF} \end{vmatrix} = \begin{vmatrix} \cos\Omega t & -\sin\Omega t & & & & \\ \sin\Omega t & \cos\Omega t & & & & \\ & & 1 & & & \\ & & & \cos\Omega t & -\sin\Omega t & \\ & & & \sin\Omega t & \cos\Omega t & \\ & & & & & 1 \end{vmatrix} \begin{vmatrix} F_{xRT} \\ F_{yRT} \\ F_{zRT} \\ M_{xRT} \\ M_{yRT} \\ M_{zRT} \end{vmatrix}$$

However, the general form for load in the rotating system is,

$$Q = A_o + \sum_{1}^{n} A_n \cos n\Omega t + \sum_{1}^{n} B_N \sin n\Omega t$$

Therefore, the following general expressions must be evaluated,

$$Q\cos\Omega t = A_o\cos\Omega t + \cos\Omega t\sum_1^n A_n\cos n\Omega t + \cos\Omega t\sum_1^n B_n\sin n\Omega t$$

$$= A_o\cos\Omega t + \sum_1^n A_n\cos\Omega t\cos n\Omega t + \sum_1^n B_n\cos\Omega t\sin n\Omega t$$

$$= A_o\cos\Omega t + \sum_1^n \tfrac{1}{2}A_n\left[\cos(1-n)\Omega t + \cos(1+n)\Omega t\right] + \sum_1^n \tfrac{1}{2}B_n\left[\sin(n-1)\Omega t + \sin(1+n)\Omega t\right]$$

$$Q\sin\Omega t = A_o\sin\Omega t + \sin\Omega t\sum_1^n A_n\cos n\Omega t + \sin\Omega t\sum_1^n B_n\sin n\Omega t$$

$$= A_o\sin\Omega t + \sum_1^n A_n\sin\Omega t\cos n\Omega t + \sum_1^n B_n\sin\Omega t\sin n\Omega t$$

$$= A_o\sin\Omega t + \sum_1^n \tfrac{1}{2}A_n\left[\sin(1-n)\Omega t + \sin(1+n)\Omega t\right] + \sum_1^n \tfrac{1}{2}B_n\left[\cos(1-n)\Omega t - \cos(1+n)\Omega t\right]$$

$$Q\left[-\sin\Omega t\right] = -A_o\sin\Omega t - \sum_1^n \tfrac{1}{2}A_n\left[\sin(1-n)\Omega t + \sin(1+n)\Omega t\right]$$

$$- \sum_1^n \tfrac{1}{2}B_n\left[\cos(1-n)\Omega t - \cos(1+n)\Omega t\right]$$

For three harmonics in the fixed system,

$$Q\cos\Omega t = A_o\cos\Omega t + \tfrac{1}{2}A_1\left[1 + \cos 2\Omega t\right] + \tfrac{1}{2}B_1\left[0 + \sin 2\Omega t\right]$$

$$+ \tfrac{1}{2}A_2\left[\cos(-\Omega t) + \cos 3\Omega t\right] + \tfrac{1}{2}B_2\left[\sin(\Omega t) + \sin 3\Omega t\right]$$

$$+ \tfrac{1}{2}A_3\left[\cos(-2\Omega t) + \cos 4\Omega t\right] + \tfrac{1}{2}B_3\left[\sin(2\Omega t) + \sin 4\Omega t\right]$$

$$+ \tfrac{1}{2}A_4\left[\cos(-3\Omega t) + \cos 5\Omega t\right] + \tfrac{1}{2}B_4\left[\sin(3\Omega t) + \sin 5\Omega t\right]$$

$$Q\cos\Omega t = \tfrac{1}{2}A_1 + \tfrac{1}{2}B_2\sin\Omega t + (A_o + \tfrac{1}{2}A_2)\cos\Omega t + (\tfrac{1}{2}B_1 + \tfrac{1}{2}B_3)\sin 2\Omega t$$

$$+(\tfrac{1}{2}A_1 + \tfrac{1}{2}A_3)\cos 2\Omega t + (\tfrac{1}{2}B_2 + \tfrac{1}{2}B_4)\sin 3\Omega t + (\tfrac{1}{2}A_2 + \tfrac{1}{2}A_4)\cos 3\Omega t$$

$$Q\sin\Omega t = A_o\sin\Omega t + \tfrac{1}{2}A_1\left[0 + \sin 2\Omega t\right] + \tfrac{1}{2}B_1\left[1 - \cos 2\Omega t\right]$$

$$+ \tfrac{1}{2}A_2\left[\sin(-\Omega t) + \sin 3\Omega t\right] + \tfrac{1}{2}B_2\left[\cos(-\Omega t) - \cos 3\Omega t\right] + \tfrac{1}{2}A_3\left[\sin(-2\Omega t) + \sin 4\Omega t\right]$$

$$+ \tfrac{1}{2}B_3\left[\cos(-2\Omega t) - \cos 4\Omega t\right] + \tfrac{1}{2}A_4\left[\sin(-3\Omega t) + \sin 5\Omega t\right] + \tfrac{1}{2}B_4\left[\cos(-3\Omega t) - \cos 5\Omega t\right]$$

$$Q \sin\Omega t = \tfrac{1}{2}B_1 + \tfrac{1}{2}B_2 \cos\Omega t + (A_0 - \tfrac{1}{2}A_2)\sin\Omega t + (-\tfrac{1}{2}B_1 + \tfrac{1}{2}B_3)\cos 2\Omega t$$
$$+(\tfrac{1}{2}A_1 - \tfrac{1}{2}A_3)\sin 2\Omega t + (-\tfrac{1}{2}B_2 + \tfrac{1}{2}B_4)\cos 3\Omega t + (\tfrac{1}{2}A_2 - \tfrac{1}{2}A_4)\sin 3\Omega t$$

$$-Q \sin\Omega t = -\tfrac{1}{2}B_1 + \tfrac{1}{2}B_2 \cos\Omega t + (-A_0 + \tfrac{1}{2}A_2)\sin\Omega t + (+\tfrac{1}{2}B_1 - \tfrac{1}{2}B_3)\cos 2\Omega t$$
$$+(-\tfrac{1}{2}A_1 + \tfrac{1}{2}A_3)\sin 2\Omega t + (\tfrac{1}{2}B_2 - \tfrac{1}{2}B_4)\cos 3\Omega t + (-\tfrac{1}{2}A_2 + \tfrac{1}{2}A_4)\sin 3\Omega t$$

Letting a second subscript denote the loads in the following order,

1, F_{xRT}	4, M_{xRT}
2, F_{yRT}	5, M_{yRT}
3, F_{zRT}	6, M_{zRT}

The fixed system loads can be written as,

$$F_{xF} = \tfrac{1}{2}A_{11} + \tfrac{1}{2}B_{21}\sin\Omega t + (A_{01} + \tfrac{1}{2}A_{21})\cos\Omega t + (\tfrac{1}{2}B_{11} + \tfrac{1}{2}B_{31})\sin 2\Omega t$$
$$+ (\tfrac{1}{2}A_{11} + \tfrac{1}{2}A_{31})\cos 2\Omega t + (\tfrac{1}{2}B_{21} + \tfrac{1}{2}B_{41})\sin 3\Omega t + (\tfrac{1}{2}A_{21} + \tfrac{1}{2}A_{41})\cos 3\Omega t$$
$$-\tfrac{1}{2}B_{12} - \tfrac{1}{2}B_{22}\cos\Omega t + (-A_{02} + \tfrac{1}{2}A_{22})\sin\Omega t + (\tfrac{1}{2}B_{12} - \tfrac{1}{2}B_{32})\cos 2\Omega t$$
$$+(-\tfrac{1}{2}A_{12} + \tfrac{1}{2}A_{32})\sin 2\Omega t + (\tfrac{1}{2}B_{22} - \tfrac{1}{2}B_{42})\cos 3\Omega t + (-\tfrac{1}{2}A_{22} + \tfrac{1}{2}A_{42})\sin 3\Omega t$$

$$F_{xF} = (\tfrac{1}{2}A_{11} - \tfrac{1}{2}B_{12}) + (\tfrac{1}{2}B_{21} - A_{02} + \tfrac{1}{2}A_{22})\sin\Omega t + (A_{01} + \tfrac{1}{2}A_{21} - \tfrac{1}{2}B_{22})\cos\Omega t$$
$$+ (\tfrac{1}{2}B_{11} + \tfrac{1}{2}B_{31} - \tfrac{1}{2}A_{12} + \tfrac{1}{2}A_{32})\sin 2\Omega t + (\tfrac{1}{2}A_{11} + \tfrac{1}{2}A_{31} + \tfrac{1}{2}B_{12} - \tfrac{1}{2}B_{32})\cos 2\Omega t$$
$$+ (\tfrac{1}{2}B_{21} + \tfrac{1}{2}B_{41} - \tfrac{1}{2}A_{22} + \tfrac{1}{2}A_{42})\sin 3\Omega t + (\tfrac{1}{2}A_{21} + \tfrac{1}{2}A_{41} + \tfrac{1}{2}B_{22} - \tfrac{1}{2}B_{42})\cos 3\Omega t$$

$$F_{yF} = \tfrac{1}{2}B_{11} + \tfrac{1}{2}B_{21}\cos\Omega t + (A_{01} - \tfrac{1}{2}A_{21})\sin\Omega t + (-\tfrac{1}{2}B_{11} + \tfrac{1}{2}B_{31})\cos 2\Omega t$$
$$+ (\tfrac{1}{2}A_{11} - \tfrac{1}{2}A_{31})\sin 2\Omega t + (-\tfrac{1}{2}B_{21} + \tfrac{1}{2}B_{41})\cos 3\Omega t + (\tfrac{1}{2}A_{21} - \tfrac{1}{2}A_{41})\sin 3\Omega t$$
$$+ \tfrac{1}{2}A_{12} + \tfrac{1}{2}B_{22}\sin\Omega t + (A_{02} + \tfrac{1}{2}A_{22})\cos\Omega t + (\tfrac{1}{2}B_{12} + \tfrac{1}{2}B_{32})\sin 2\Omega t$$
$$+ (\tfrac{1}{2}A_{12} + \tfrac{1}{2}A_{32})\cos 2\Omega t + (\tfrac{1}{2}B_{22} + \tfrac{1}{2}B_{42})\sin 3\Omega t + (\tfrac{1}{2}A_{22} + \tfrac{1}{2}A_{42})\cos 3\Omega t$$

$$F_{yF} = \tfrac{1}{2}B_{11} + \tfrac{1}{2}A_{12} + (A_{01} - \tfrac{1}{2}A_{21} + \tfrac{1}{2}B_{22})\sin\Omega t + (A_{02} + \tfrac{1}{2}A_{22} + \tfrac{1}{2}B_{21})\cos\Omega t$$
$$+ (\tfrac{1}{2}A_{11} - \tfrac{1}{2}A_{31} + \tfrac{1}{2}B_{12} + \tfrac{1}{2}B_{32})\sin 2\Omega t + (-\tfrac{1}{2}B_{11} + \tfrac{1}{2}B_{31} + \tfrac{1}{2}A_{12} + \tfrac{1}{2}A_{32})\cos 2\Omega t$$
$$+ (\tfrac{1}{2}A_{21} - \tfrac{1}{2}A_{41} + \tfrac{1}{2}B_{22} + \tfrac{1}{2}B_{42})\sin 3\Omega t + (-\tfrac{1}{2}B_{21} + \tfrac{1}{2}B_{41} + \tfrac{1}{2}A_{22} + \tfrac{1}{2}A_{42})\cos 3\Omega t$$

Fixed System Loads (Continued)

$$F_{zF} = A_{03} + A_{13}\cos\Omega t + B_{13}\sin\Omega t + A_{23}\cos 2\Omega t + B_{23}\sin 2\Omega t + A_{33}\cos 3\Omega t + B_{33}\sin 3\Omega t$$

$$M_{xF} = \tfrac{1}{2}A_{14} + \tfrac{1}{2}B_{24}\sin\Omega t + (A_{04} + \tfrac{1}{2}A_{24})\cos\Omega t + (\tfrac{1}{2}B_{14} + \tfrac{1}{2}B_{34})\sin 2\Omega t + (\tfrac{1}{2}A_{14} + \tfrac{1}{2}A_{34})\cos 2\Omega t + (\tfrac{1}{2}B_{24} + \tfrac{1}{2}B_{44})\sin 3\Omega t + (\tfrac{1}{2}A_{24} + \tfrac{1}{2}A_{44})\cos 3\Omega t - \tfrac{1}{2}B_{15} - \tfrac{1}{2}B_{25}\cos\Omega t + (-A_{05} + \tfrac{1}{2}A_{25})\sin\Omega t + (\tfrac{1}{2}B_{15} - \tfrac{1}{2}B_{35})\cos 2\Omega t + (-\tfrac{1}{2}A_{15} + \tfrac{1}{2}A_{35})\sin 2\Omega t + (\tfrac{1}{2}B_{25} - \tfrac{1}{2}B_{45})\cos 3\Omega t + (-\tfrac{1}{2}A_{25} + \tfrac{1}{2}A_{45})\sin 3\Omega t$$

$$M_{xF} = \tfrac{1}{2}A_{14} - \tfrac{1}{2}B_{10} + (\tfrac{1}{2}B_{24} - A_{05} + \tfrac{1}{2}A_{25})\sin\Omega t + (A_{04} + \tfrac{1}{2}A_{24} - \tfrac{1}{2}B_{26})\cos\Omega t + (\tfrac{1}{2}B_{14} + \tfrac{1}{2}B_{34} - \tfrac{1}{2}A_{15} + \tfrac{1}{2}A_{35})\sin 2\Omega t + (\tfrac{1}{2}A_{14} + \tfrac{1}{2}A_{34} + \tfrac{1}{2}B_{15} - \tfrac{1}{2}B_{35})\cos 2\Omega t + (\tfrac{1}{2}B_{24} + \tfrac{1}{2}B_{44} - \tfrac{1}{2}A_{25} + \tfrac{1}{2}A_{45})\sin 3\Omega t + (\tfrac{1}{2}A_{24} + \tfrac{1}{2}A_{44} + \tfrac{1}{2}B_{25} - \tfrac{1}{2}B_{45})\cos 3\Omega t$$

$$M_{yF} = \tfrac{1}{2}B_{14} + \tfrac{1}{2}B_{24}\cos\Omega t + (A_{04} - \tfrac{1}{2}A_{24})\sin\Omega t + (-\tfrac{1}{2}B_{14} + \tfrac{1}{2}B_{34})\cos 2\Omega t + (\tfrac{1}{2}A_{14} - \tfrac{1}{2}A_{34})\sin 2\Omega t + (-\tfrac{1}{2}B_{24} + \tfrac{1}{2}B_{44})\cos 3\Omega t + (\tfrac{1}{2}A_{24} - \tfrac{1}{2}A_{44})\sin 3\Omega t + \tfrac{1}{2}A_{15} + \tfrac{1}{2}B_{25}\sin\Omega t + (A_{05} + \tfrac{1}{2}A_{25})\cos\Omega t + (\tfrac{1}{2}B_{15} + \tfrac{1}{2}B_{35})\sin 2\Omega t + (\tfrac{1}{2}A_{15} + \tfrac{1}{2}A_{35})\cos 2\Omega t + (\tfrac{1}{2}B_{25} + \tfrac{1}{2}B_{45})\sin 3\Omega t + (\tfrac{1}{2}A_{25} + \tfrac{1}{2}A_{45})\cos 3\Omega t$$

$$M_{yF} = \tfrac{1}{2}B_{14} + \tfrac{1}{2}A_{15} + (A_{04} - \tfrac{1}{2}A_{24} + \tfrac{1}{2}B_{25})\sin\Omega t + (\tfrac{1}{2}B_{24} + A_{05} + \tfrac{1}{2}A_{25})\cos\Omega t + (\tfrac{1}{2}A_{14} - \tfrac{1}{2}A_{34} + \tfrac{1}{2}B_{15} + \tfrac{1}{2}B_{35})\sin 2\Omega t + (-\tfrac{1}{2}B_{14} + \tfrac{1}{2}B_{54} + \tfrac{1}{2}A_{15} + \tfrac{1}{2}A_{35})\cos 2\Omega t + (\tfrac{1}{2}A_{24} - \tfrac{1}{2}A_{44} + \tfrac{1}{2}B_{25} + \tfrac{1}{2}B_{45})\sin 3\Omega t + (-\tfrac{1}{2}B_{24} + \tfrac{1}{2}B_{44} + \tfrac{1}{2}A_{25} + \tfrac{1}{2}A_{45})\cos 3\Omega t$$

$$M_{zF} = A_{06} + A_{16}\cos\Omega t + B_{16}\sin\Omega t + A_{26}\cos 2\Omega t + B_{26}\sin 2\Omega t + A_{36}\cos 3\Omega t + B_{36}\sin 3\Omega t$$

Adding a third subscript F, to denote loads in the fixed system, the fixed system equations are,

$$F_{xF} = A_{01F} + A_{11F}\cos\Omega t + B_{11F}\sin\Omega t + A_{21F}\cos 2\Omega t + B_{21F}\sin 2\Omega t + A_{31F}\cos 3\Omega t + B_{31F}\sin 3\Omega t$$

$$F_{yF} = A_{02F} + A_{12F}\cos\Omega t + B_{12F}\sin\Omega t + A_{22F}\cos 2\Omega t + B_{22F}\sin 2\Omega t + A_{32F}\cos 3\Omega t + B_{32F}\sin 3\Omega t$$

$$F_{zF} = F_{03F} + A_{13F}\cos\Omega t + B_{13F}\sin\Omega t + A_{23F}\cos 2\Omega t + B_{23F}\sin 2\Omega t + A_{33F}\cos 3\Omega t + B_{33F}\sin 3\Omega t$$

$$M_{xF} = A_{04F} + A_{14F}\cos\Omega t + B_{14F}\sin\Omega t + A_{24F}\cos 2\Omega t + B_{24F}\sin 2\Omega t + A_{34F}\cos 3\Omega t + B_{34F}\sin 3\Omega t$$

$$M_{yF} = A_{05F} + A_{15F}\cos\Omega t + B_{15F}\sin\Omega t + A_{25F}\cos 2\Omega t + B_{25F}\sin 2\Omega t + A_{35F}\cos 3\Omega t + B_{35F}\sin 3\Omega t$$

$$M_{zF} = A_{06F} + A_{16F}\cos\Omega t + B_{16F}\sin\Omega t + A_{26F}\cos 2\Omega t + B_{26F}\sin 2\Omega t + A_{36F}\cos 3\Omega t + B_{36F}\sin 3\Omega t$$

Solving for fixed system coefficients in terms of rotating system coefficients,

STEADY

$$A_{01F} = \tfrac{1}{2}A_{11} - \tfrac{1}{2}B_{12}$$

$$A_{02F} = \tfrac{1}{2}B_{11} + \tfrac{1}{2}A_{12}$$

$$A_{03F} = A_{03}$$

$$A_{04F} = \tfrac{1}{2}A_{14} - \tfrac{1}{2}B_{15}$$

$$A_{05F} = \tfrac{1}{2}B_{14} + \tfrac{1}{2}A_{15}$$

$$A_{06F} = A_{06}$$

1ST HARMONIC

cos Terms

$A_{11F} = A_{01} + \frac{1}{2}A_{21} - \frac{1}{2}B_{22}$

$A_{12F} = A_{02} + \frac{1}{2}B_{21} + \frac{1}{2}A_{22}$

$A_{13F} = A_{13}$

$A_{14F} = A_{04} + \frac{1}{2}A_{24} - \frac{1}{2}B_{25}$

$A_{15F} = A_{05} + \frac{1}{2}B_{24} + \frac{1}{2}A_{25}$

$A_{16F} = A_{16}$

sin Terms

$B_{11F} = -A_{02} + \frac{1}{2}B_{21} + \frac{1}{2}A_{22}$

$B_{12F} = A_{01} - \frac{1}{2}A_{21} + \frac{1}{2}B_{22}$

$B_{13F} = B_{13}$

$B_{14F} = -A_{05} + \frac{1}{2}B_{24} + \frac{1}{2}A_{25}$

$B_{15F} = A_{04} - \frac{1}{2}A_{24} + \frac{1}{2}B_{25}$

$B_{16F} = B_{16}$

2ND HARMONIC

cos Terms

$A_{21F} = \frac{1}{2}A_{11} + \frac{1}{2}B_{12} + \frac{1}{2}A_{31} - \frac{1}{2}B_{32}$

$A_{22F} = -\frac{1}{2}B_{11} + \frac{1}{2}A_{12} + \frac{1}{2}B_{31} + \frac{1}{2}A_{32}$

$A_{23F} = A_{23}$

$A_{24F} = \frac{1}{2}A_{14} + \frac{1}{2}B_{15} + \frac{1}{2}A_{34} - \frac{1}{2}B_{35}$

$A_{25F} = -\frac{1}{2}B_{14} + \frac{1}{2}A_{15} + \frac{1}{2}B_{34} + \frac{1}{2}A_{35}$

$A_{26F} = A_{26}$

sin Terms

$B_{21F} = \frac{1}{2}B_{11} - \frac{1}{2}A_{12} + \frac{1}{2}B_{31} + \frac{1}{2}A_{32}$

$B_{22F} = \frac{1}{2}A_{11} + \frac{1}{2}B_{12} - \frac{1}{2}A_{31} + \frac{1}{2}B_{32}$

$B_{23F} = B_{23}$

$B_{24F} = \frac{1}{2}B_{14} - \frac{1}{2}A_{15} + \frac{1}{2}B_{34} + \frac{1}{2}A_{35}$

$B_{25F} = \frac{1}{2}A_{14} + \frac{1}{2}B_{15} - \frac{1}{2}A_{34} + \frac{1}{2}B_{35}$

$B_{26F} = B_{26}$

3RD HARMONIC

cos Terms

$A_{31F} = \frac{1}{2}A_{21} + \frac{1}{2}B_{22} + \frac{1}{2}A_{41} - \frac{1}{2}B_{42}$

$A_{32F} = -\frac{1}{2}B_{21} + \frac{1}{2}A_{22} + \frac{1}{2}B_{41} + \frac{1}{2}A_{42}$

$A_{33F} = A_{33}$

$A_{34F} = \frac{1}{2}A_{24} + \frac{1}{2}B_{25} + \frac{1}{2}A_{44} - \frac{1}{2}B_{45}$

$A_{35F} = -\frac{1}{2}B_{24} + \frac{1}{2}A_{25} + \frac{1}{2}B_{44} + \frac{1}{2}A_{45}$

$A_{36F} = A_{36}$

sin Terms

$B_{31F} = \frac{1}{2}B_{21} - \frac{1}{2}A_{22} + \frac{1}{2}B_{41} + \frac{1}{2}A_{42}$

$B_{32F} = \frac{1}{2}A_{21} + \frac{1}{2}B_{22} - \frac{1}{2}A_{41} + \frac{1}{2}B_{42}$

$B_{33F} = B_{33}$

$B_{34F} = \frac{1}{2}B_{24} - \frac{1}{2}A_{25} + \frac{1}{2}B_{44} + \frac{1}{2}A_{45}$

$B_{35F} = \frac{1}{2}A_{24} + \frac{1}{2}B_{25} - \frac{1}{2}A_{44} + \frac{1}{2}B_{45}$

$B_{36F} = B_{36}$

These coefficients convert the measured shaft loads from the rotating system to the fixed system.

The lateral and longitudinal motions of the rotor were measured by accelerometers located as shown in the following plan view of the rotor.

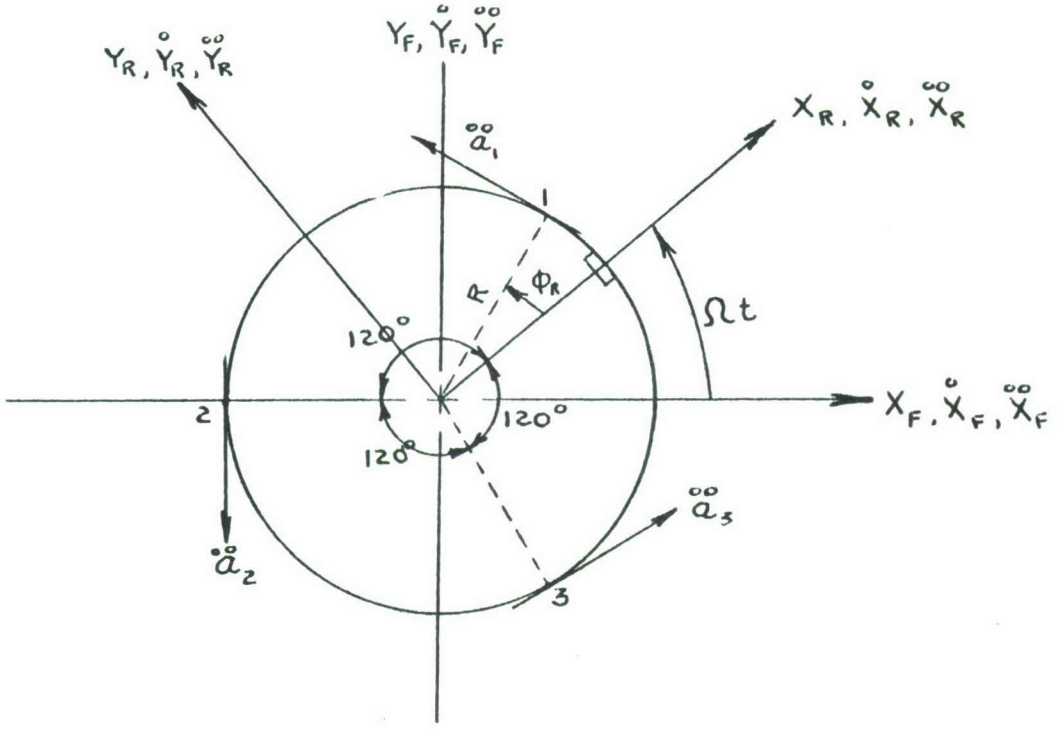

Forward Rotor

Let $\ddot{\gamma}$ = **shaft rotational acceleration**

Then,

$$\ddot{a}_1 = R\ddot{\gamma} - \ddot{x}_R \sin\Phi_R + \ddot{y}_R \cos\Phi_R$$

$$\ddot{a}_2 = R\ddot{\gamma} - \ddot{x}_R \sin(\Phi_R + 120^\circ) + \ddot{y}_R \cos(\Phi_R + 120^\circ)$$

$$\ddot{a}_3 = R\ddot{\gamma} - \ddot{x}_R \sin(\Phi_R + 240^\circ) + \ddot{y}_R \cos(\Phi_R + 120^\circ)$$

The measured values of acceleration must be corrected for a 1st harmonic acceleration resulting from a steady gravity force. The in-plane effect of gravity produced by a steady pitching attitude is shown in the following diagrams.

Letting β = pitching attitude, nose down positive

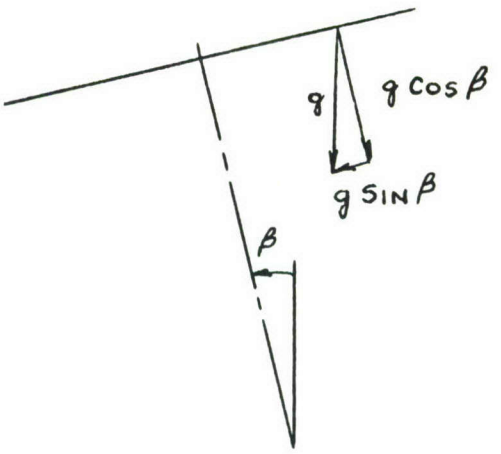

Considering the effect of g sin β on the in-plane accelerations of the system

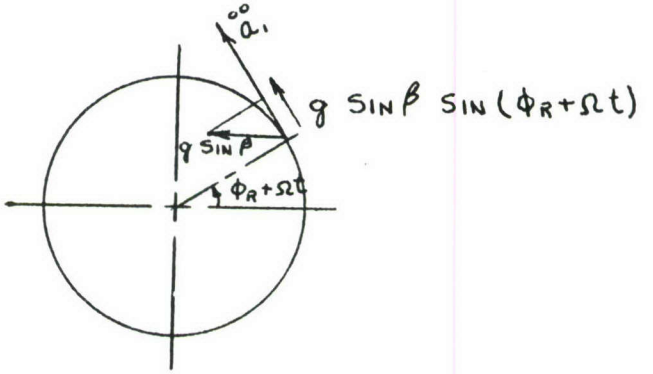

Then, the in-plane acceleration becomes,

$$\ddot{a}_1 = \underset{\text{(measured)}}{\ddot{\bar{a}}_1} - g \sin\beta \sin(\phi_R + \Omega t)$$

$$\ddot{a}_2 = \underset{\text{(measured)}}{\ddot{\bar{a}}_2} - g \sin\beta \sin(120^\circ + \phi_R + \Omega t)$$

$$\ddot{a}_3 = \underset{\text{(measured)}}{\ddot{\bar{a}}_3} - g \sin\beta \sin(240^\circ + \phi_R + \Omega t)$$

or

$$\ddot{a}_1 = \ddot{\bar{a}}_1 - g \sin\beta \sin\phi_R \cos\Omega t - g \sin\beta \cos\phi_R \sin\Omega t$$

$$\ddot{a}_2 = \ddot{\bar{a}}_2 - g \sin\beta \sin(\phi_R + 120^\circ) \cos\Omega t - g \sin\beta \cos(\phi_R + 120^\circ) \sin\Omega t$$

$$\ddot{a}_3 = \ddot{\bar{a}}_3 - g \sin\beta \sin(\phi_R + 240^\circ) \cos\Omega t - g \sin\beta \cos(\phi_R + 240^\circ) \sin\Omega t$$

Letting the measured accelerations be of the form,

$$\ddot{a}_1 = \ddot{a}_{1-0} + \ddot{a}_{1-1}\cos\Omega t + \ddot{b}_{1-1}\sin\Omega t + \ddot{a}_{1-2}\cos 2\Omega t + \ddot{b}_{1-2}\sin 2\Omega t + \ddot{a}_{1-3}\cos 3\Omega t + \ddot{b}_{1-3}\sin 3\Omega t + \ddot{a}_{1-4}\cos 4\Omega t + \ddot{b}_{1-4}\sin 4\Omega t$$

$$\ddot{a}_2 = \ddot{a}_{2-0} + \ddot{a}_{2-1}\cos\Omega t + \ddot{b}_{2-1}\sin\Omega t + \ddot{a}_{2-2}\cos 2\Omega t + \ddot{b}_{2-2}\sin 2\Omega t + \ddot{a}_{2-3}\cos 3\Omega t + \ddot{b}_{2-3}\sin 3\Omega t + \ddot{a}_{2-4}\cos 4\Omega t + \ddot{b}_{2-4}\sin 4\Omega t$$

$$\ddot{a}_3 = \ddot{a}_{3-0} + \ddot{a}_{3-1}\cos\Omega t + \ddot{b}_{3-1}\sin\Omega t + \ddot{a}_{3-2}\cos 2\Omega t + \ddot{b}_{3-2}\sin 2\Omega t + \ddot{a}_{3-3}\cos 3\Omega t + \ddot{b}_{3-3}\sin 3\Omega t + \ddot{a}_{3-4}\cos 4\Omega t + \ddot{b}_{3-4}\sin 4\Omega t$$

Subtracting the 1/rev effect of the steady g loading,

$$\ddot{a}_1 = \ddot{a}_{1-0} + \left[\ddot{a}_{1-1} - g\sin\beta\sin\phi_R\right]\cos\Omega t + \left[\ddot{b}_{1-1} - g\sin\beta\cos\phi_R\right]\sin\Omega t + \ddot{a}_{1-2}\cos 2\Omega t + \ddot{b}_{1-2}\sin 2\Omega t + \ddot{a}_{1-3}\cos 3\Omega t + \ddot{b}_{1-3}\sin 3\Omega t + \ddot{a}_{1-4}\cos 4\Omega t + \ddot{b}_{1-4}\sin 4\Omega t$$

$$\ddot{a}_2 = \ddot{a}_{2-0} + \left[\ddot{a}_{2-1} - g\sin\beta\sin(\phi_R + 120^\circ)\right]\cos\Omega t + \left[\ddot{b}_{2-1} - g\sin\beta\cos(\phi_R + 120^\circ)\right]\sin\Omega t + \ddot{a}_{2-2}\cos 2\Omega t + \ddot{b}_{2-2}\sin 2\Omega t + \ddot{a}_{2-3}\cos 3\Omega t + \ddot{b}_{2-3}\sin 3\Omega t + \ddot{a}_{2-4}\cos 4\Omega t + \ddot{b}_{2-4}\sin 4\Omega t$$

$$\ddot{a}_3 = \ddot{a}_{3-0} + \ddot{a}_{3-1} - g\sin\beta\sin(\phi_R + 120^\circ)\cos\Omega t + \ddot{b}_{3-1} - g\sin\beta\cos(\phi_R + 120^\circ)\sin\Omega t + \ddot{a}_{3-2}\cos 2\Omega t + \ddot{b}_{3-2}\sin 2\Omega t + \ddot{a}_{3-3}\cos 3\Omega t + \ddot{b}_{3-3}\sin 3\Omega t + \ddot{a}_{3-4}\cos 4\Omega t + \ddot{b}_{3-4}\sin 4\Omega t$$

Rewriting the equations of actual in-plane accelerations in matrix form,

$$\begin{bmatrix} \ddot{a}_1 \\ \ddot{a}_2 \\ \ddot{a}_3 \end{bmatrix} = \begin{bmatrix} -\sin\phi_R & \cos\phi_R & R \\ -\sin(\phi_R + 120^\circ) & \cos(\phi_R + 120^\circ) & R \\ -\sin(\phi_R + 240^\circ) & \cos(\phi_R + 240^\circ) & R \end{bmatrix} \begin{bmatrix} \ddot{X}_R \\ \ddot{Y}_R \\ \ddot{\gamma} \end{bmatrix}$$

Solving for $\ddot{X}_R$, $\ddot{Y}_R$, $\ddot{\gamma}$

Evaluating the determinant of the coefficients, $|C|$,

$$|C| = -\sin\phi_R \left[R\cos(\phi_R + 120^\circ) - R\cos(\phi_R + 240^\circ)\right]$$
$$- \cos\phi_R \left[-R\sin(\phi_R + 120^\circ) + R\sin(\phi_R + 240^\circ)\right]$$
$$R\left[-\sin(\phi_R + 120^\circ)\cos(\phi_R + 240^\circ) + \sin(\phi_R + 240^\circ)\cos(\phi_R + 120^\circ)\right]$$

$$|C| = -R\sin\phi_R \cos(\phi_R + 120^\circ) + R\sin\phi_R \cos(\phi_R + 240^\circ)$$
$$+R\cos\phi_R \sin(\phi_R + 120^\circ) - R\cos\phi_R \sin(\phi_R + 240^\circ)$$
$$-R\sin(\phi_R + 120^\circ)\cos(\phi_R + 240^\circ) + R\cos(\phi_R + 120^\circ)\sin(\phi_R + 240^\circ)$$

$$|C| = -\tfrac{1}{2}R\sin(-120^\circ) + \tfrac{1}{2}R\sin(-240^\circ) + \tfrac{1}{2}R\sin 120^\circ - \tfrac{1}{2}R\sin 240^\circ$$
$$-\tfrac{1}{2}R\sin(-120^\circ) + \tfrac{1}{2}R\sin(120^\circ)$$

$$|C| = \tfrac{1}{2}R\left[\sin 120^\circ - \sin 240^\circ + \sin 120^\circ - \sin 240^\circ + \sin 120^\circ + \sin 120^\circ\right]$$

$$|C| = \tfrac{1}{2}R\left[\tfrac{1}{2}\sqrt{3} - (-\tfrac{1}{2}\sqrt{3}) + \tfrac{1}{2}\sqrt{3} - (-\tfrac{1}{2}\sqrt{3}) + \tfrac{1}{2}\sqrt{3} + \tfrac{1}{2}\sqrt{3}\right]$$

$$|C| = \tfrac{1}{2}R \quad 6\,(\tfrac{1}{2}\sqrt{3}) = \tfrac{1}{2}3\sqrt{3}\ R = \tfrac{1}{2}9R\frac{1}{\sqrt{3}}$$

Solving for $\overset{\circ\circ}{x}_R$

$$\overset{\circ\circ}{x}_R = \frac{\begin{vmatrix} \overset{\circ\circ}{a}_1 & \cos\phi_R & R \\ \overset{\circ\circ}{a}_2 & \cos(\phi_R + 120^\circ) & R \\ \overset{\circ\circ}{a}_3 & \cos(\phi_R + 240^\circ) & R \end{vmatrix}}{\frac{9R}{2\sqrt{3}}} = \frac{2\sqrt{3}}{9R} \begin{vmatrix} \overset{\circ\circ}{a}_1 & \cos\phi_R & R \\ \overset{\circ\circ}{a}_2 & \cos(\phi_R + 120^\circ) & R \\ \overset{\circ\circ}{a}_3 & \cos(\phi_R + 240^\circ) & R \end{vmatrix}$$

$$\overset{\circ\circ}{x}_R = \frac{2\sqrt{3}}{9R}\left\{\overset{\circ\circ}{a}_1\left[R\cos(\phi_R + 120^\circ) - R\cos(\phi_R + 240^\circ)\right] - \overset{\circ\circ}{a}_2\left[R\cos\phi_R - R\cos(\phi_R + 240^\circ)\right]\right.$$
$$\left. + \overset{\circ\circ}{a}_3\left[R\cos(\phi_R) - R\cos(\phi_R + 120^\circ)\right]\right\}$$

$$\overset{oo}{x}_R = \frac{2\sqrt{3}}{9}\left\{\overset{oo}{a}_1\left[\cos\phi_R\cos 120^o - \sin\phi_R \sin 120^o - \cos\phi_R \cos 240^o + \sin\phi_R\sin 240^o\right]\right.$$

$$-\overset{oo}{a}_2\left[\cos\phi_R - \cos\phi_R \cos 240^o + \sin\phi_R \sin 240^o\right]$$

$$\left.+\overset{oo}{a}_3\left[\cos\phi_R - \cos\phi_R \cos 120^o + \sin\phi_R \sin 120^o\right]\right\}$$

$$\overset{oo}{x}_R = \frac{2\sqrt{3}}{9}\left\{\overset{oo}{a}_1\left[(-\sqrt{3})\sin\phi_R\right] - \overset{oo}{a}_2\left[\frac{3}{2}\cos\phi_R - \frac{\sqrt{3}}{2}\sin\phi_R\right] + \overset{oo}{a}_3\left[\frac{3}{2}\cos\phi_R + \frac{\sqrt{3}}{2}\sin\phi_R\right]\right\}$$

$$\overset{oo}{x}_R = \left[-\frac{2}{3}\sin\phi_R\right]\overset{oo}{a}_1 + \left[-\frac{\sqrt{3}}{3}\cos\phi_R + \frac{1}{3}\sin\phi_R\right]\overset{oo}{a}_2 + \left[\frac{\sqrt{3}}{3}\cos\phi_R + \frac{1}{3}\sin\phi_R\right]\overset{oo}{a}_3$$

Solving for $\overset{oo}{y}_R$

$$\overset{oo}{y}_R = \frac{2\sqrt{3}}{9R}\begin{vmatrix} -\sin\phi_R & \overset{oo}{a}_1 & R \\ -\sin(\phi_R + 120^o) & \overset{oo}{a}_2 & R \\ -\sin(\phi_R + 240^o) & \overset{oo}{a}_3 & R \end{vmatrix}$$

$$\overset{oo}{y}_R = \frac{2\sqrt{3}}{9R}\left\{-\sin\phi_R\left[\overset{oo}{a}_2 R - \overset{oo}{a}_3 R\right] + \sin(\phi_R + 120^o)\left[\overset{oo}{a}_1 R - \overset{oo}{a}_3 R\right]\right.$$

$$\left.-\sin(\phi_R + 240^o)\left[\overset{oo}{a}_1 R - \overset{oo}{a}_2 R\right]\right\}$$

$$\overset{oo}{y}_R = \frac{2\sqrt{3}}{9}\overset{oo}{a}_1\left[\sin(\phi_R + 120^o) - \sin(\phi_R + 240^o)\right] + \overset{oo}{a}_2\left[\sin(\phi_R + 240^o) - \sin\phi_R\right]$$

$$+ \overset{oo}{a}_3\left[\sin\phi_R - \sin(\phi_R + 120^o)\right]$$

$$\overset{oo}{y}_R = \frac{2\sqrt{3}}{9}\left\{\overset{oo}{a}_1\left[\sin\phi_R \cos 120^o + \cos\phi_R \sin 120^o - \sin\phi_R \cos 240^o - \cos\phi_R \sin 240^o\right]\right.$$

$$+ \overset{oo}{a}_2\left[\sin\phi_R \cos 240^o + \cos\phi_R \sin 240^o - \sin\phi_R\right]$$

$$\left.+ \overset{oo}{a}_3\left[\sin\phi_R - \sin\phi_R \cos 120^o - \cos\phi_R \sin 120^o\right]\right\}$$

$$\overset{oo}{y}_R = \frac{2\sqrt{3}}{9}\left\{\overset{oo}{a}_1\left[-\frac{1}{2}\sin\phi_R + \frac{\sqrt{3}}{2}\cos\phi_R + \frac{1}{2}\sin\phi_R + \frac{\sqrt{3}}{2}\cos\phi_R\right]\right.$$

$$\left.+ \overset{oo}{a}_2\left[-\frac{1}{2}\sin\phi_R - \frac{\sqrt{3}}{2}\cos\phi_R - \sin\phi_R\right] + \overset{oo}{a}_3\left[\sin\phi_R + \frac{1}{2}\sin\phi_R - \frac{\sqrt{3}}{2}\cos\phi_R\right]\right\}$$

$$\overset{oo}{y}_R = \frac{2\sqrt{3}}{9}\left\{\overset{oo}{a}_1\left[\sqrt{3}\cos\phi_R\right] + a\left[-\frac{3}{2}\sin\phi_R - \frac{\sqrt{3}}{2}\cos\phi_R\right] + a\left[+\frac{3}{2}\sin\phi_R - \frac{\sqrt{3}}{2}\cos\phi_R\right]\right\}$$

$$\overset{oo}{y}_R = \frac{2}{3}\cos\phi_R \times \overset{oo}{a}_1 + \left[-\frac{\sqrt{3}}{3}\sin\phi_R - \frac{1}{3}\cos\phi_R\right]\overset{oo}{a}_2 + \left[\frac{\sqrt{3}}{3}\sin\phi_R - \frac{1}{3}\cos\phi_R\right]\overset{oo}{a}_3$$

Solving for $\overset{\circ\circ}{\gamma}_R$

$$\overset{\circ\circ}{\gamma}_R = \frac{2\sqrt{3}}{9R}\begin{vmatrix} -\sin\Phi_R & \cos\Phi_R & \overset{\circ\circ}{a}_1 \\ -\sin(\Phi_R + 120^\circ) & \cos(\Phi_R + 120^\circ) & \overset{\circ\circ}{a}_2 \\ -\sin(\Phi_R + 240^\circ) & \cos(\Phi_R + 240^\circ) & \overset{\circ\circ}{a}_3 \end{vmatrix}$$

$$\overset{\circ\circ}{\gamma}_R = \frac{2\sqrt{3}}{9R}\Big\{\overset{\circ\circ}{a}_1\left[-\sin(\Phi_R + 120^\circ)\cos(\Phi_R + 240^\circ) + \sin(\Phi_R + 240^\circ)\cos(\Phi_R + 120^\circ)\right]$$

$$+ \overset{\circ\circ}{a}_2\left[+\sin\Phi_R\cos(\Phi_R + 240^\circ) - \cos\Phi_R\sin(\Phi_R + 240^\circ)\right]$$

$$+ \overset{\circ\circ}{a}_3\left[-\sin\Phi_R\cos(\Phi_R + 120^\circ) + \sin(\Phi_R + 120^\circ)\cos\Phi_R\right]\Big\}$$

$$\overset{\circ\circ}{\gamma}_R = \frac{2\sqrt{3}}{9R}\Big\{\overset{\circ\circ}{a}_1\left[-\frac{1}{2}\sin(360^\circ + 2\Phi_R) + \sin(-120^\circ) + \frac{1}{2}\sin(360^\circ + 2\Phi_R) + \sin(120^\circ)\right]$$

$$+ \overset{\circ\circ}{a}_2\left[\frac{1}{2}\sin(240^\circ + 2\Phi_R) + \sin(-240^\circ) - \frac{1}{2}\sin(240^\circ + 2\Phi_R) + \sin(240^\circ)\right]$$

$$+ \overset{\circ\circ}{a}_3\left[-\frac{1}{2}\sin(120^\circ + 2\Phi_R) + \sin(-120^\circ) + \frac{1}{2}\sin(120^\circ + 2\Phi_R) + \sin 120^\circ\right]\Big\}$$

$$\overset{\circ\circ}{\gamma}_R = \frac{2\sqrt{3}}{9R}\Big\{\overset{\circ\circ}{a}_1\left[\frac{1}{2}\sin 120^\circ + \frac{1}{2}\sin 120^\circ\right] + \overset{\circ\circ}{a}_2\left[-\frac{1}{2}\sin 240^\circ - \frac{1}{2}\sin 240^\circ\right]$$

$$+ \overset{\circ\circ}{a}_3\left[+\frac{1}{2}\sin 120^\circ + \frac{1}{2}\sin 120^\circ\right]\Big\}$$

$$\overset{\circ\circ}{\gamma}_R = \frac{2\sqrt{3}}{9R}\left\{\frac{\sqrt{3}}{2}\overset{\circ\circ}{a}_1 + \frac{\sqrt{3}}{2}\overset{\circ\circ}{a}_2 + \frac{\sqrt{3}}{2}\overset{\circ\circ}{a}_3\right\}$$

$$\overset{\circ\circ}{\gamma}_R = \frac{2\sqrt{3}\sqrt{3}}{9\cdot 2\,R}\left\{\overset{\circ\circ}{a}_1 + \overset{\circ\circ}{a}_2 + \overset{\circ\circ}{a}_3\right\}$$

$$R = \frac{1}{3R}\left\{\overset{\circ\circ}{a}_1 + \overset{\circ\circ}{a}_2 + \overset{\circ\circ}{a}_3\right\}$$

Therefore the coefficient of the Fourier Series can be converted from the actual test location to the rotating axes by

$$\begin{bmatrix} \overset{\circ\circ}{x}_R \\ \overset{\circ\circ}{y}_R \\ \overset{\circ\circ}{\gamma} \end{bmatrix} = \left[\begin{array}{c|c|c} -\frac{2}{3}\sin\Phi_R & -\frac{\sqrt{3}}{3}\cos\Phi_R + \frac{1}{3}\sin\Phi_R & \frac{\sqrt{3}}{3}\cos\Phi_R + \frac{1}{3}\sin\Phi_R \\ \frac{2}{3}\cos\Phi_R & -\frac{\sqrt{3}}{3}\sin\Phi_R - \frac{1}{3}\cos\Phi_R & \frac{\sqrt{3}}{3}\sin\Phi_R - \frac{1}{3}\cos\Phi_R \\ \frac{1}{3R} & \frac{1}{3R} & \frac{1}{3R} \end{array}\right] \begin{bmatrix} \overset{\circ\circ}{a}_1 \\ \overset{\circ\circ}{a}_2 \\ \overset{\circ\circ}{a}_3 \end{bmatrix}$$

Consider the following final form of the x_R, y_R, and γ_R acceleration equations in the rotating system.

$$\ddot{x}_R = \ddot{A}_{01} + \ddot{A}_{11}\cos\Omega t + \ddot{B}_{11}\sin\Omega t + \ddot{A}_{21}\cos 2\Omega t + \ddot{B}_{21}\sin 2\Omega t + \ddot{A}_{31}\cos 3\Omega t + \ddot{B}_{31}\sin 3\Omega t + \ddot{A}_{41}\cos 4\Omega t + \ddot{B}_{41}\sin 4\Omega t$$

$$\ddot{y}_R = \ddot{A}_{02} + \ddot{A}_{12}\cos\Omega t + \ddot{B}_{12}\sin\Omega t + \ddot{A}_{22}\cos 2\Omega t + \ddot{B}_{22}\sin 2\Omega t + \ddot{A}_{32}\cos 3\Omega t + \ddot{B}_{32}\sin 3\Omega t + \ddot{A}_{42}\cos 4\Omega t + \ddot{B}_{42}\sin 4\Omega t$$

$$\ddot{\gamma}_R = \ddot{A}_{06} + \ddot{A}_{16}\cos\Omega t + \ddot{B}_{16}\sin\Omega t + \ddot{A}_{26}\cos 2\Omega t + \ddot{B}_{26}\sin 2\Omega t + \ddot{A}_{36}\cos 3\Omega t + \ddot{B}_{36}\sin 3\Omega t + \ddot{A}_{46}\cos 4\Omega t + \ddot{B}_{46}\sin 4\Omega t$$

Consider the following acceleration equations in the fixed system, where α_F, β_F are the angular coordinates along the corresponding x and y axis in the fixed system.

$$\ddot{x}_F = \ddot{A}_{01F} + \ddot{A}_{11F}\cos\Omega t + \ddot{B}_{11F}\sin\Omega t + \ddot{A}_{21F}\cos 2\Omega t + \ddot{B}_{21F}\sin 2\Omega t + \ddot{A}_{31F}\cos 3\Omega t + \ddot{B}_{31F}\sin 3\Omega t$$

$$\ddot{y}_F = \ddot{A}_{02F} + \ddot{A}_{12F}\cos\Omega t + \ddot{B}_{12F}\sin\Omega t + \ddot{A}_{22F}\cos 2\Omega t + \ddot{B}_{22F}\sin 2\Omega t + \ddot{A}_{23F}\cos 3\Omega t + \ddot{B}_{23F}\sin 3\Omega t$$

$$\ddot{z}_F = \ddot{A}_{03F} + \ddot{A}_{13F}\cos\Omega t + \ddot{B}_{13F}\sin\Omega t + \ddot{A}_{23F}\cos 2\Omega t + \ddot{B}_{23}\sin 2\Omega t + \ddot{A}_{33F}\cos 3\Omega t + \ddot{B}_{33F}\sin 3\Omega t$$

$$\ddot{\alpha}_F = \ddot{A}_{04F} + \ddot{A}_{14F}\cos\Omega t + \ddot{B}_{14F}\sin\Omega t + \ddot{A}_{24F}\cos 2\Omega t + \ddot{B}_{24F}\sin 2\Omega t + \ddot{A}_{34F}\cos 3\Omega t + \ddot{B}_{34F}\sin 3\Omega t$$

$$\ddot{\beta}_F = \ddot{A}_{05F} + \ddot{A}_{15F}\cos\Omega t + \ddot{B}_{15F}\sin\Omega t + \ddot{A}_{25F}\cos 2\Omega t + \ddot{B}_{25F}\sin 2\Omega t + \ddot{A}_{35F}\cos 3\Omega t + \ddot{B}_{35F}\sin 3\Omega t$$

$$\ddot{\gamma}_F = \ddot{A}_{06F} + \ddot{A}_{16F}\cos\Omega t + \ddot{B}_{16F}\sin\Omega t + \ddot{A}_{26F}\cos 2\Omega t + \ddot{B}_{26F}\sin 2\Omega t + \ddot{A}_{36F}\cos 3\Omega t + \ddot{B}_{36F}\sin 3\Omega t$$

Considering the $\ddot{x}_F$, $\ddot{y}_F$ rotor hub accelerations in the fixed system and the fixed system linear acceleration equations of the transmission upper bearing.

From Page 86.

$$\ddot{x}_F = \ddot{A}_{01F} + \ddot{A}_{11F}\cos\Omega t + \ddot{B}_{11F}\sin\Omega t + \ddot{A}_{21F}\cos 2\Omega t + \ddot{B}_{21F}\sin 2\Omega t + \ddot{A}_{31F}\cos 3\Omega t + \ddot{B}_{31F}\sin 3\Omega t$$

$$\ddot{y}_F = \ddot{A}_{02F} + \ddot{A}_{12F}\cos\Omega t + \ddot{B}_{12F}\sin\Omega t + \ddot{A}_{22F}\cos 2\Omega t + \ddot{B}_{22F}\sin 2\Omega t + \ddot{A}_{32F}\cos 3\Omega t + \ddot{B}_{32F}\sin\Omega t$$

And, letting the transmission upper bearing linear accelerations be represented as

$$\ddot{x}_{Fu} = \ddot{A}_{01Fu} + \ddot{A}_{11Fu}\cos\Omega t + \ddot{B}_{11Fu}\sin\Omega t + \ddot{A}_{21Fu}\cos\Omega t + \ddot{B}_{21Fu}\sin 2\Omega t + \ddot{A}_{31Fu}\cos 3\Omega t + \ddot{B}_{31Fu}\sin 3\Omega t$$

$$\ddot{y}_{Fu} = \ddot{A}_{02Fu} + \ddot{A}_{12Fu}\cos\Omega t + \ddot{B}_{12Fu}\sin\Omega t + \ddot{A}_{22Fu}\cos 2\Omega t + \ddot{B}_{22Fu}\sin 2\Omega t + \ddot{A}_{32Fu}\cos 3\Omega t + \ddot{B}_{32Fu}\sin 3\Omega t$$

Neglecting shaft flexibility, the coefficients of the $\ddot{\alpha}_F$, and $\ddot{\beta}_F$ angular acceleration equations, can be written as the difference between linear accelerations at the hub and upper transmission bearing divided by the distance, ℓ, between these locations.

$$\ddot{A}_{04F} = -\frac{\ddot{A}_{02F} - \ddot{A}_{02Fu}}{\ell} \qquad \ddot{A}_{05F} = \frac{\ddot{A}_{01F} - \ddot{A}_{01Fu}}{\ell}$$

$$\ddot{A}_{14F} = -\frac{\ddot{A}_{12F} - \ddot{A}_{12Fu}}{\ell} \qquad \ddot{A}_{15F} = \frac{\ddot{A}_{11F} - \ddot{A}_{11Fu}}{\ell}$$

$$\ddot{B}_{14F} = -\frac{\ddot{B}_{12F} - \ddot{B}_{12Fu}}{\ell} \qquad \ddot{B}_{15F} = \frac{\ddot{B}_{11F} - \ddot{B}_{11Fu}}{\ell}$$

$$\ddot{A}_{24F} = -\frac{\ddot{A}_{22F} - \ddot{A}_{22Fu}}{\ell} \qquad \ddot{A}_{25F} = \frac{\ddot{A}_{21F} - \ddot{A}_{21Fu}}{\ell}$$

$$\ddot{B}_{24F} = -\frac{\ddot{B}_{22F} - \ddot{B}_{22Fu}}{\ell} \qquad \ddot{B}_{25F} = \frac{\ddot{B}_{21F} - \ddot{B}_{21Fu}}{\ell}$$

$$\ddot{A}_{34F} = -\frac{\ddot{A}_{32F} - \ddot{A}_{32Fu}}{\ell} \qquad \ddot{A}_{35F} = \frac{\ddot{A}_{31F} - \ddot{A}_{31Fu}}{\ell}$$

$$\ddot{B}_{34F} = -\frac{\ddot{B}_{32F} - \ddot{B}_{32Fu}}{\ell} \qquad \ddot{B}_{36F} = \frac{\ddot{B}_{31F} - \ddot{B}_{31Fu}}{\ell}$$

For the forward rotor, from Pages 78 and 79 and knowing that the coefficients for α , β , and z accelerations are determined using data measured in the fixed system, the Fourier Series coefficients in the fixed system become,

STEADY

$$\overset{oo}{A}_{01F} = \tfrac{1}{2}\overset{oo}{A}_{11} - \tfrac{1}{2}\overset{oo}{B}_{12}$$

$$\overset{oo}{A}_{02F} = \tfrac{1}{2}\overset{oo}{B}_{11} + \tfrac{1}{2}\overset{oo}{A}_{12}$$

$$\overset{oo}{A}_{03F} = \overset{oo}{A}_{03F}$$

$$\left.\begin{matrix}\overset{oo}{A}_{04F} = \\ \overset{oo}{A}_{05F} =\end{matrix}\right\}\text{See Pg. 87}$$

$$\overset{oo}{A}_{06F} + \overset{oo}{A}_{06}$$

1ST HARMONIC

cos Terms

$$\overset{oo}{A}_{11F} = \overset{oo}{A}_{01} + \tfrac{1}{2}\overset{oo}{A}_{21} - \tfrac{1}{2}\overset{oo}{B}_{22}$$

$$\overset{oo}{A}_{12F} = \overset{oo}{A}_{02} + \tfrac{1}{2}\overset{oo}{B}_{21} + \tfrac{1}{2}\overset{oo}{A}_{22}$$

$$\overset{oo}{A}_{13F} = \overset{oo}{A}_{13F}$$

$$\left.\begin{matrix}\overset{oo}{A}_{14F} = \\ \overset{oo}{A}_{15F} =\end{matrix}\right\}\text{See Pg.87}$$

$$\overset{oo}{A}_{16F} = \overset{oo}{A}_{16}$$

sin Terms

$$\overset{oo}{B}_{11F} = -\overset{oo}{A}_{02} + \tfrac{1}{2}\overset{oo}{B}_{21} + \tfrac{1}{2}\overset{oo}{A}_{22}$$

$$\overset{oo}{B}_{12F} = \overset{oo}{A}_{01} - \tfrac{1}{2}\overset{oo}{A}_{21} + \tfrac{1}{2}\overset{oo}{B}_{22}$$

$$\overset{oo}{B}_{13F} = \overset{oo}{B}_{13F}$$

$$\left.\begin{matrix}\overset{oo}{B}_{14F} = \\ \overset{oo}{B}_{15F} =\end{matrix}\right\}\text{See Pg. 87}$$

$$\overset{oo}{B}_{16F} = \overset{oo}{B}_{16}$$

2ND HARMONIC

cos Terms

$$\overset{oo}{A}_{21F} = \tfrac{1}{2}\overset{oo}{A}_{11} + \tfrac{1}{2}\overset{oo}{B}_{12} + \tfrac{1}{2}\overset{oo}{A}_{31} - \tfrac{1}{2}\overset{oo}{B}_{32}$$

$$\overset{oo}{A}_{22F} = -\tfrac{1}{2}\overset{oo}{B}_{11} + \tfrac{1}{2}\overset{oo}{A}_{12} + \tfrac{1}{2}\overset{oo}{B}_{31} + \tfrac{1}{2}\overset{oo}{A}_{32}$$

$$\overset{oo}{A}_{23F} = \overset{oo}{A}_{23F}$$

$$\left.\begin{matrix}\overset{oo}{A}_{24F} = \\ \overset{oo}{A}_{25F} =\end{matrix}\right\}\text{See Pg.87}$$

$$\overset{oo}{A}_{26F} = \overset{oo}{A}_{26}$$

sin Terms

$$\overset{oo}{B}_{21F} = \tfrac{1}{2}\overset{oo}{B}_{11} - \tfrac{1}{2}\overset{oo}{A}_{12} + \tfrac{1}{2}\overset{oo}{B}_{31} + \tfrac{1}{2}\overset{oo}{A}_{32}$$

$$\overset{oo}{B}_{22F} = \tfrac{1}{2}\overset{oo}{A}_{11} + \tfrac{1}{2}\overset{oo}{B}_{12} - \tfrac{1}{2}\overset{oo}{A}_{31} + \tfrac{1}{2}\overset{oo}{B}_{32}$$

$$\overset{oo}{B}_{23F} = \overset{oo}{B}_{23F}$$

$$\left.\begin{matrix}\overset{oo}{B}_{24F} = \\ \overset{oo}{B}_{25F} =\end{matrix}\right\}\text{See Pg. 87}$$

$$\overset{oo}{B}_{26F} = \overset{oo}{B}_{26}$$

Fixed System Acceleration Coefficients (Continued)

3RD HARMONIC

cos Terms

$$A^{oo}_{31F} + \tfrac{1}{2}A^{oo}_{21} + \tfrac{1}{2}B^{oo}_{22} + \tfrac{1}{2}A^{oo}_{41} - \tfrac{1}{2}B^{oo}_{42}$$

$$A^{oo}_{32F} = -\tfrac{1}{2}B^{oo}_{21} + \tfrac{1}{2}A^{oo}_{22} + \tfrac{1}{2}B^{oo}_{41} + \tfrac{1}{2}A^{oo}_{42}$$

$$A^{oo}_{33F} = A^{oo}_{33F}$$

$$\left.\begin{matrix} A^{oo}_{34F} = \\ A^{oo}_{35F} = \end{matrix}\right\} \text{See Pg. 87}$$

$$A^{oo}_{36F} = A^{oo}_{36}$$

sin Terms

$$B^{oo}_{31F} = \tfrac{1}{2}B^{oo}_{21} - \tfrac{1}{2}A^{oo}_{22} + \tfrac{1}{2}B^{oo}_{41} + \tfrac{1}{2}A^{oo}_{42}$$

$$B^{oo}_{32F} = \tfrac{1}{2}A^{oo}_{21} + \tfrac{1}{2}B^{oo}_{22} - \tfrac{1}{2}A^{oo}_{41} + \tfrac{1}{2}B^{oo}_{42}$$

$$B^{oo}_{33F} = B^{oo}_{33F}$$

$$\left.\begin{matrix} B^{oo}_{34F} = \\ B^{oo}_{35F} = \end{matrix}\right\} \text{See Pg. 87}$$

$$B^{oo}_{36F} = B^{oo}_{36}$$

APPENDIX B

ROTOR SHAFT LOAD IN THE FIXED SYSTEM

ACTING ON THE HELICOPTER

AFT ROTOR

For the aft rotor, the forces and moments acting on the helicopter in the rotating system below the rotor are obtained by the same procedure as that used on the forward rotor. The coefficients of the pitch link and shaft can be combined by the procedure on Page 74, namely:

$$\begin{bmatrix} F_{xRT} \\ F_{yRT} \\ F_{zRT} \\ M_{xRT} \\ M_{yRT} \\ M_{zRT} \end{bmatrix} = \left[\begin{array}{c|c|c|c|c|c|c|c|c} 1 & & & & & & & & \\ & 1 & & & & & & & \\ & & 1 & & & & & & \\ & & & 1 & & & 1 & 1 & 1 \\ & & & & 1 & & P_{1y} & P_{2y} & -P_{3y} \\ & & & & & 1 & -P_{1x} & P_{2x} & P_{3x} \end{array}\right] \begin{bmatrix} F_{xR} \\ F_{yR} \\ F_{zR} \\ M_{xR} \\ M_{yR} \\ M_{zR} \\ F_{zRp1} \\ F_{zRP2} \\ F_{zRP3} \end{bmatrix}$$

The aft rotor fixed system loads are obtained by the same procedure as the forward rotor with the one exception of using a negative rotational speed as the rotor rotates contrary to the established sign convention. Using this method derived on Page 75, the fixed system load equations can be written as,

Load equations in the fixed system -

$$F_{xF} = \tfrac{1}{2}A_{11} + \tfrac{1}{2}B_{12} + (\tfrac{1}{2}B_{21} + A_{02} - \tfrac{1}{2}A_{22}) \sin\Omega t + (A_{01} + \tfrac{1}{2}A_{21} + \tfrac{1}{2}B_{22}) \cos\Omega t$$
$$+ (\tfrac{1}{2}B_{11} + \tfrac{1}{2}B_{31} + \tfrac{1}{2}A_{12} - \tfrac{1}{2}A_{32}) \sin 2\Omega t + (\tfrac{1}{2}A_{11} + \tfrac{1}{2}A_{31} - \tfrac{1}{2}B_{12} + \tfrac{1}{2}B_{32}) \cos 2\Omega t$$
$$+ (\tfrac{1}{2}B_{21} + \tfrac{1}{2}B_{41} + \tfrac{1}{2}A_{22} - \tfrac{1}{2}A_{42}) \sin 3\Omega t + (\tfrac{1}{2}A_{21} + \tfrac{1}{2}A_{41} - \tfrac{1}{2}B_{22} + \tfrac{1}{2}B_{42}) \cos 3\Omega t$$

$$F_{yF} = -\tfrac{1}{2}B_{11} + \tfrac{1}{2}A_{12} + (-A_{01} + \tfrac{1}{2}A_{21} + \tfrac{1}{2}B_{22}) \sin\Omega t + (-\tfrac{1}{2}B_{21} + A_{02} + \tfrac{1}{2}A_{22}) \cos\Omega t$$
$$+ (-\tfrac{1}{2}A_{11} + \tfrac{1}{2}A_{31} + \tfrac{1}{2}B_{12} + \tfrac{1}{2}B_{32}) \sin 2\Omega t + (\tfrac{1}{2}B_{11} - \tfrac{1}{2}B_{31} + \tfrac{1}{2}A_{12} + \tfrac{1}{2}A_{32}) \cos 2\Omega t$$
$$+ (-\tfrac{1}{2}A_{21} + \tfrac{1}{2}A_{41} + \tfrac{1}{2}B_{22} + \tfrac{1}{2}B_{42}) \sin 3\Omega t + (\tfrac{1}{2}B_{21} - \tfrac{1}{2}B_{41} + \tfrac{1}{2}A_{22} + \tfrac{1}{2}A_{42}) \cos 3\Omega t$$

$$F_{zF} = A_{03} + A_{13} \cos\Omega t + B_{13} \sin\Omega t + A_{23} \cos 2\Omega t$$
$$+ B_{23} \sin 2\Omega t + A_{33} \cos 3\Omega t + B_{33} \sin 3\Omega t$$

Load equation in the fixed system (Continued)

$$M_{xF} = \tfrac{1}{2}A_{14} + \tfrac{1}{2}B_{15} + (\tfrac{1}{2}B_{24} + A_{05} - \tfrac{1}{2}A_{25}) \sin\Omega t + (A_{04} + \tfrac{1}{2}A_{24} + \tfrac{1}{2}B_{25}) \cos\Omega t$$
$$+ (\tfrac{1}{2}B_{14} + \tfrac{1}{2}B_{34} + \tfrac{1}{2}A_{15} - \tfrac{1}{2}A_{35}) \sin 2\Omega t + (\tfrac{1}{2}A_{14} + \tfrac{1}{2}A_{34} - \tfrac{1}{2}B_{15} + \tfrac{1}{2}B_{35}) \cos 2\Omega t$$
$$+ (\tfrac{1}{2}B_{24} + \tfrac{1}{2}B_{44} + \tfrac{1}{2}A_{25} - \tfrac{1}{2}A_{45}) \sin 3\Omega t + (\tfrac{1}{2}A_{24} + \tfrac{1}{2}A_{44} - \tfrac{1}{2}B_{25} + \tfrac{1}{2}B_{45}) \cos 3\Omega t$$

$$M_{yF} = -\tfrac{1}{2}B_{14} + \tfrac{1}{2}A_{15} + (-A_{04} + \tfrac{1}{2}A_{24} + \tfrac{1}{2}B_{25}) \sin\Omega t + (-\tfrac{1}{2}B_{24} + A_{05} + \tfrac{1}{2}A_{25}) \cos\Omega t$$
$$+ (-\tfrac{1}{2}A_{14} + \tfrac{1}{2}A_{34} + \tfrac{1}{2}B_{15} + \tfrac{1}{2}B_{35}) \sin 2\Omega t + (\tfrac{1}{2}B_{14} - \tfrac{1}{2}B_{34} + \tfrac{1}{2}A_{15} + \tfrac{1}{2}A_{35}) \cos 2\Omega t$$
$$+ (-\tfrac{1}{2}A_{24} + \tfrac{1}{2}A_{44} + \tfrac{1}{2}B_{25} + \tfrac{1}{2}B_{45}) \sin 3\Omega t + (\tfrac{1}{2}B_{24} - \tfrac{1}{2}B_{44} + \tfrac{1}{2}A_{25} + \tfrac{1}{2}A_{45}) \cos 3\Omega t$$

$$M_{zF} = A_{06} + A_{16} \cos\Omega t + B_{16} \sin\Omega t + A_{26} \cos 2\Omega t + B_{26} \sin 2\Omega t$$
$$+ A_{36} \cos 3\Omega t + B_{36} \sin 3\Omega t$$

The fixed system equations can be written in the following form,

$$F_{xF} = A_{01F} + A_{11F} \cos\Omega t + B_{11F} \sin\Omega t + A_{21F} \cos 2\Omega t + B_{21F} \sin 2\Omega t$$
$$+ A_{31F} \cos 3\Omega t + B_{31F} \sin 3\Omega t$$

$$F_{yF} = A_{02F} + A_{12F} \cos\Omega t + B_{12F} \sin\Omega t + A_{22F} \cos 2\Omega t + B_{22F} \sin 2\Omega t$$
$$+ A_{32F} \cos 3\Omega t + B_{32F} \sin 3\Omega t$$

$$F_{zF} = A_{03F} + A_{13F} \cos\Omega t + B_{13F} \sin\Omega t + A_{23F} \cos 2\Omega t + B_{23F} \sin 2\Omega t$$
$$+ A_{33F} \cos 3\Omega t + B_{33F} \sin 3\Omega t$$

$$M_{xF} = A_{04F} + A_{14F} \cos\Omega t + B_{14F} \sin\Omega t + A_{24F} \cos 2\Omega t + B_{24F} \sin 2\Omega t$$
$$+ A_{34F} \cos 3\Omega t + B_{34F} \sin 3\Omega t$$

$$M_{yF} = A_{05F} + A_{15F} \cos\Omega t + B_{15F} \sin\Omega t + A_{25F} \cos 2\Omega t + B_{25F} \sin 2\Omega t$$
$$+ A_{35F} \cos 3\Omega t + B_{35F} \sin 3\Omega t$$

$$M_{zF} = A_{06F} + A_{16F} \cos\Omega t + B_{16F} \sin\Omega t + A_{26F} \cos 2\Omega t + B_{26F} \sin 2\Omega t$$
$$+ A_{36F} \cos 3\Omega t + B_{36F} \sin 3\Omega t$$

Writing the fixed system coefficients

STEADY

$$A_{01F} = \tfrac{1}{2}A_{11} + \tfrac{1}{2}B_{12}$$

$$A_{02F} = -\tfrac{1}{2}B_{11} + \tfrac{1}{2}A_{12}$$

$$A_{03F} = A_{03}$$

$$A_{04F} = \tfrac{1}{2}A_{14} + \tfrac{1}{2}B_{15}$$

$$A_{05F} = -\tfrac{1}{2}B_{14} + \tfrac{1}{2}A_{15}$$

$$A_{06F} = A_{06}$$

1ST HARMONIC

cos Terms

$$A_{11F} = A_{01} + \tfrac{1}{2}A_{21} + \tfrac{1}{2}B_{22}$$

$$A_{12F} = A_{02} - \tfrac{1}{2}B_{21} + \tfrac{1}{2}A_{22}$$

$$A_{13F} = A_{13}$$

$$A_{14F} = A_{04} + \tfrac{1}{2}A_{24} + \tfrac{1}{2}B_{25}$$

$$A_{15F} = +A_{05} - \tfrac{1}{2}B_{24} + \tfrac{1}{2}A_{25}$$

$$A_{16F} = A_{16}$$

sin Terms

$$B_{11F} = \tfrac{1}{2}B_{21} + A_{02} - \tfrac{1}{2}A_{22}$$

$$B_{12F} = \tfrac{1}{2}A_{21} - A_{01} + \tfrac{1}{2}B_{22}$$

$$B_{13F} = B_{13}$$

$$B_{14F} = \tfrac{1}{2}B_{24} + A_{05} - \tfrac{1}{2}A_{25}$$

$$B_{15F} = \tfrac{1}{2}A_{24} - A_{04} + \tfrac{1}{2}B_{25}$$

$$B_{16F} = B_{16}$$

2ND HARMONIC

cos Terms

$$A_{21F} = \tfrac{1}{2}A_{11} + \tfrac{1}{2}A_{31} - \tfrac{1}{2}B_{12} + \tfrac{1}{2}B_{32}$$

$$A_{22F} = \tfrac{1}{2}B_{11} - \tfrac{1}{2}B_{31} + \tfrac{1}{2}A_{12} + \tfrac{1}{2}A_{32}$$

$$A_{23F} = A_{23}$$

$$A_{24F} = \tfrac{1}{2}A_{14} + \tfrac{1}{2}A_{34} - \tfrac{1}{2}B_{15} + \tfrac{1}{2}B_{35}$$

$$A_{25F} = \tfrac{1}{2}B_{14} - \tfrac{1}{2}B_{34} + \tfrac{1}{2}A_{15} + \tfrac{1}{2}A_{35}$$

$$A_{26F} = A_{26}$$

sin Terms

$$B_{21F} = \tfrac{1}{2}B_{11} + \tfrac{1}{2}B_{31} + \tfrac{1}{2}A_{12} - \tfrac{1}{2}A_{32}$$

$$B_{22F} = -\tfrac{1}{2}A_{11} + \tfrac{1}{2}A_{31} + \tfrac{1}{2}B_{12} + \tfrac{1}{2}B_{32}$$

$$B_{23F} = B_{23}$$

$$B_{24F} = \tfrac{1}{2}B_{14} + \tfrac{1}{2}B_{34} + \tfrac{1}{2}A_{15} - \tfrac{1}{2}A_{35}$$

$$B_{25F} = -\tfrac{1}{2}A_{14} + \tfrac{1}{2}A_{34} + \tfrac{1}{2}B_{15} + \tfrac{1}{2}B_{35}$$

$$B_{26F} = B_{26}$$

Fixed System Coefficients (Continued)

3RD HARMONIC

cos Terms	sin Terms
$A_{31F} + \frac{1}{2}A_{21} + \frac{1}{2}A_{41} - \frac{1}{2}B_{22} + \frac{1}{2}B_{42}$	$B_{31F} = \frac{1}{2}B_{21} + \frac{1}{2}B_{41} + \frac{1}{2}A_{22} - \frac{1}{2}A_{42}$
$A_{32F} = \frac{1}{2}B_{21} - \frac{1}{2}B_{41} + \frac{1}{2}A_{22} + \frac{1}{2}A_{42}$	$B_{32F} = -\frac{1}{2}A_{21} + \frac{1}{2}A_{41} + \frac{1}{2}B_{22} + \frac{1}{2}B_{42}$
$A_{33F} = A_{33}$	$B_{33F} = B_{33}$
$A_{34F} = \frac{1}{2}A_{24} + \frac{1}{2}A_{44} - \frac{1}{2}B_{25} + \frac{1}{2}B_{45}$	$B_{34F} = \frac{1}{2}B_{24} + \frac{1}{2}B_{44} + \frac{1}{2}A_{25} - \frac{1}{2}A_{45}$
$A_{35F} = \frac{1}{2}B_{24} - \frac{1}{2}B_{44} + \frac{1}{2}A_{25} + \frac{1}{2}A_{45}$	$B_{35F} = -\frac{1}{2}A_{24} + \frac{1}{2}A_{44} + \frac{1}{2}B_{25} + \frac{1}{2}B_{45}$
$A_{36F} = A_{36}$	$B_{36F} = B_{36}$

Similar to the forward rotor Page 80, the in-plane accelerations are measured by accelerometers located at ϕ_R, $\phi_R + 120^o$, $\phi_R + 240^o$.

From Page 81, using a negative rotor speed the in-plane accelerations become

$$\ddot{a}_1 = \underset{\text{measured}}{\ddot{\bar{a}}_1} - g \sin\beta \sin(\phi_R - \Omega t)$$

$$\ddot{a}_2 = \underset{\text{measured}}{\ddot{\bar{a}}_2} - g \sin\beta \sin(120^o + \phi_R - \Omega t)$$

$$\ddot{a}_3 = \underset{\text{measured}}{\ddot{\bar{a}}} - g \sin\beta \sin(240^o + \phi_R - \Omega t)$$

or

$$\ddot{a}_1 = \ddot{\bar{a}}_1 - g \sin\beta \sin\phi_R \cos\Omega t + g \sin\beta \cos\phi_R \sin\Omega t$$

$$\ddot{a}_2 = \ddot{\bar{a}}_1 - g \sin\beta \sin(\phi_R + 120^o) \cos\Omega t + g \sin\beta \cos(\phi_R + 120^o) \sin\Omega t$$

$$\ddot{a}_3 = \ddot{\bar{a}} - g \sin\beta \sin(\phi_R + 240^o) \cos\Omega t + g \sin\beta \cos(\phi_R + 240^o) \sin\Omega t$$

Letting, the aft rotor measured acceleration be of the form

$$\ddot{\bar{a}}_1 = \ddot{a}_{1-0} + \ddot{a}_{1-1}\cos\Omega t + \ddot{b}_{1-1}\sin\Omega t + \ddot{a}_{1-2}\cos 2\Omega t + \ddot{b}_{1-2}\sin 2\Omega t$$
$$+ \ddot{a}_{1-3}\cos 3\Omega t + \ddot{b}_{1-3}\sin 3\Omega t + \ddot{a}_{1-4}\cos 4\Omega t + \ddot{b}_{1-4}\sin 4\Omega t$$

$$\ddot{\bar{a}}_2 = \ddot{a}_{2-0} + \ddot{a}_{2-1}\cos\Omega t + \ddot{b}_{2-1}\sin\Omega t + \ddot{a}_{2-2}\cos 2\Omega t + \ddot{b}_{2-2}\sin 2\Omega t$$
$$+ \ddot{a}_{2-3}\cos 3\Omega t + \ddot{b}_{2-3}\sin 3\Omega t + \ddot{a}_{2-4}\cos 4\Omega t + \ddot{b}_{2-4}\sin 4\Omega t$$

$$\ddot{\bar{a}}_3 = \ddot{a}_{3-0} + \ddot{a}_{3-1}\cos\Omega t + \ddot{b}_{3-1}\sin\Omega t + \ddot{a}_{3-2}\cos 2\Omega t + \ddot{b}_{3-2}\sin 2\Omega t$$
$$+ \ddot{a}_{3-3}\cos 3\Omega t + \ddot{b}_{3-3}\sin 3\Omega t + \ddot{a}_{3-4}\cos 4\Omega t + \ddot{b}_{3-4}\sin 4\Omega t$$

Subtracting the 1/rev effect of the steady g loading,

$$\ddot{a}_1 = \ddot{a}_{1-0} + \left[\ddot{a}_{1-1} - g\sin\beta\sin\phi_R\right]\cos\Omega t + \left[\ddot{b}_{1-1} + g\sin\beta\cos\phi_R\right]\sin\Omega t$$
$$+ \ddot{a}_{1-2}\cos 2\Omega t + \ddot{b}_{1-2}\sin 2\Omega t + \ddot{a}_{1-3}\cos 3\Omega t + \ddot{b}_{1-3}\sin 3\Omega t$$
$$+ \ddot{a}_{1-4}\cos 4\Omega t + \ddot{b}_{1-4}\sin 4\Omega t$$

$$\ddot{a}_2 = \ddot{a}_{2-0} + \left[\ddot{a}_{2-1} - g\sin\beta\sin(\phi_R + 120^\circ)\right]\cos\Omega t$$
$$+ \left[\ddot{b}_{2-1} + g\sin\beta\cos(\phi_R + 120^\circ)\right]\sin\Omega t + \ddot{a}_{2-2}\cos 2\Omega t + \ddot{b}_{2-2}\sin 2\Omega t$$
$$+ \ddot{a}_{2-3}\cos 3\Omega t + \ddot{b}_{2-3}\sin 3\Omega t + \ddot{a}_{2-4}\cos 4\Omega t + \ddot{b}_{2-4}\sin 4\Omega t$$

$$\ddot{a}_3 = \ddot{a}_{3-0} + \left[\ddot{a}_{3-1} - g\sin\beta\sin(\phi_R + 240^\circ)\right]\cos\Omega t$$
$$+ \left[\ddot{b}_{3-1} + g\sin\beta\cos(\phi_R + 240^\circ)\right]\sin\Omega t + \ddot{a}_{3-2}\cos 2\Omega t + \ddot{b}_{3-2}\sin 2\Omega t$$
$$+ \ddot{a}_{3-3}\cos 3\Omega t + \ddot{b}_{3-3}\sin 3\Omega t + \ddot{a}_{3-4}\cos 4\Omega t + \ddot{b}_{3-4}\sin 4\Omega t$$

The acceleration coefficients of in-plant equations of $\ddot{a}_1$, $\ddot{a}_2$, $\ddot{a}_3$ can be converted to the rotating coordinate system by the following procedure which is derived on pages 103 through 106

$$\begin{bmatrix} \ddot{x}_R \\ \ddot{y}_R \\ \ddot{\gamma}_R \end{bmatrix} = \left[\begin{array}{c|c|c} -2/3 \sin\phi_R & -\sqrt{3}/3 \cos\phi_R + 1/3 \sin\phi_R & \sqrt{3}/3 \cos\phi_R + 1/3 \sin\phi_R \\ 2/3 \cos\phi_R & -\sqrt{3}/3 \sin\phi_R - 1/3 \cos\phi_R & \sqrt{3}/3 \sin\phi_R - 1/3 \cos\phi_R \\ 1/3R & 1/3R & 1/3R \end{array}\right] \cdot \begin{bmatrix} \ddot{a}_1 \\ \ddot{a}_2 \\ \ddot{a}_3 \end{bmatrix}$$

Consider the following form of the x_R, y_R, z_R and γ_R acceleration equation in the rotating system,

$$\ddot{x}_R = \ddot{A}_{01} + \ddot{A}_{11} \cos\Omega t + \ddot{B}_{11} \sin\Omega t + \ddot{A}_{21} \cos 2\Omega t + \ddot{B}_{21} \sin 2\Omega t + \ddot{A}_{31} \cos 3\Omega t + \ddot{B}_{31} \sin 3\Omega t + \ddot{A}_{41} \cos 4\Omega t + \ddot{B}_{41} \sin 4\Omega t$$

$$\ddot{y}_R = \ddot{A}_{02} + \ddot{A}_{12} \cos\Omega t + \ddot{B}_{12} \sin\Omega t + \ddot{A}_{22} \cos 2\Omega t + \ddot{B}_{22} \sin 2\Omega t + \ddot{A}_{32} \cos 3\Omega t + \ddot{B}_{32} \sin 3\Omega t + \ddot{A}_{42} \cos 4\Omega t + \ddot{B}_{42} \sin 4\Omega t$$

$$\ddot{z}_R = \ddot{A}_{03} + \ddot{A}_{13} \cos\Omega t + \ddot{B}_{13} \sin\Omega t + \ddot{A}_{23} \cos 2\Omega t + \ddot{B}_{23} \sin 2\Omega t + \ddot{A}_{33} \cos 3\Omega t + \ddot{B}_{33} \sin 3\Omega t + \ddot{A}_{43} \cos 3\Omega t + \ddot{B}_{43} \sin 3\Omega t$$

$$\ddot{\gamma}_R = \ddot{A}_{06} + \ddot{A}_{16} \cos\Omega t + \ddot{B}_{16} \sin\Omega t + \ddot{A}_{26} \cos 2\Omega t + \ddot{B}_{26} \sin 2\Omega t + \ddot{A}_{36} \cos 3\Omega t + \ddot{B}_{36} \sin 3\Omega t + \ddot{A}_{46} \cos 4\Omega t$$

For the aft rotor, consider the following fixed system acceleration equations, where α_F, α_β are the angular coordinates along the corresponding x & y fixed system direction.

$$\ddot{x}_F = \ddot{A}_{01F} + \ddot{A}_{11F} \cos\Omega t + \ddot{B}_{11F} \sin\Omega t + \ddot{A}_{21F} \cos 2\Omega t + \ddot{B}_{21F} \sin 2\Omega t + \ddot{A}_{31F} \cos 3\Omega t + \ddot{B}_{31F} \sin 3\Omega t$$

$$\ddot{y}_F = \ddot{A}_{02F} + \ddot{A}_{12F} \cos\Omega t + \ddot{B}_{12F} \sin\Omega t + \ddot{A}_{22} \cos 2\Omega t + \ddot{B}_{22} \sin 2\Omega t + \ddot{A}_{32F} \cos 3\Omega t + \ddot{B}_{32F} \sin 3\Omega t$$

$$\ddot{z}_F = \ddot{A}_{03F} + \ddot{A}_{13F} \cos\Omega t + \ddot{B}_{13F} \sin\Omega t + \ddot{A}_{23} \cos 2\Omega t + \ddot{B}_{23} \sin 2\Omega t + \ddot{A}_{33} \cos 3\Omega t + \ddot{B}_{33F} \sin 3\Omega t$$

Fixed System Acceleration Equations (Continued)

$$\ddot{\alpha}_F = \ddot{A}_{04F} + \ddot{A}_{14F}\cos\Omega t + \ddot{B}_{14F}\sin\Omega t + \ddot{A}_{24F}\cos 2\Omega t + \ddot{B}_{24F}\sin 2\Omega t + \ddot{A}_{34F}\cos 3\Omega t + \ddot{B}_{34F}\sin 3\Omega t$$

$$\ddot{\beta}_F = \ddot{A}_{05F} + \ddot{A}_{15F}\cos\Omega t + \ddot{B}_{15F}\sin\Omega t + \ddot{A}_{25F}\cos 2\Omega t + \ddot{B}_{25F}\sin 2\Omega t + \ddot{A}_{35F}\cos 3\Omega t + \ddot{B}_{35F}\sin 3\Omega t$$

$$\ddot{\gamma}_F = \ddot{A}_{06F} + \ddot{A}_{16F}\cos\Omega t + \ddot{B}_{16F}\sin\Omega t + \ddot{A}_{26F}\cos 2\Omega t + \ddot{B}_{26F}\sin 2\Omega t + \ddot{A}_{36F}\cos 3\Omega t + \ddot{B}_{36F}\sin 3\Omega t$$

Using the procedure established on page 87 , the α_F, β_F acceleration coefficients can be written as,

$$\ddot{A}_{04F} = -\frac{\ddot{A}_{02F} - \ddot{A}_{02FU}}{\ell} \qquad \ddot{A}_{05F} = \frac{\ddot{A}_{01F} - \ddot{A}_{01FU}}{\ell}$$

$$\ddot{A}_{14F} = -\frac{\ddot{A}_{12F} - \ddot{A}_{12FU}}{\ell} \qquad \ddot{A}_{15F} = \frac{\ddot{A}_{11F} - \ddot{A}_{11FU}}{\ell}$$

$$\ddot{B}_{14F} = -\frac{\ddot{B}_{12F} - \ddot{B}_{12FU}}{\ell} \qquad \ddot{B}_{15F} = \frac{\ddot{B}_{11F} - \ddot{B}_{11FU}}{\ell}$$

$$\ddot{A}_{24F} = -\frac{\ddot{A}_{22F} - \ddot{A}_{22FU}}{\ell} \qquad \ddot{A}_{25F} = \frac{\ddot{A}_{21F} - \ddot{A}_{21FU}}{\ell}$$

$$\ddot{B}_{24F} = -\frac{\ddot{B}_{22F} - \ddot{B}_{22FU}}{\ell} \qquad \ddot{B}_{25F} = \frac{\ddot{B}_{21F} - \ddot{B}_{21FU}}{\ell}$$

$$\ddot{A}_{34F} = -\frac{\ddot{A}_{32F} - \ddot{A}_{32FU}}{\ell} \qquad \ddot{A}_{35F} = \frac{\ddot{A}_{31F} - \ddot{A}_{31FU}}{\ell}$$

$$\ddot{B}_{34F} = -\frac{\ddot{B}_{32F} - \ddot{B}_{32FU}}{\ell} \qquad \ddot{B}_{35F} = \frac{\ddot{B}_{31F} - \ddot{B}_{31FU}}{\ell}$$

Using the procedure established on Pages 94 and 95 and knowing that the acceleration coefficients for α, β, and z are measured in the fixed system, the coefficients in the fixed system become

STEADY

$$\ddot{\ddot{A}}_{01F} = \tfrac{1}{2}\ddot{\ddot{A}}_{11} + \tfrac{1}{2}\ddot{\ddot{B}}_{12}$$

$$\ddot{\ddot{A}}_{02F} = -\tfrac{1}{2}\ddot{\ddot{B}}_{11} + \tfrac{1}{2}\ddot{\ddot{A}}_{12}$$

$$\ddot{\ddot{A}}_{03F} = \ddot{\ddot{A}}_{03F}$$

$$\left.\begin{aligned}\ddot{\ddot{A}}_{04F} &= \\ \ddot{\ddot{A}}_{05F} &=\end{aligned}\right\} \text{See Page 98}$$

$$\ddot{\ddot{A}}_{06F} = \ddot{\ddot{A}}_{06F}$$

1ST HARMONIC

cos Terms

$$\ddot{\ddot{A}}_{11F} = \ddot{\ddot{A}}_{01} + \tfrac{1}{2}\ddot{\ddot{A}}_{21} + \tfrac{1}{2}\ddot{\ddot{B}}_{22}$$

$$\ddot{\ddot{A}}_{12F} = \ddot{\ddot{A}}_{02} - \tfrac{1}{2}\ddot{\ddot{B}}_{21} + \tfrac{1}{2}\ddot{\ddot{A}}_{22}$$

$$\ddot{\ddot{A}}_{13F} = \ddot{\ddot{A}}_{13F}$$

$$\left.\begin{aligned}\ddot{\ddot{A}}_{14F} &= \\ \ddot{\ddot{A}}_{15F} &=\end{aligned}\right\} \text{See Page 98}$$

$$\ddot{\ddot{A}}_{16F} = \ddot{\ddot{A}}_{16}$$

sin Terms

$$\ddot{\ddot{B}}_{11F} + \tfrac{1}{2}\ddot{\ddot{B}}_{21} + \ddot{\ddot{A}}_{02} - \tfrac{1}{2}\ddot{\ddot{A}}_{22}$$

$$\ddot{\ddot{B}}_{12F} = \tfrac{1}{2}\ddot{\ddot{A}}_{21} - \ddot{\ddot{A}}_{01} + \tfrac{1}{2}\ddot{\ddot{B}}_{22}$$

$$\ddot{\ddot{B}}_{13F} = \ddot{\ddot{B}}_{13F}$$

$$\left.\begin{aligned}\ddot{\ddot{B}}_{14F} &= \\ \ddot{\ddot{B}}_{15F} &=\end{aligned}\right\} \text{See Page 98}$$

$$\ddot{\ddot{B}}_{16F} = \ddot{\ddot{B}}_{16}$$

2ND HARMONIC

cos Terms

$$\ddot{\ddot{A}}_{21F} = \tfrac{1}{2}\ddot{\ddot{A}}_{11} + \tfrac{1}{2}\ddot{\ddot{A}}_{31} - \tfrac{1}{2}\ddot{\ddot{B}}_{12} + \tfrac{1}{2}\ddot{\ddot{B}}_{32}$$

$$\ddot{\ddot{A}}_{22F} = \tfrac{1}{2}\ddot{\ddot{B}}_{11} - \tfrac{1}{2}\ddot{\ddot{B}}_{31} + \tfrac{1}{2}\ddot{\ddot{A}}_{12} + \tfrac{1}{2}\ddot{\ddot{A}}_{32}$$

$$\ddot{\ddot{A}}_{23F} = \ddot{\ddot{A}}_{23F}$$

$$\left.\begin{aligned}\ddot{\ddot{A}}_{24F} &= \\ \ddot{\ddot{A}}_{25F} &=\end{aligned}\right\} \text{See Page 98}$$

$$\ddot{\ddot{A}}_{26F} = \ddot{\ddot{A}}_{26}$$

sin Terms

$$\ddot{\ddot{B}}_{21F} = \tfrac{1}{2}\ddot{\ddot{B}}_{11} + \tfrac{1}{2}\ddot{\ddot{B}}_{31} + \tfrac{1}{2}\ddot{\ddot{A}}_{12} - \tfrac{1}{2}\ddot{\ddot{A}}_{32}$$

$$\ddot{\ddot{B}}_{22F} = -\tfrac{1}{2}\ddot{\ddot{A}}_{11} + \tfrac{1}{2}\ddot{\ddot{A}}_{31} + \tfrac{1}{2}\ddot{\ddot{B}}_{12} + \tfrac{1}{2}\ddot{\ddot{B}}_{32}$$

$$\ddot{\ddot{B}}_{23F} = \ddot{\ddot{B}}_{23F}$$

$$\left.\begin{aligned}\ddot{\ddot{B}}_{24F} &= \\ \ddot{\ddot{B}}_{25F} &=\end{aligned}\right\} \text{See Page 98}$$

$$\ddot{\ddot{B}}_{26F} = \ddot{\ddot{B}}_{26}$$

3RD HARMONIC

cos Terms	sin Terms
$\ddot{\ddot{A}}_{31F} = \frac{1}{2}\ddot{\ddot{A}}_{21} + \frac{1}{2}\ddot{\ddot{A}}_{41} - \frac{1}{2}\ddot{\ddot{B}}_{22} + \frac{1}{2}\ddot{\ddot{B}}_{42}$	$\ddot{\ddot{B}}_{31F} = \frac{1}{2}\ddot{\ddot{B}}_{21} + \frac{1}{2}\ddot{\ddot{B}}_{41} + \frac{1}{2}\ddot{\ddot{A}}_{22} - \frac{1}{2}\ddot{\ddot{A}}_{42}$
$\ddot{\ddot{A}}_{32F} = \frac{1}{2}\ddot{\ddot{B}}_{21} - \frac{1}{2}\ddot{\ddot{B}}_{41} + \frac{1}{2}\ddot{\ddot{A}}_{22} + \frac{1}{2}\ddot{\ddot{A}}_{42}$	$\ddot{\ddot{B}}_{32F} = -\frac{1}{2}\ddot{\ddot{A}}_{21} + \frac{1}{2}\ddot{\ddot{A}}_{41} + \frac{1}{2}\ddot{\ddot{B}}_{22} + \frac{1}{2}\ddot{\ddot{B}}_{42}$
$\ddot{\ddot{A}}_{33F} = \ddot{\ddot{A}}_{33F}$	$\ddot{\ddot{B}}_{33F} = \ddot{\ddot{B}}_{33F}$
$\ddot{\ddot{A}}_{34F} =$ See Page 98	$\ddot{\ddot{B}}_{34F} =$ See Page 98
$\ddot{\ddot{A}}_{35F} =$	$\ddot{\ddot{B}}_{35F} =$
$\ddot{\ddot{A}}_{36F} = \ddot{\ddot{A}}_{36}$	$\ddot{\ddot{B}}_{36F} = \ddot{\ddot{B}}_{36}$

APPENDIX C

INSTRUMENTATION

APPENDIX C

INSTRUMENTATION

A. General

The aircraft instrumentation used in this program can be grouped into three major categories:

(1) Rotor shaft strain gage instrumentation.

(2) Vibration measuring instrumentation.

(3) Torque bridges on the interconnecting and engine shaft for measuring horsepower.

Presented herein is a description of instrumentation used during the in-flight measurements of Reference 4 corresponding to Items 1 and 2. Strain gage bridges on each rotor shaft and pitch link measure strain variations; in combination with the necessary load calibrations these define the forces and moments acting on the helicopter at the rotor hub. Velocity pickups on the forward and aft transmission, and accelerometers on the rotor hubs are used to define the fixed system accelerations and velocities at the forward and aft rotor hubs. Additional velocity pickups are located at the cockpit floor to measure vertical, lateral and longitudinal vibration.

The sign conventions for the rotor shaft loads and the velocity pickups are presented in Figure 27.

B. Rotor Shaft Instrumentation

1. Description

Instrumentation for the measurement of the magnitude and phasing of the fuselage exciting forces was installed on the forward and aft rotor shafts, since these shafts are the main load carrying link between the rotors where the loads originate, and the fuselage. Shaft loads, which include bending moments in two mutually perpendicular directions, shear forces in two mutually perpendicular directions, shaft torque and lift, together with pitch link loads form the major external loads acting on the helicopter.

The rotor shafts are among the most important structural components in the helicopter, since they must support its entire weight and transmit the torque required to develop the thrust necessary to support the helicopter and propel it through the air. In addition, they are subjected to rather severe oscillatory loads, yet must for safety have virtually infinite life. As a result of these design considerations, the shafts are quite strong, and the oscillatory stress levels quite low, and therefore difficult to measure. This is particularly true of tension and torsion where the steady loads are quite high compared to the oscillatory forces. In these cases it was necessary to

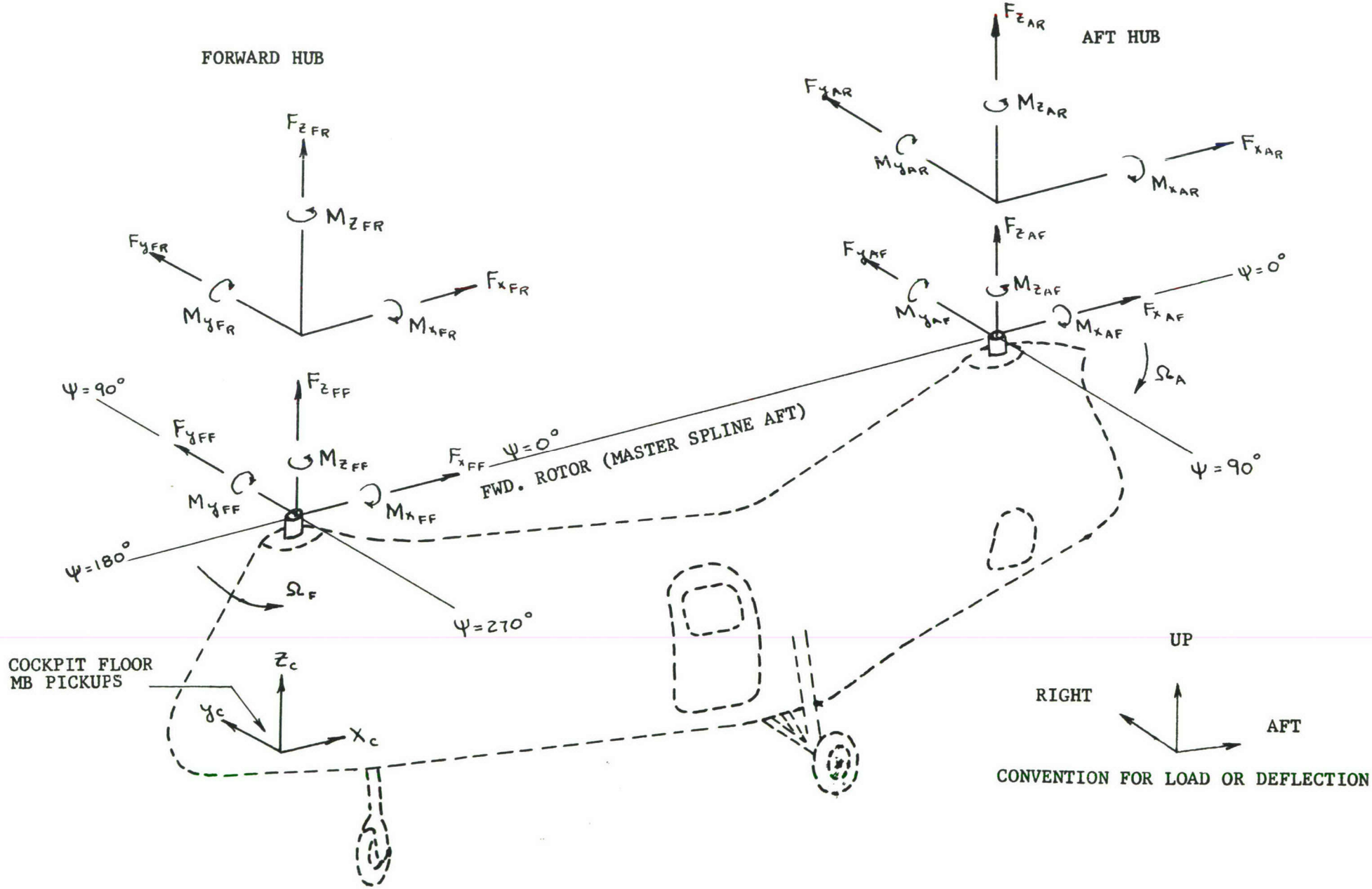

Figure 27 Sign Convention for Instrumentation in H-21C #96

use two sets of strain gages - one set to measure the large steady loads - and a second high-sensitivity set to record the alternating signals of relatively low strength. A somewhat similar problem existed in the measurement of the longitudinal and lateral shear forces which had to be determined from the difference between relatively large bending moments at two horizontal shaft locations. This difficulty was overcome by electrically connecting the two bridges so as to yield the difference between them, and then performing calculations for the shear loads on the shaft.

The strain gage installation is shown in Figure 28, a developed view of the rotor shaft. Duplicate bridge sets are located on the 0^{o} - 180^{o} azimuth and the 90^{o} - 270^{o} azimuth. The top bridge at 7.42 in. below the rotor plane, and the bottom bridge at 15.74 in. are designated as shear bridges. These are actually two moment bridges wired, as noted above, to measure the difference in bending moment. The next lower bridge measures bending moment 8.44 in. below the rotor. Next are two torque bridges, one with low sensitivity for the steady torque, and the second with high sensitivity for the alternating torque. At 13.04 in. and 14.90 in. below the rotor are the two lift bridges, one for steady and one for alternating loads.

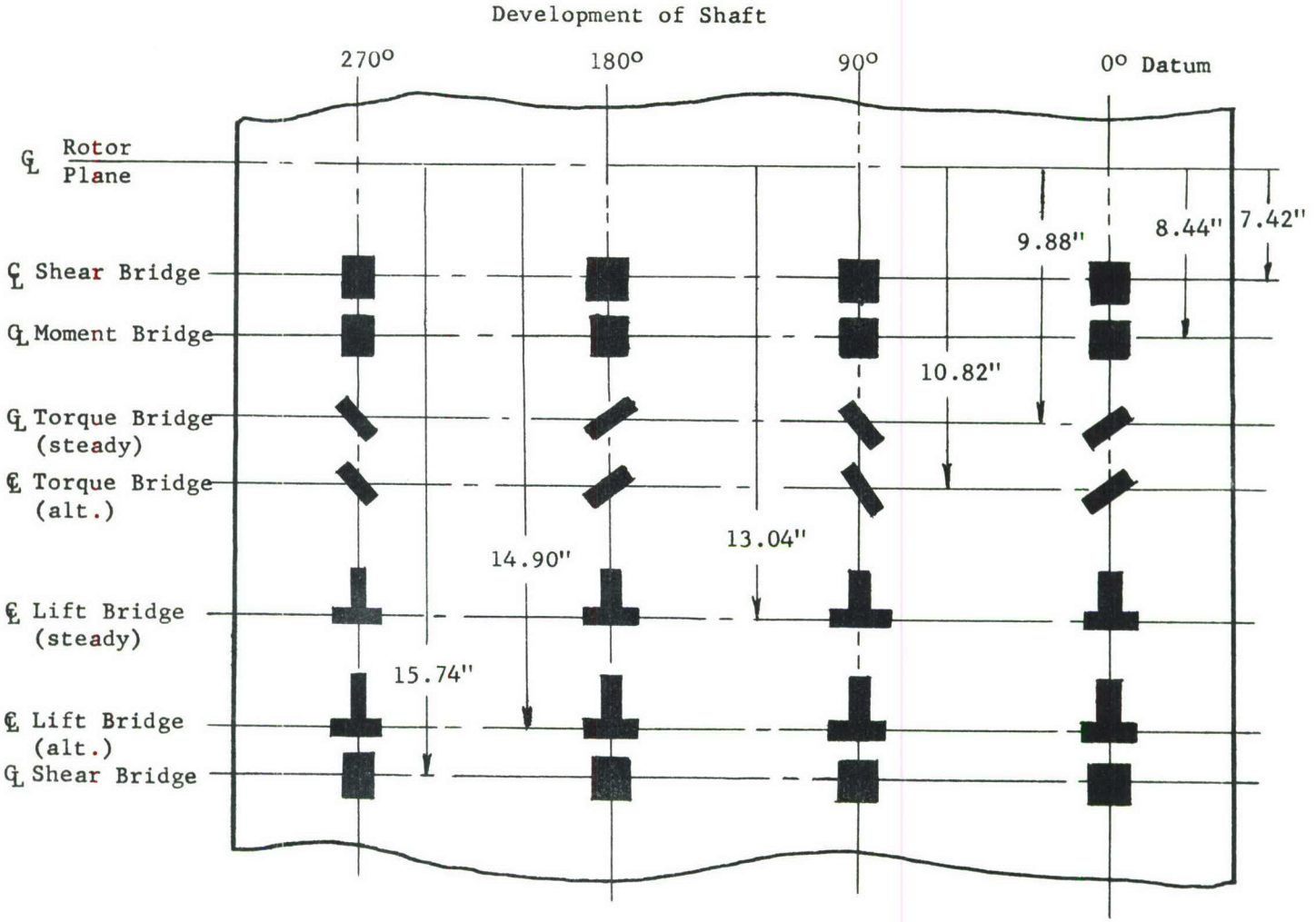

Install Type EB-F 13S Plus Strain Gages with Armstrong Adhesive, Type A-6, Using Activator "A." Locate Gages as Shown Above.

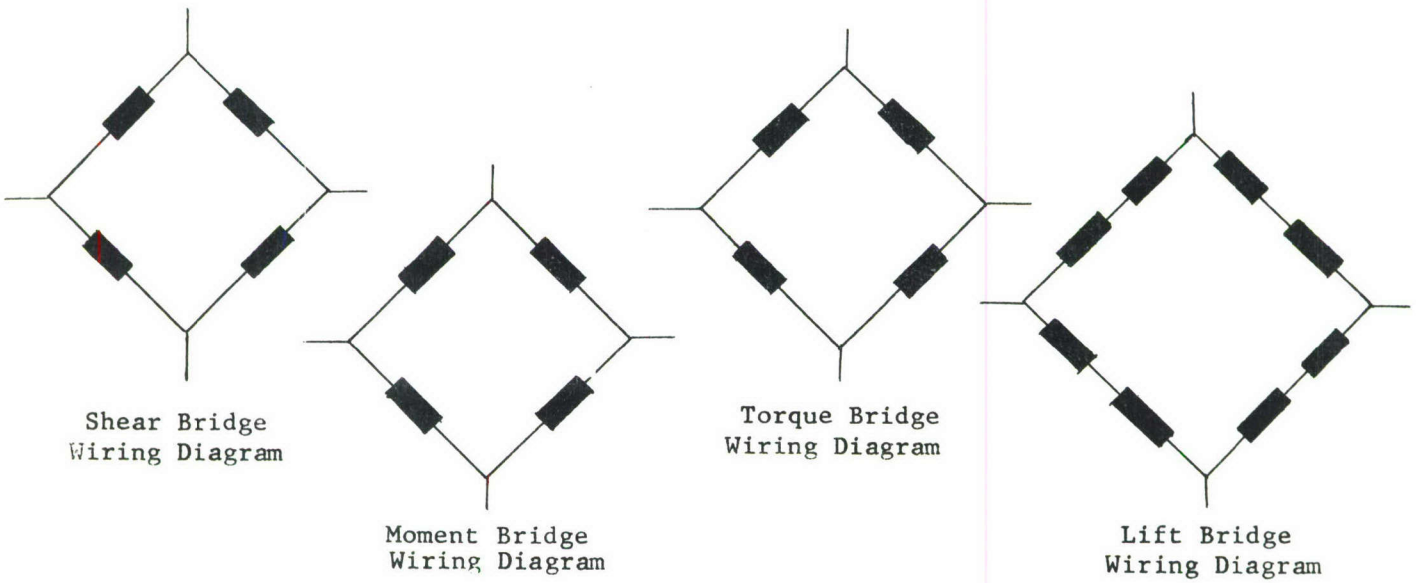

Figure 28 Shaft Instrumentation

Reference Dwg. No.
FT 1960 - Rev. B

2. Load Calibration

Load calibration of the instrumented forward and aft rotor shaft was performed with the shaft mounted in loading jigs as illustrated in Figure 4 for the shear load calibration. Incremental loads were applied to the shaft, and the output from each strain gage bridge was recorded on oscillograph tape using the flight recording equipment shown in Tables I and II. Before and aft each load application a known resistance was placed across each strain gage bridge to provide a sensitivity check of the circuit for adjusting the calibration.

This load data was analyzed, using the Benson-Lehner Data Reader shown in Figure 1, in order to convert the oscillographic analog information to digital data; an arbitrary linear unit peculiar to this Reader was chosen for denoting trace deflection from a datum line. The value of this unit is 1/131 inch and the unit itself is referred to in this report as a "count".

Figure 29 is a typical calibration curve for shear load. Using this calibration curve, the calibration constant for shear load (90^{o}-270^{o}) is obtained by dividing the load variation (1200 lb - 0) by the trace deflection (364-210), $K = \frac{1200 \text{ lb}}{154 \text{ cts.}} =$ 78 lb/count. Similarly, calibration constants for all loadings were obtained by using the recorded trace deflection from the appropriate strain gage bridge. This curve indicates that, as intended, the predominant gage response occurs between the applied shear load and the strain gage bridge representing shear. This is the pair of bending gages which are wired together to measure differential moment, and designated as shear bridge in Figure 28. It is also apparent that other gages show response which is not in the direction of the calibration load. One of the obvious examples is the "lift alternative" bridge which shows a relatively large response. Such side effects may be due to an unfavorable location of a particular gage with respect to a load direction it is not intended to measure, or to Poisson's ratio effect. These side effects are accounted for by an "interaction matrix" which also contains the main load calibrations. This matrix represents the complete relationship between the measurements and the loads on the shaft in all directions at the rotor plane.

TABLE I

FORWARD ROTOR SHAFT

Data	Amp. S/N	Galvo Type	Galvo S/N	Attenuation	Gage Resistance (ohms)	Gage Factor
F_x = 0°-180° shear	246 DH 06	7-323	577 DK	X10 120 K ohms	350	2.06
F_y = 90°-270° shear	580 DB 15		5080			
M_x = 90°-270° bending	424 DH 16		606 DK			
M_y = 0°-180° bending	706 DH 16		582 DK			
M_z (alt.) = Alternating Torque	00 CU 14	7-323	629 DK	X10 120 K ohms		
F_z (alt.) = Alternating Lift	584 DH 16	7-344	2331	X150 120 K ohms		
M_z (st'd.) = Steady Torque	317 DH 16	7-323	613 DK	X10 120 K ohms		
F_z (st'd.) = Steady Torque	468 DH 16	7-323	630 DK	X15 120 K ohms	350	2.06

TABLE II

AFT ROTOR SHAFT

Data	Amp. S/N	Galvo Type	Attenuation & R_{cal}	Gage Resistance (ohms)	Gage Factor
F_x = 0°-180° shear	476 DH 16	7-323	X10 120 K ohms	350	2.06
F_y = 90°-270° shear	537 DH 16				
M_x = 90°-270° bending	226 DB 15				
M_y = 0°-180° bending	386 DH 16				
M_z (alt.) = Alternating Torque	261 DH 16	7-323	X10 120 K ohms		
F_z (alt.) = Alternating Lift	241 DH 16	7-344	X150 120 K ohms		
M_z (st'd.) = Steady Torque	751 CU 14	7-323	X10 120 K ohms		
F_z (st'd.) = Steady Lift	594 DB 15	7-323	X15 120 K ohms	350	2.06

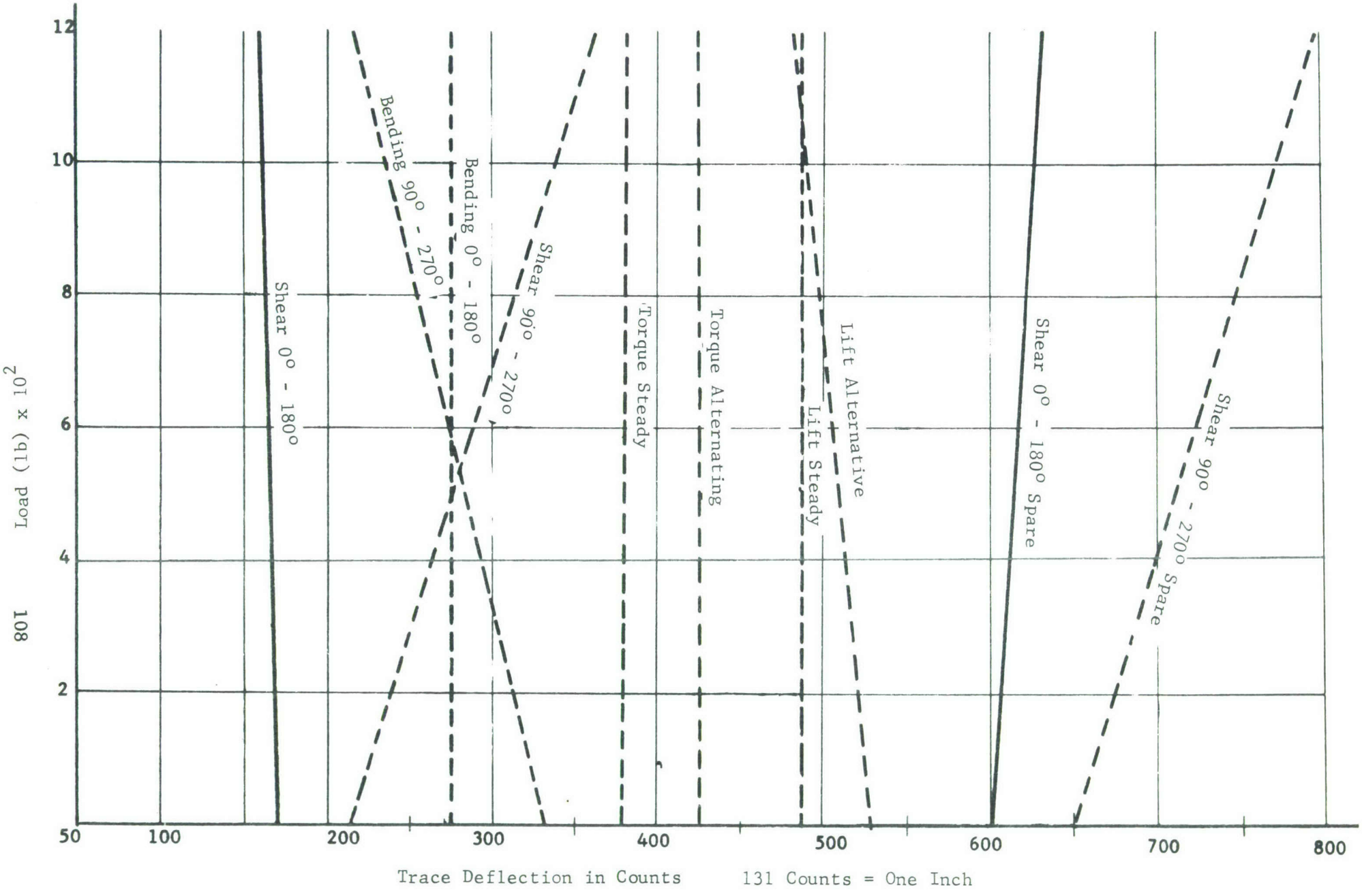

Figure 29 Rotor Shaft Loads Calibration C-96 Forward Transmission Shear Only 90° 0' Approx. (See Diagram)

The result is an interaction matrix of the form,

$$\begin{bmatrix} \overline{F_x} \\ \overline{F_y} \\ \overline{F_z} \\ \overline{M_\alpha} \\ \overline{M_\beta} \\ \overline{M_\gamma} \end{bmatrix} = \begin{bmatrix} i_{ax} & i_{ay} & i_{az} & i_{a\alpha} & i_{a\alpha} & i_{a\alpha} \\ i_{bx} & i_{by} & i_{bz} & i_{b\alpha} & . & . \\ i_{cx} & i_{cy} & i_{cz} & . & . & . \\ i_{dx} & i_{dy} & . & . & . & . \\ i_{ex} & . & . & . & . & . \\ i_{fx} & . & . & . & . & . \end{bmatrix} \begin{bmatrix} F_x \\ F_y \\ F_z \\ M_\alpha \\ M_\beta \\ M_\gamma \end{bmatrix}$$

F_x, F_y, F_z = actual loads in the x, y, z direction

M_x, M_y, M_z = actual moments about the x, y, z axis

i_{ax}, i_{ay}, i_{az} = interaction of gage "a" to unit x, y, z forces

$i_{a\alpha}$, $i_{a\beta}$, $i_{a\gamma}$ = interaction of gage "a" to unit α, β, γ moments

$\overline{F_x}$, $\overline{F_y}$, $\overline{F_z}$ are loads corresponding to the strain measurements

$\overline{M_x}$, $\overline{M_y}$, $\overline{M_z}$,

Shear

Application of shear loads for calibration of the strain gage bridges was performed as shown in Figure 3. The shear load was applied to the rotor shaft by a hydraulic jack mounted at its base on a ball joint pivot to insure loading through the center line of the shaft. During the loading, the applied shear load was accurately monitored and limited to a peak value of 1200 lb using a load cell and strain indicator from the 50,000 lb capacity weighing kit shown in the figure. In order to obtain calibration curves for both of the shear gage bridges used in the test, the shaft was loaded on the 0^o - 180^o axis in addition to the 90^o - 270^o axis. To maintain the accuracy of load position, the inclinometer shown in Figure 4 was used to set the angular position of the calibration loads relative to the master spline. The sighting scope shown was not used for the shear load calibration. It is noted that an independent calibration for the spare strain gage bridges was unnecessary since the responses recorded during the initial load calibration could be used for this purpose.

Lift.

Lift calibration loads were applied with a hydraulic jack as shown in Figure 3. To insure accurate alignment of the load through the center of the shaft, an optical system was employed consisting of a sighting scope and target. The sighting scope was mounted on the rotor shaft parallel to the ℄ as shown in Figure 4 and a target scribed with radial lines at 90° increments was mounted at right angles to the loading link as illustrated in Figure 3. Upon rotation of the target and loading shaft at 90° increments, it was possible to determine and adjust the alignment of lift load by relocating the load attachment point until the sightings indicated equal radial dimensions for all incremental positions. Lift loads were set using the 50,000 lb capacity load cell and strain indicator in increments of 2000 lb to a maximum of 7500 lb.

Moment

Calibration loads for bending moment were imposed on the rotor shaft using the test arrangement shown below, and partially in Figure 2:

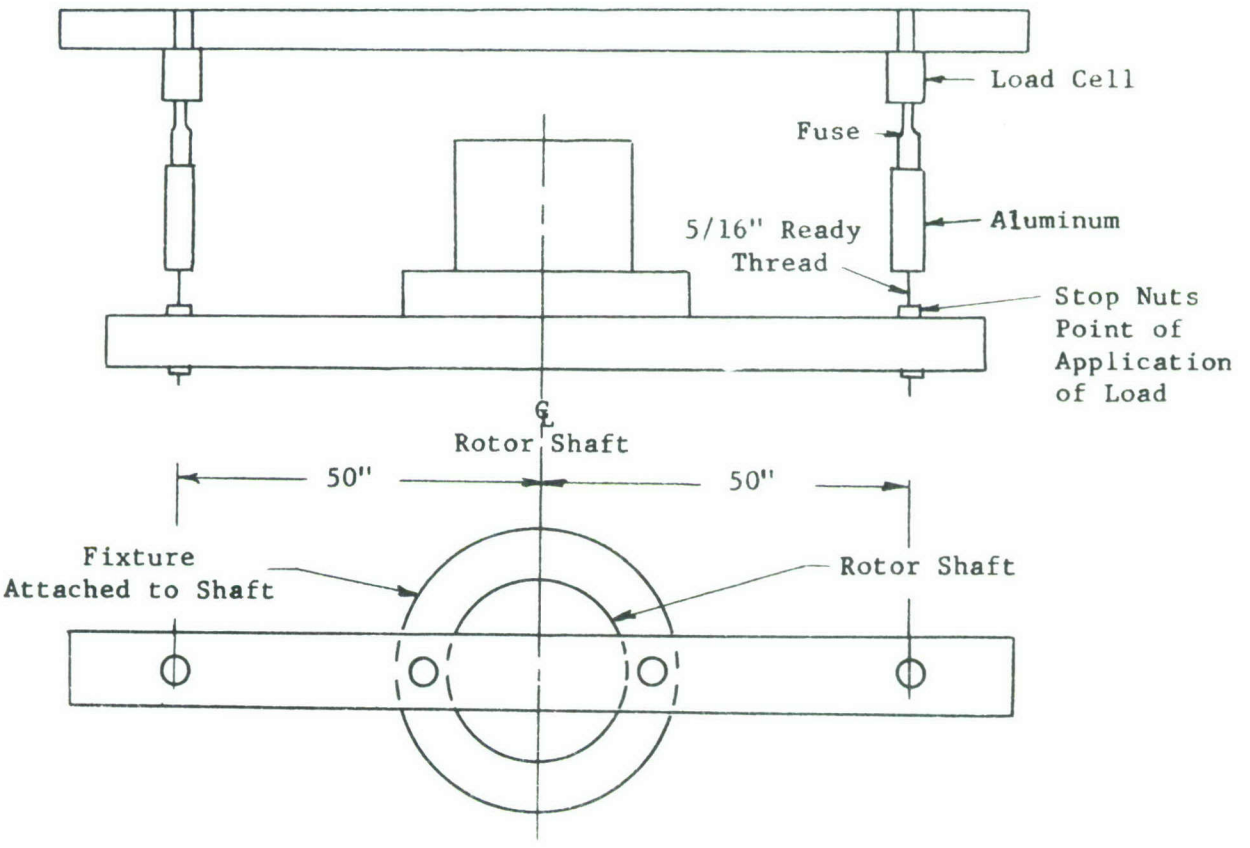

Using the adjustments located at each end of the 50" moment arm, this setup permitted one side to be loaded in tension while the other was in compression, thus producing a pure moment at the centerline of the shaft in the presence of a large steady lift load.

During application of the loads, a load cell in combination with a strain indicator was employed to monitor the forces on each arm of the beam. Initial calibrations were performed for the 0^{o}-180^{o} bending bridges by applying equal tension and compression loads along the axis; the 90^{o}-270^{o} bending bridges were calibrated in the same manner after the shaft had been rotated 90^{o}. In order to define a representative calibration curve, loads were applied in increments of 25 lb (2500 in lb) from 0 lb to a maximum value of 150 lb (15,000 in lb).

Torque

Initially, the torque calibration used a load balance system as shown in the lower half of Figure 2, but this system was replaced by a closed loop system to improve the accuracy. Final torque load calibration was performed using the test setup shown in the upper half of Figure 2. A schematic of this loading system showing the closed loop cable arrangement is given below:

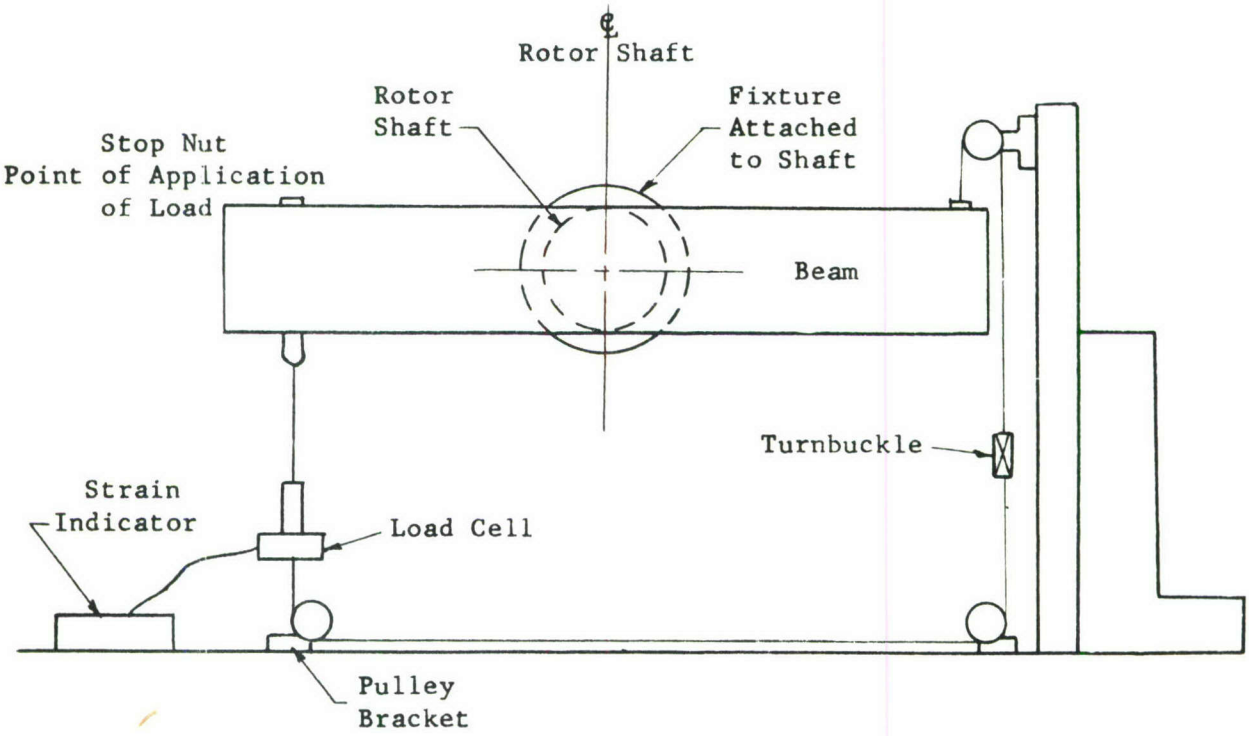

The force was applied by a turnbuckle on the right-hand side of the jig and transmitted to both ends of the beam by a flexible cable. A load cell was placed at the opposite end of the cable to measure the applied forces which ranged from 0 lb to a maximum of 2,000 lb (200,000 in lb) in increments of 250 lb (25,000 in lb). The moment on the shaft due to the weight of the "I" section beam was nullified by lifting the equivalent weight of the beam with the hydraulic jack shown in Figure 2.

Final Interaction Matrices

From the load calibration data, the following interaction matrices were obtained:

FORWARD ROTOR SHAFT

STEADY LOADS

$$\begin{bmatrix} F_x \\ F_y \\ F_z \\ M_x \\ M_y \\ M_z \end{bmatrix} = \begin{bmatrix} 1 & +0.0633 & +0.0021 & +0.0001 & -0.0089 & -0.0016 \\ -0.1171 & 1 & +0.0010 & +0.0067 & -0.0030 & +0.0006 \\ -0.0379 & +0.0416 & 1 & +0.0015 & +0.0091 & -0.0151 \\ 0 & -9.517 & -0.0124 & 1 & -0.0104 & +0.0005 \\ +9.415 & -0.0256 & +0.0881 & +0.0156 & 1 & +0.0074 \\ -0.0858 & -0.0144 & -0.0068 & -0.0205 & -0.0331 & 1 \end{bmatrix} \begin{bmatrix} F_x \\ F_y \\ F_z \\ M_x \\ M_y \\ M_z \end{bmatrix}$$

Measured — Actual

ALTERNATING LOADS

$$\begin{bmatrix} F_x \\ F_y \\ F_z \\ M_x \\ M_y \\ M_z \end{bmatrix} = \begin{bmatrix} 1 & +0.0633 & -0.0021 & +0.0001 & -0.0089 & -0.0016 \\ -0.1171 & 1 & +0.0010 & -0.0067 & -0.0030 & +0.0006 \\ +0.0583 & +0.1008 & 1 & 0.0\ 52 & -0.0088 & +0.0029 \\ 0 & -9.517 & -0.0124 & 1 & -0.0104 & +0.0005 \\ +0.415 & -0.0256 & +0.0881 & +0.0156 & 1 & +0.0074 \\ -0.1567 & +0.1142 & -0.0343 & -0.0289 & -0.0467 & 1 \end{bmatrix} \begin{bmatrix} F_x \\ F_y \\ F_z \\ M_x \\ M_y \\ M_z \end{bmatrix}$$

AFT ROTOR SHAFT

STEADY LOADS

$$\begin{bmatrix} F_x \\ F_y \\ F_z \\ M_x \\ M_y \\ M_z \end{bmatrix} = \begin{bmatrix} 1 & +0.017 & -0.002 & +0.004 & -0.002 & -0.001 \\ -0.022 & 1 & -0.001 & +0.011 & +0.005 & +0.007 \\ +0.106 & -0.113 & 1 & -0.005 & +0.002 & -0.004 \\ -0.597 & -9.935 & +0.028 & 1 & +0.052 & -0.048 \\ +10.06 & -0.563 & +0.122 & -0.049 & 1 & +0.024 \\ +0.103 & -0.021 & 0 & -0.009 & -0.020 & 1 \end{bmatrix} \begin{bmatrix} F_x \\ F_y \\ F_z \\ M_x \\ M_y \\ M_z \end{bmatrix}$$

Measured Actual

ALTERNATING LOADS

$$\begin{bmatrix} F_x \\ F_y \\ F_z \\ M_x \\ M_y \\ M_z \end{bmatrix} = \begin{bmatrix} 1 & +0.017 & -0.002 & +0.004 & -0.013 & -0.001 \\ -0.022 & 1 & -0.001 & +0.011 & +0.005 & +0.001 \\ +0.076 & +0.008 & 1 & -0.001 & +0.006 & +0.008 \\ -0.597 & -9.935 & +0.028 & 1 & +0.052 & -0.024 \\ +10.06 & -0.563 & +0.122 & -0.049 & 1 & +0.012 \\ +0.335 & +0.019 & -0.039 & -0.029 & -0.006 & 1 \end{bmatrix} \begin{bmatrix} F_x \\ F_y \\ F_z \\ M_x \\ M_y \\ M_z \end{bmatrix}$$

It is noted that the interaction matrices for the steady and alternating loads are composed of the same elements in the rows and columns involving interaction between the shear and bending moment. However, the elements associated with lift and torque loads usually exhibit unlike elements, partly resulting from the nonlinear load characteristics existing between the steady and alternating load ranges used in the calibration and partly because independent strain gage bridges were used for the steady and alternating lift and torque loads.

C. Motion Pickups

1. Description

In addition to the shaft loads, the helicopter was instrumented to record cockpit floor vibration level, pitch link loads, transmission motions, rotor hub accelerations and helicopter pitch attitude. Vibration was measured at the cockpit floor along the vertical, lateral, and longitudinal axes of the aircraft and motion about the lateral axis was sensed by a pitch attitude gyro with the equipment shown in Table III.

The pitch attitude gyro was installed to determine the rotor shaft angle in flight. This was required in order to correct the first harmonic error in the rotating system rotor hub accelerations. As shown schematically below, the angular tilt of the rotor shaft from the vertical position (rotor plane horizontal) introduces a steady acceleration force, g sin β, in the plane perpendicular to the shaft.

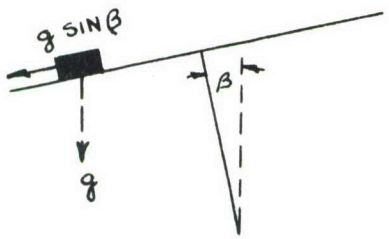

Accelerometers located on the rotor hub are influenced by this steady acceleration, but each accelerometer senses only the component in the direction of measurement. Viewing the accelerometers in the rotor plane,

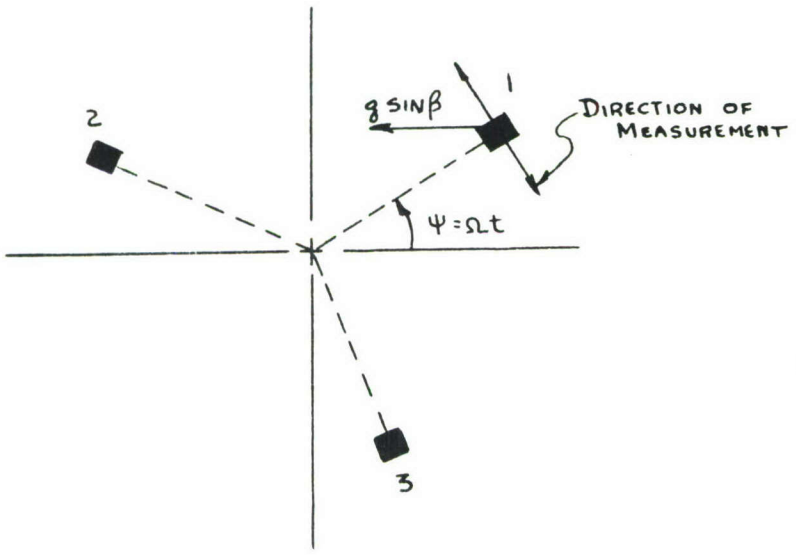

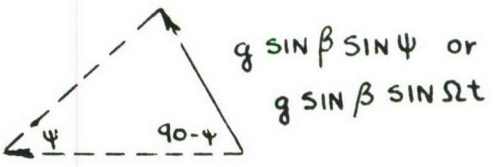

TABLE III

Item	Galvanometer Type	Galvanometer S/N	MB S/N	Amp. S/N	Attenuation
Cockpit Floor Vertical Vibration	7-317	5638	5712	7059	15
Cockpit Floor Lateral Vibration	7-317	295AD	5700	170DF-5	15
Cockpit Floor Longitudinal Vibration	7-317	5562	6965	8093	15
Pitch Attitude Gyro	7-315				GVDC

TABLE IV

Item	Accel. S/N	Galvanometer Type	Galvanometer S/N	RCAL	Gage Factor
Red Pitch Link		7-315		60K	2.06
Yellow Pitch Link		7-315		60K	2.06
Green Pitch Link		7-315		60K	2.06
Accel. - 0^{o}	164	7-339	9135	120K	
Accel. - 120^{o}	132	7-339	9742	120K	
Accel. - 240^{o}	123	7-339	9758	120K	

TABLE V

Item	AFT ROTOR HUB Accel. S/N	Galvanometer Type	Galvanometer S/N	RCAL	Gage Factor
Red Pitch Link		7-315		60K	2.06
Accel. - 0^{o}	124	7-339	8556	120K	
Accel. - 120^{o}	128	7-339	11695	120K	
Accel. - 240^{o}	165	7-339	8612	120K	

As shown in the vector diagram, accelerometer No. 1 indicates an additional first harmonic acceleration from shaft tilt which must be removed to obtain the correct in-plane acceleration.

Similar shaft tilt corrections were necessary for each of the three forward and aft rotor hub accelerometers identified in Tables IV and V.

Although of secondary importance, the pitch links were instrumented for axial load, thereby providing a complete picture of the loads transmitted between each rotor and the fuselage. Each pitch link on the forward head was instrumented for recording loads, but only one pitch link was instrumented on the aft head because of the normal assumption of similar loads on each link displaced by 120 degrees. Confirmation of this assumption was obtained from axial load measurements on all three links at the forward rotor head during the check flight. Identification of the instrumentation for the three forward and one aft pitch link is presented in Tables IV and V.

Space limitations prevented the location of sufficient instrumentation on the rotor hubs to define hub motions other than in-plane motions. However, to supplement this measured data, velocity pickups were located at the forward and aft transmissions to completely define the motion. The velocity pickups mounted on the forward and aft transmissions were located as shown in Figure 30. In addition, Tables VI and VII present a detailed description of this instrumentation.

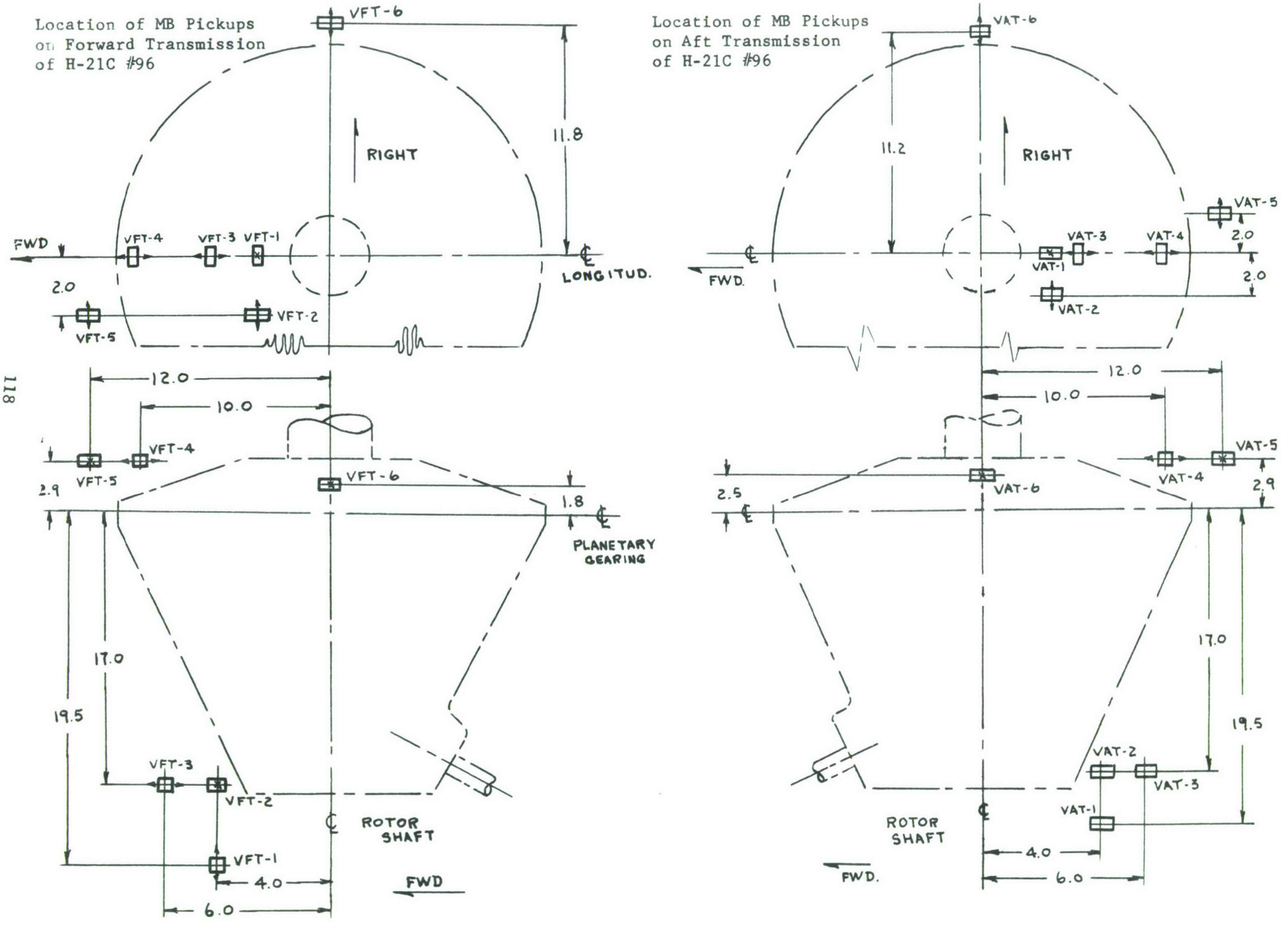

Figure 30 Location of M.B. Pickups

TABLE VI

FORWARD TRANSMISSION

Pickup No.	Direction	Amp. S/N	Galvo Type	Galvo S/N	MB S/N	Attenuation
VFT-1	Vertical	7127	7-317	5644	4548	15
VFT-2	Lateral	216 DF 5	7-317	5516	7132	15
VFT-3	Longitudinal	8076	7-317	5524	2850	15
VFT-4	Longitudinal	219 DF 5	7-317	5648	5066	15
VFT-5	Lateral	964 DE 5	7-317	5650	6258	15
VFT-6	Lateral	7006	7-315	5647	5455	15

TABLE VII

AFT TRANSMISSION

Pickup No.	Direction	Amp. S/N	Galvo Type	Galvo S/N	MB S/N	Attenuation
VAT-1	Vertical	244 DF 5	7-317	5395	5524	15
VAT-2	Lateral	8066	7-317	381AD	2832	15
VAT-3	Longitudinal	8173	7-317	5622	7041	15
VAT-4	Longitudinal	101 DF 5	7-317	643 DF	2826	15
VAT-5	Lateral	7193	7-217	249 AN	5488	15
VAT-6	Lateral	7027	7-217	239 AN	2847	15

2. Calibration

Equipment

1. MB Type T112031 (S/N 245) Vibration Equipment with MB Type C1 (S/N 24) Shaker Table.

2. MB Type OC1 Microscope with Scale calibrated from 0 to 0.1 inches for measuring table displacement.

3. Hewlett Packard Model 200C Audio Signal Generator for sensitivity calibration.

4. Ballantine Model 300 RMS AC Voltmeter for measuring calibrating signals.

5. Berkley Model 5500 Universal Counter for accurately measuring frequencies of table displacement.

6. Ballantine Model 316 Peak-to-Peak AC Meter for checking velocity of table by output of signal coil.

7. Fifteen (15) MB Type 124 Velocity Pickups

8. Fifteen (15) CEC Type 1-112C Linear - Integrate Amplifiers

Description of Calibrating Equipment

1. The MB Type T112031 Vibration Calibrating Equipment consists of the following components:

a. A Type C-1J Calibrator-Exciter intended for the calibration of velocity, acceleration, and displacement-type vibration pickups by direct attachment to the vibration table. Rigidly attached to the table assembly is a signal coil which moves in a fixed magnetic field so that the voltage developed across it is proportional to the table velocity and, hence, 90^{o} leading in phase with reference to displacement. By using a sensitivity curve furnished by the manufacturer and checked periodically in the laboratory, the displacement of the table can be measured directly. For direct measurement of table displacement, the MB Type OC-1 Microscope is used. In use, the microscope is affixed to the body of the shaker assembly so that it can be focused on a minute point of light on the moving table. When the light point is sufficiently small and sharply defined, the displacement of the table may be read to .005" on the 0 to 0.1" scale of the instrument. The light point source is obtained by beaming light onto a painted surface on the table, on which grit particles have been imbedded.

b. The PALL G Power Amplifier is used to drive the C-1J Exciter to its rated output of 75g's (resonant mechanical load).

c. The A20 Audio Oscillator excites the power amplifier with sine wave voltage variable from 5 cycles per second to 600 KC.

2. The Hewlett Packard Model 200C Oscillator and the Ballantine Model 200 VTVM are used to initiate a signal of known frequency and amplitude, which can be injected into the input of the system and recorded at the output, thereby establishing a sensitivity reference.

3. The Berkley Model 5500 Universal Counter and Timer is an electronic counter with oven-crystal controlled grating which provides a counting accuracy of $\pm$ .001%. It is used in this system to measure the vibration frequency of the shaker table.

4. The Ballantine Model 316 Peak-to-Peak AC Voltmeter has an accuracy of 2% through a frequency range of 2 to 40 cycles per second. It was used in this application to facilitate reading the voltage output of the signal coil at low frequency, thereby making it possible to use the signal coil output for a double check on the table velocity.

5. The MB Type 124 Vibration Pickup is a transducer with an output voltage proportional to the velocity of its motion. Its overall physical dimensions are 1 19/32" x 1 7/16" x 2 13/32" x its weight 9.7 ounces. It can be adjusted for sensing movement in either a vertical or a horizontal plane. The voltage sensitivity is in the order of 20 millivolts per .001" per 100 cycles per second in the flat portion of the frequency response curve (8 cycles per second to 100 cycles per second). The natural frequency of the MB pickup is 4.75 cycles per second with 65% of critical damping (this pickup is referred to simply as an "MB" during the remainder of the report).

6. The CEC Type 1-112C Linear Integrate Amplifier, in this system, is operated in the integrate-low mode. In this mode it has the following characteristics: Magnification - 190 millivolts at 100 cycles per second - will cause full scale output. Response - uniform $\pm$ 5% from 5 to 5,000 cycles per second. Input attenuator - 20 steps, 1 to 1,000 and off. Full scale output - 40 milliamps into a 25 ohm load.

7. The CEC Type 7-317 Galvo is fluid damped. It has a natural frequency of 3700 cps and a flat range to 2200 cps. The phase shift is negligible at the frequencies of interest in this application. The undamped dc sensitivity is 41.4 milliamps per inch.

Functional Check of Amplifiers

Prior to the system calibration each amplifier to be used in the test program was bench checked and its sensitivity set so that an input signal level of 0.3 volts at 18 cps would produce an output of 0.3 volts across a 25 ohm load. This was done with the Attenuation Set at 20 and the mode of operation on "integrate."

Phase Calibration of Amplifiers

The amplifiers were phase calibrated using the Hewlett Packard 200C Generator and a recording oscillograph connected as shown below:

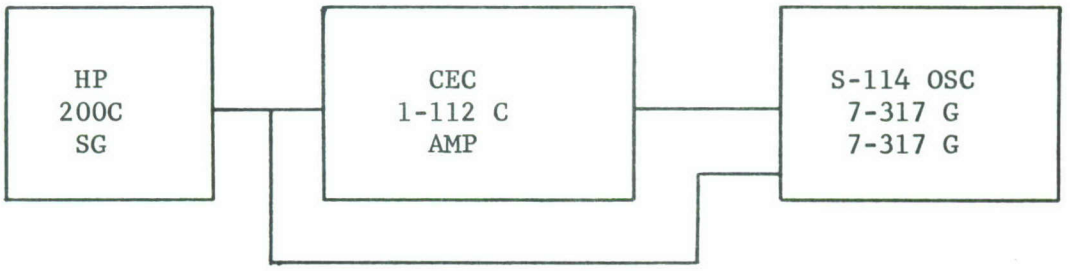

Using this arrangement, two paths are provided from the signal generator to the recording oscillographs, one containing the amplifier to be calibrated and the other a direct connection to serve as a reference trace. For each amplifier, the phase displacement between the reference trace and the amplifier trace was measured and plotted for output frequencies of 5, 6, 7, 8, 10, 12, 20 and 30 cps. Figure 31 shows typical phase calibration curves which were used later in the system calibration to correct for amplifier phase shift.

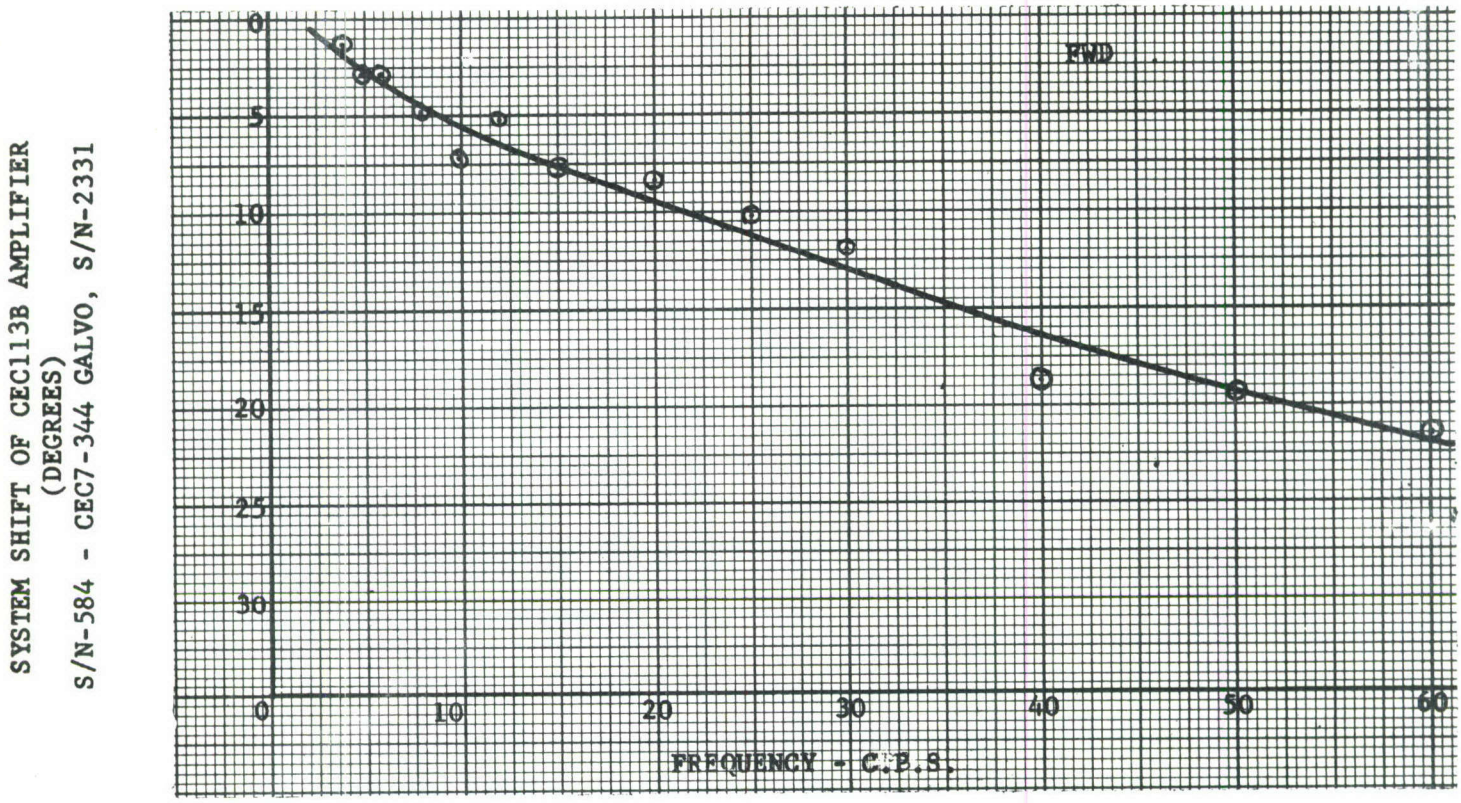

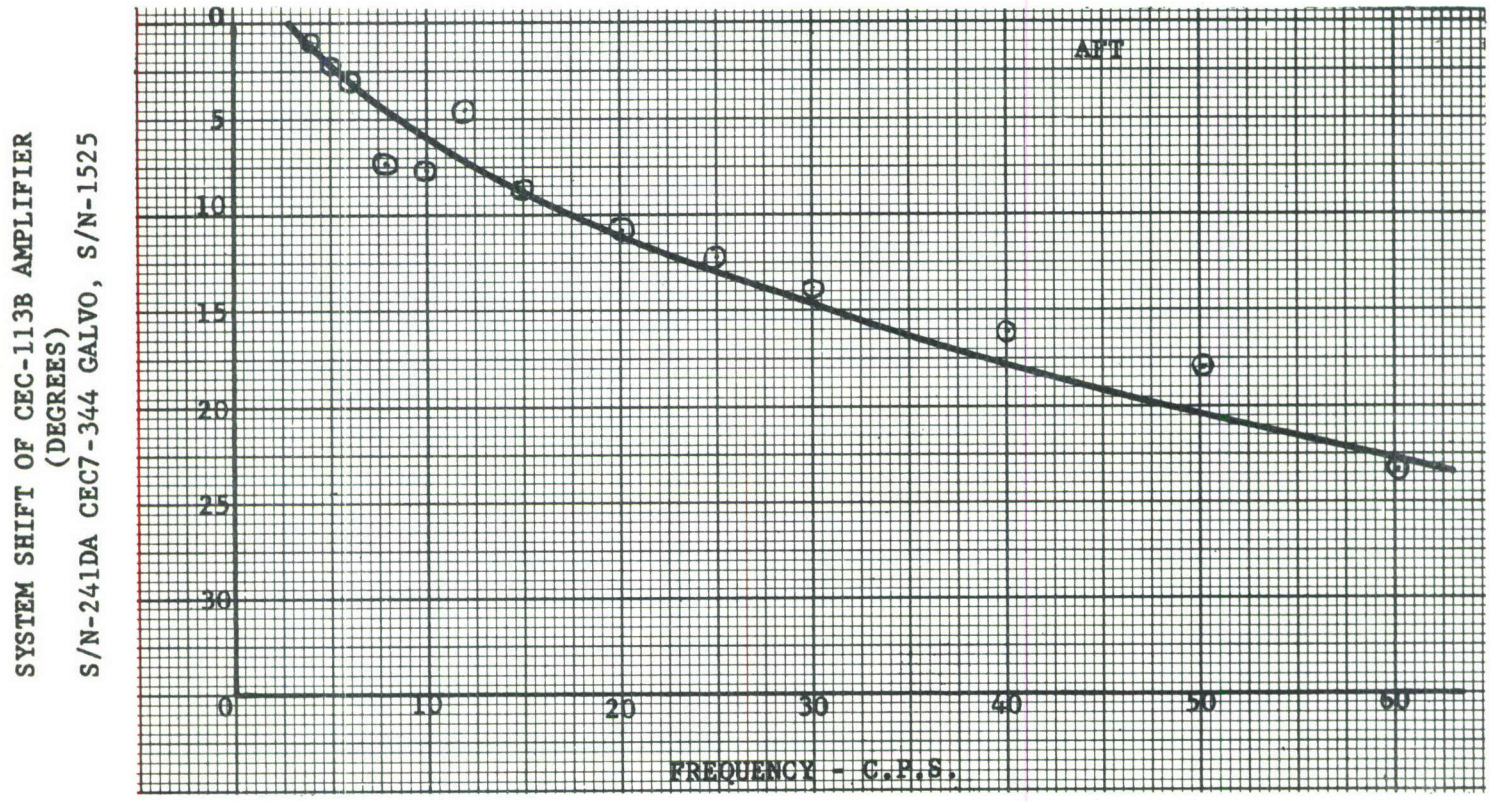

Figure 31 Phase Calibration Curves

Calibration of MB Pickups

The calibration equipment for each vibration pickup-amplifier-galvanometer combination is shown in Figure 32, and although just one vibration channel is shown, the remaining fourteen channels were calibrated similarly. It is obvious that once calibrated, the vibration pickup-amplifier-galvanometer combinations must remain grouped. Furthermore, the polarity of the generated signal has to be held constant between channels and correlated to the motion of the oscillogram trace at the beginning of each calibration. This was accomplished with a linear potentiometer which was mechanically coupled to the shaker table and then supplied to a conventional indicator bridge circuit. This output was recorded simultaneously with that of the signal coil and velocity pickup, and from manual operation of the shaker table the oscillograph trace polarity was determined.

With the velocity pickup secured to the vibration table - zero amplitude displacement - the signal generator output was adjusted to a given frequency and fed to the amplifier input circuit. Once the attenuator had been set to give sufficient deflection on the oscillograph, it was held constant for the remaining amplifiers. In addition, the generated signal was recorded and used as a sensitivity reference for the entire system.

The shaker table was excited at 9 frequencies for each of two amplitudes. Frequencies were measured with the counter, and the amplitude of the velocity pickup was read directly by means of the calibrated microscope. As a check on the visual measurement, the voltage of the peak-to-peak voltmeter was used to determine the table displacement.

The phase reference for the system was determined from the signal coil voltage recorded simultaneously with the velocity pickup, recording through an amplifier identical with those used for the velocity pickup channels. The displacement of the recorded velocity pickup trace and signal coil trace on the recorded type could then be taken as a measure of the phase lead of the velocity pickup. A measure of the overall phase shift between original displacement and the recorded trace was obtained by substracting the phase lag of the integrate amplifier and adding the 90^{o} phase lead of the signal coil. Calibration curves for phase angle and displacement amplitude have been plotted as functions of frequency. Typical curves are presented in Figure 33.

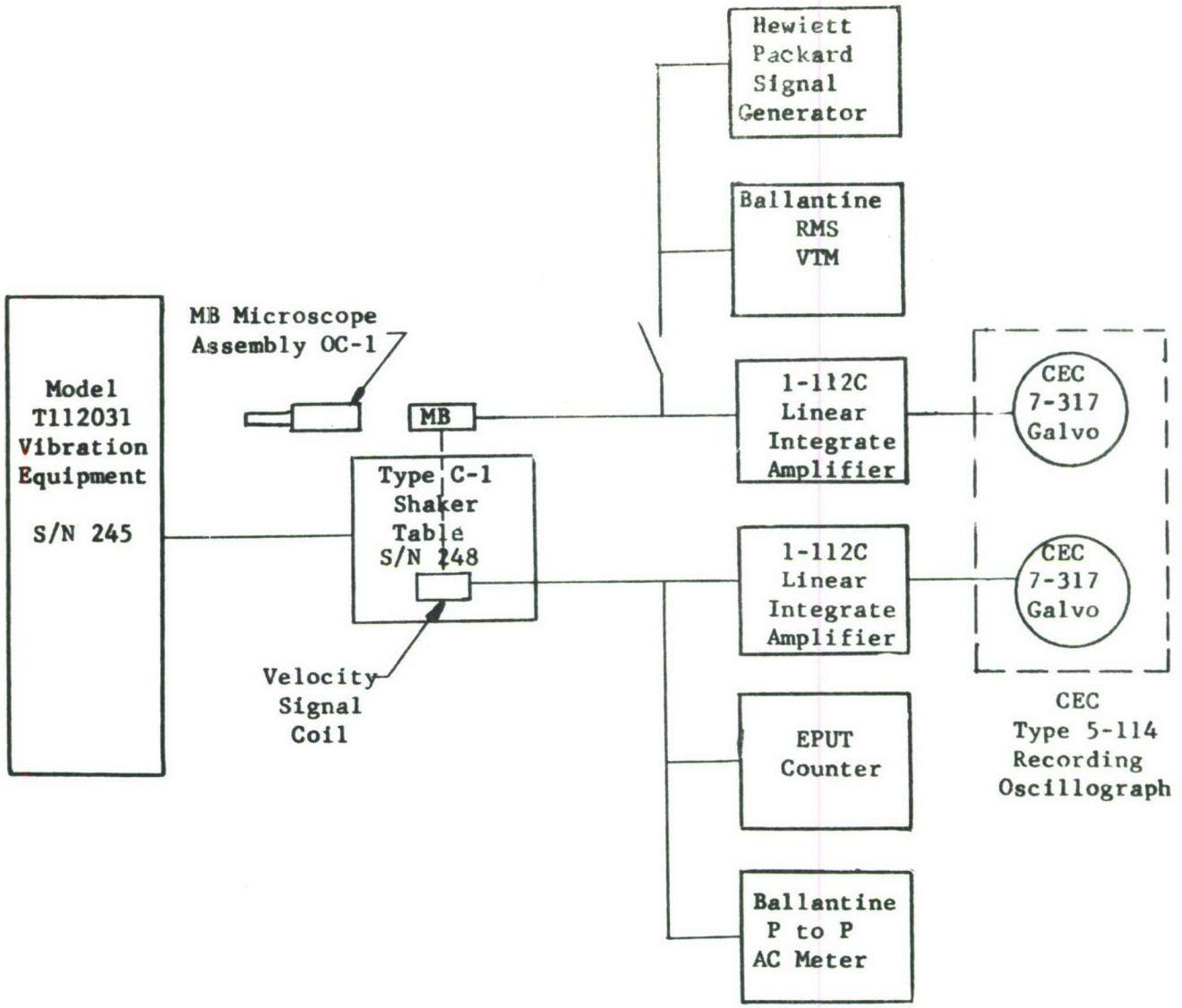

BLOCK DIAGRAM FOR TYPICAL VIBRATION
MEASURING SYSTEM IN H-21 #96

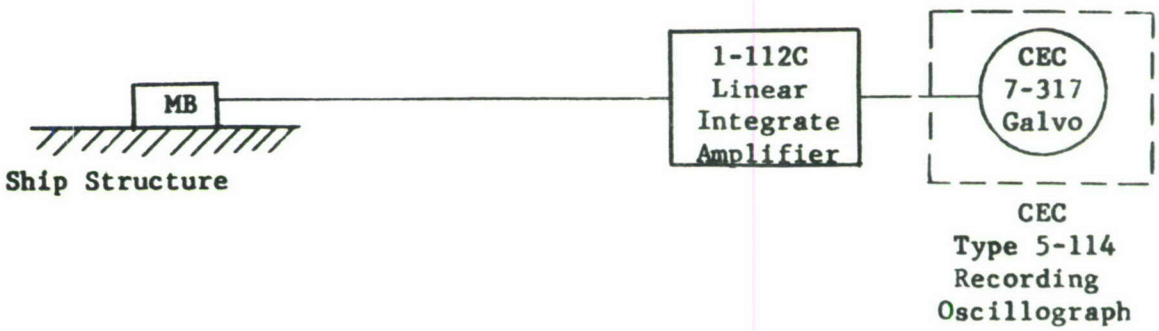

Figure 32 Block Diagram For Instrumentation Used In Calibrating M.B. Pickups.

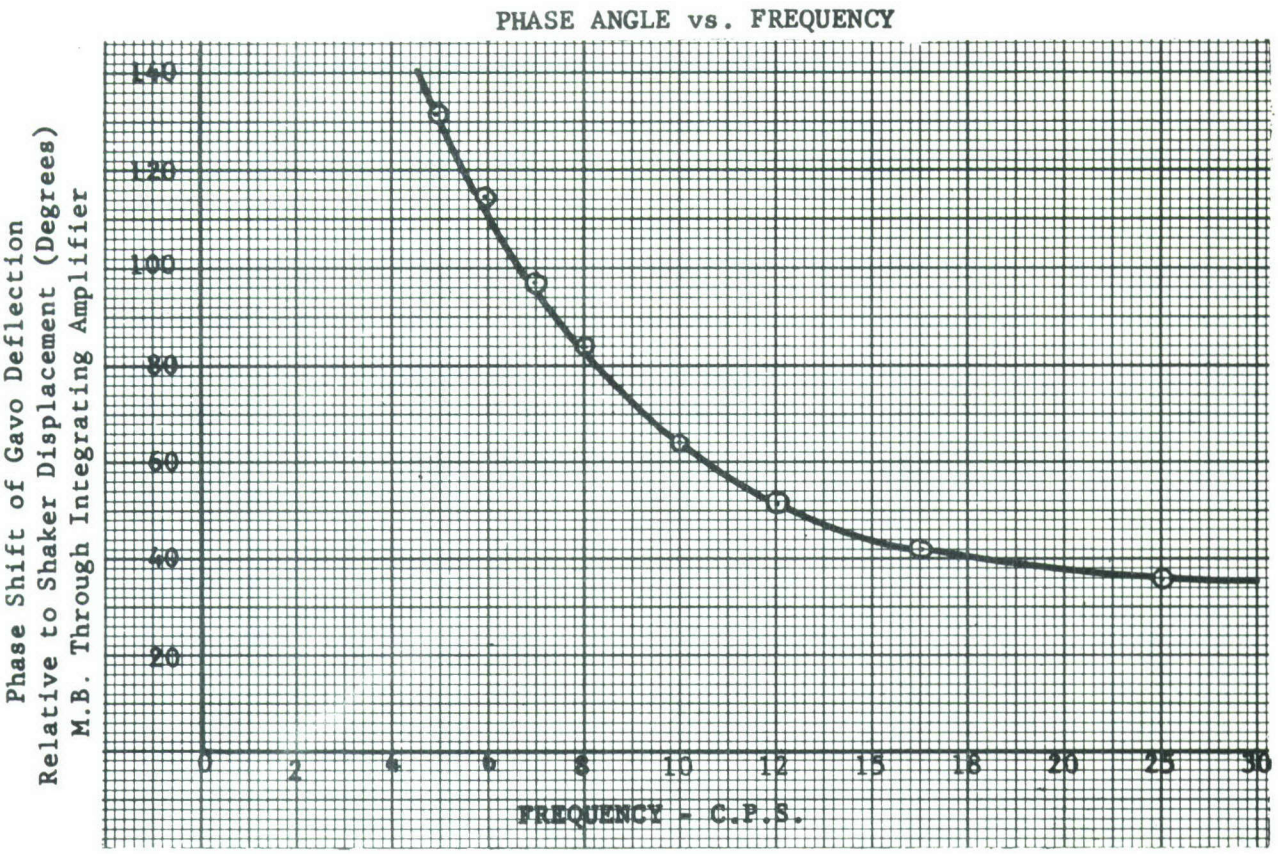

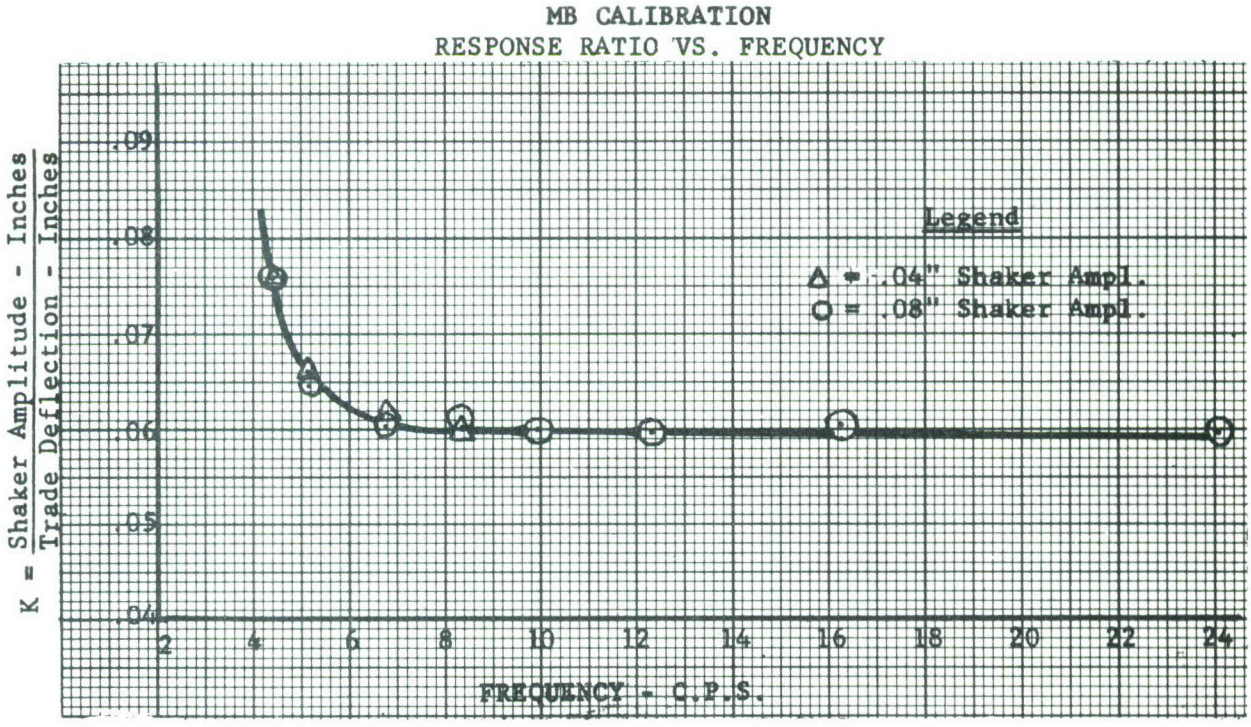

Figure 33 Calibration Curves For Phase Angles And Displacement Amplitudes